

VERÖFFENTLICHUNGEN

des Fachgebietes Bodenmechanik und Grundbau
der Technischen Universität Kaiserslautern

Herausgeber: Prof. Dr.-Ing. C. Vrettos

Heft 19

STATIC AND DYNAMIC BEHAVIOUR OF
SAND-RUBBER CHIPS MIXTURES

von

Gerard Banzibaganye

KAISERSLAUTERN 2022

Vom Fachbereich Bauingenieurwesen
der Technischen Universität Kaiserslautern

zur
Verleihung des akademischen Grades
DOKTOR-INGENIEUR (Dr.-Ing.)
genehmigte

DISSERTATION

D 386

Tag der Einreichung: 22. November 2021

Tag der mündlichen Prüfung: 7. Februar 2022

Dekan: Prof. Dr.-Ing. Hamid Sadegh-Azar

Berichterstatter: Prof. Dr.-Ing. habil. Christos Vrettos
apl. Prof. Dr.-Ing. Andreas Becker
Prof. Dr.-Ing. Jürgen Grabe

Autor dieses Heftes ist

Gerard Banzibaganye

Wissenschaftlicher Mitarbeiter am Fachgebiet Bodenmechanik und
Grundbau der Technischen Universität Kaiserslautern

Editor's Foreword

During the last decades, chipped and shredded scrap tires mixed with soil have found a wide range of innovative civil engineering applications including the use as highway embankment fill, retaining walls and bridge abutment backfill, for liquefaction mitigation, for seismic isolation of building foundations, as barrier for vibration protection, or to reduce swelling of expansive clays. Several studies have addressed the behaviour of the composite material with respect to compressibility, shear strength, or liquefaction susceptibility. The degree of improvement depends on the size and shape of the rubber particles as well as the gradation of the rubber and the sand. Most investigations hitherto dealt with rubber granulate or small-size chips.

The present experimental work focuses on the behaviour of large, irregularly shaped rubber chips mixed with different sands. Extensive static, cyclic and dynamic laboratory tests have been carried out in order to enhance our understanding about the complex interactions between the two constituents, capture the pertinent properties of the composite material at various rubber contents, and identify the optimal mixing ratio in dependence of the loading pattern. The behaviour of pure sand, inferred from the respective laboratory tests, serves as a benchmark for the quality of the tests and point of reference for the assessment of the mechanical properties of the sand-rubber mixtures. Of great interest are the findings for cyclic drained or undrained loading. The equations for shear modulus and damping derived from the wide range resonant column tests can directly be used in design.

The dissertation provides a valuable insight into the behaviour of this particular type of composite granular medium, and can be used as a starting point for the investigation of mixtures with other rubber chips geometries and soils types, aiming at optimizing the application in geotechnics.

Christos Vrettos

Preface

This dissertation work was carried out at the Technical University of Kaiserslautern and was supported partly by the Deutscher Akademischer Austauschdienst (DAAD) and partly by a scholarship from the Division of Soil Mechanics and Foundation Engineering of the Technical University of Kaiserslautern.

At this point I would like to express my deepest appreciation to my supervisor Prof. Dr. Ing. habil. Christos Vrettos for supporting me during this incomparable journey and for supervising my scientific work.

I would also like to thank apl. Prof. Dr. Ing. habil. Andreas Becker for his helpful advice and Prof. Dr. Ing. Jürgen Grabe for reviewing my dissertation.

Appreciation goes to Mr. Ronald Günther for helping to solve problems encountered during the experimental works.

Last but not least, I would like to thank my wife Marie Adolatha Umutoni who supported me a long journey towards a doctoral degree.

Gerard Banzibaganye

Table of Contents

	Page
Editor's Foreword	i
Preface	iii
Table of Contents	v
List of Symbols	ix
Latin Symbols.....	ix
Greek Symbols	ix
Abbreviations	x
Abstract	xi
1 Introduction	1
2 State of the art	4
2.1 Static behaviour of sand and tyre-chips mixtures	4
2.1.1 Compressibility.....	4
2.1.2 Shear strength	5
2.2 Cyclic behaviour.....	9
2.3 Dynamic behaviour	10
2.4 Effect of using tyre rubber on the environment	12
3 Material investigated	14
3.1 Sands.....	14
3.2 Waste tyre rubber chips.....	15

3.3 Sand rubber chips mixtures	16
3.3.1 Densities	17
3.3.2 Permeability	20
4 Static tests	22
4.1 Oedometer tests	22
4.2 Direct shear tests	25
4.2.1 Equipment and testing procedure	25
4.2.2 Results.....	28
4.3 Triaxial tests	31
4.3.1 Equipment and testing procedure	31
4.3.2 Results for saturated sand	36
4.3.2 Results of drained test on dry and wet sand	39
4.3.3 Results for unsaturated sand rubber mixtures	44
4.4 Discussion.....	51
5 Cyclic triaxial tests.....	53
5.1 Equipment and testing procedure.....	53
5.2 Results of undrained tests on saturated material	59
5.2.1 Cyclic resistance of pure sand	59
5.2.2 Cyclic resistance of sand rubber chips mixtures from CAU tests	65
5.3 Results of drained tests on saturated material	73
5.3.1 Volume change	73

5.3.1 Accumulated axial strain	75
5.4 Link between undrained and drained test results	77
5.5 Long term cyclic response of unsaturated material.....	79
5.5.1 Stress-strain curves and accumulated strain.....	79
5.5.2 Young's modulus and damping ratio	82
5.5.3 Post cyclic shear strength	85
5.6 Sample conditions before and after cyclic testing.....	86
5.7 Discussion.....	88
6 Resonant column tests	91
6.1 Equipment and calibration	91
6.1.1 Equipment.....	91
6.1.2 Device calibration.....	91
6.2 Sample preparation and testing method	97
6.3 Calculation for shear strain	100
6.4 Results for sands.....	101
6.4.1 Small strains response	101
6.4.2 Intermediate strains response.....	104
6.5 Results for sand rubber mixtures.....	107
6.5.1 Small strains response	107
6.5.2 Intermediate strain response	111
6.6 Discussion.....	124

7. Summary and outlook	126
Literature	129
Appendices.....	139
A Proctor tests	139
B Static tests	139
C Cyclic triaxial tests	144
D Resonant column tests	148

List of Symbols

Latin Symbols

c	Cohesion in the Mohr-Coulomb failure criterion
D	Damping ratio
d_{50}	Mean grain diameter
D_{\min}	Minimum damping ratio
E_d	Dynamic young modulus (secant)
E_{50}	Secant modulus at 50% of peak or maximum deviatoric stress
E_S	Constrained modulus
e	Void ratio of sand
e_{SRM}	Void ratio of sand rubber mixture
G	Shear modulus
G_d	Dynamic shear modulus (secant)
G_{\max}	Maximum shear modulus at small strains
I_D	Relative density
N_f	Cycle number at initial liquefaction
r_u	Pore pressure ratio
\bar{r}_u	Average pore pressure ratio
V_S	Shear wave velocity

Greek Symbols

ε_c	Compression strain
$\varepsilon_{1,cy}$	Cyclic axial strain
ν	Poisson's ratio
γ	Shear strain
φ	Friction angle
$\sigma_{1,cy}$	Cyclic stress amplitude
$\sigma'_{1,st}$	Pre-cyclic static stress
σ'_3	Effective confining stress
χ	Rubber chips content
ρ	Density of material

Abbreviations

CSR	Cyclic stress ratio
R	Rubber chips
S2RM	Mixture of medium sand S2 and rubber chips
S3RM	Mixture of coarse sand S3 and rubber chips
S4RM	Mixture of sand mixture S4 and rubber chips

Abstract

Reinforcing sand soils using tyre rubber chips is a novel technology that is under investigation to optimize its engineering application. Previous studies concentrated on static behaviour and very few on cyclic and dynamic behaviour of sand rubber mixtures leaving gaps that need to be addressed.

This research focuses on evaluating the static, cyclic and dynamic behaviours of sand rubber mixtures. The basic properties of sands S2, S3, S4, rubber chips and sand rubber chips mixtures at 10/20/30% rubber chips content by dry mass were first evaluated in order to obtain the parameters essential for subsequent testing. Oedometer, direct shear with larger box 300x300 mm and static triaxial compression tests were performed to assess the static behaviour of the composite material. Further, dynamic cyclic triaxial tests were performed to evaluate the cyclic behaviour of saturated, dry and wet mixtures. All specimens were first isotropically consolidated at 100 kPa. For saturated material a static deviatoric stress of 45 kPa was imposed prior to cycling to simulate the field anisotropic consolidation condition. Cycling was applied stress-controlled with amplitude of 50kPa. Both undrained and drained tests were performed. Cyclic tests in dry or wet conditions were also performed under anisotropic consolidation condition with the application of different stress amplitudes. For all cyclic tests the loading frequency was 1 Hz. With regard to dynamic behaviour of the mixtures, the resonant column tests were conducted. Calibration was first performed yielding a frequency dependent drive head inertia. Wet mixture specimens were prepared at relative density of 50% and tested at various confining stresses. Note that all specimens tested in both triaxial and resonant column were 100 mm diameter. The results from the entire investigation are promising.

In summary, rubber chips in the range of 4 to 14 mm mixed with sands were found to increase the shear resistance of the mixtures. They yield an increase of the cyclic resistance under saturated condition, to a decrease of stiffness and to an increase of damping ratio. Increased confining stress increased the shear modulus reduction and decreased damping ratio of the mixtures. Increased rubber content increased both shear modulus reduction and damping ratio. Several new design equations were proposed that can be used to compute the compression deformation, pore pressure ratio, maximum shear modulus and minimum damping ratio, as well as the modulus reduction with shear strain. Finally, chips content around 20% to 30% by dry mass can be used to reinforce

sandy soils. The use of this novel composite material in civil engineering application could consume a large volume of scrap tyres and at the same time contribute to cleaning environment and saving natural resources.

1 Introduction

The growing economy in most of the countries necessitates the development of infrastructures such as highways, railways, pipelines and others. The construction of new infrastructures and buildings is always associated with different challenges. These include but are not limited to land scarcity, environmental degradation and pollution. The land shortage problem forces engineers to use the available sites that may underlain by poor foundation soils. Removal and replacement of these soils contributes to the environmental deterioration and pollution and can also considerably increase the overall project cost. To ensure an effective structure performance (highway or building) stronger foundation is required otherwise the stable lightweight fills that can apply small stresses have to be considered.

On the other hand, a large volume of waste tyres is being discarded in different corners of the world. Managing these wastes becomes more difficult due to their bulk volume and non-biodegradability characteristics. Problems associated with discarding waste tyres include the reduction of space destined for other activities, atmospheric pollution, soil contamination, health hazard and costs (Rowhani & Rainey, 2016; Thomas et al., 2016). To minimize these problems, the European Union for example through its directive 1991/31/EC bans all waste tyres to landfills, and suggests that every member state has to find an appropriate technology to manage this waste. The characteristics that render waste tyre rubber problematic when being illegally dumped or landfilled make them a valuable resource of material for civil engineering applications. These include but are not limited to lightweight backfill behind retaining walls, road embankment and bridge abutment fills, drainage layer in landfills, building foundation seismic isolation etc.

A novel composite geomaterial can be produced by mixing sand and tyre shreds/chips. Its geotechnical characteristics including light density, compressibility, permeability, shear resistance have been evaluated in pilot studies to investigate the suitability of its usage in different civil engineering applications. Constructing highways and other earth structures using shreds/chips mixed with sandy soil may offer technical, environmental and economic benefits. These include saving of energy and natural resources, cleaning of the environment, reduction of compressibility and settlement of

foundation soil, and improved structure stability (Humphrey & Sandford 1993; Edil & Bosscher 1994).

The cyclic or dynamic loadings of soils supporting structures are of great concern. These are induced by vibrations from various sources such as natural earthquakes, highway and railway tracks, artificial explosions and soon. Vibrations in sands may lead to structure collapse or induce liquefaction failure in saturated sands. These cause severe losses of strength and stiffness which in turn induce structural damage, loss of human lives and threats to the environment. These problems may be addressed when a novel lightweight composite material is used as road fill or as damping layer within the foundation supporting the structure. They may also increase the resistance to liquefaction in saturated conditions. With respect to cyclic behaviour during repeated loading, and the associated degradation and settlement only few systematic studies have been conducted hitherto (Mashiri, 2014). Limited studies regarding the improvement of liquefaction resistance in the ground showed contradictory findings. This may be attributed to the size of tyre grains/chips, mainly non-uniform sand type, relative density, loading patterns, and liquefaction criteria. With respect to the dynamic behaviour as for example evaluated in resonant column testing, limited studies have been conducted (Anastasiadis et al., 2009 & 2011 & 2012; Senetakis et al., 2012). In these studies, only rubber granulates or fine rubber chips were mixed with sand. These studies showed that the chips reduced the shear resistance of sand. However, the influence of the chip size, the grain size distribution of the matrix material, the mix ratio and the moisture content still need further investigation for a proper material characterisation and subsequent optimization.

The main objective of the study is to evaluate the suitability of tyre chips reinforced sand material in geotechnical engineering applications through the analysis of static, cyclic and dynamic responses. For the purpose of the material optimization, an extensive laboratory study focusing on the interaction of uniform sands (medium or coarse) and a mixture of the two with tyre chips at different proportions is performed. The basic properties of the parent material and sand tyre chips mixtures are evaluated in a first series of tests. A second series covers the static behaviour of both dry and wet material and its appraisal regarding practical applications. In a third series of tests, the cyclic strength of the saturated material and the long-term cyclic response of dry and wet material are evaluated. In a fourth test series, the dynamic response of wet material is

evaluated. Finally, functional relationships for the relevant physical quantities are derived and presented in the respective sections.

Chapter 2 presents a summary of the updated state-of-the-art concerning the feasibility of using sand rubber chips mixtures in geotechnical engineering applications. Chapter 3 describes the basic properties of the investigated material. In Chapter 4 the mechanical behaviour of sand rubber chips mixtures under static loading are examined and discussed. Chapter 5 focuses on cyclic behaviour of saturated composite material as well as long-term cyclic response of dry and wet material. The dynamic response of wet composite material is addressed in Chapter 6. Chapter 7 summarizes the research findings and recommends future studies associated to this work.

2 State of the art

2.1 Static behaviour of sand and tyre-chips mixtures

Compressibility and shear strength behaviour of pure tyre shreds/chips or tyre shreds/chips sand mixtures are associated with basic properties such as permeability, specific gravity, void ratio, relative density etc. These properties have been reported in various studies, for example by Ahmed (1993), Edil & Bosscher (1994), Masad et al. (1996), Foose et al. (1996), Geosynthetic Consultants (2008), Anastasiadis et al. (2011). The specific gravity of pure tyre chips/shreds is in the range of 1-1.23 g/cm³, i.e. less than a half that of typical soils. The bulk density values of pure tyre chips/shreds are in the range of 0.225-0.714 g/cm³ and the permeability in the range of 1.5-15 cm/s. Due to their high permeability and low density, tyre shreds/chips can be a suitable material in establishing a drainage layer for landfill leachate collection or backfill behind retaining walls (Edeskar, 2006).

For sand tyre chips mixtures various authors concluded that the density decreases while void ratio increases. Mashiri et al. (2015) and Anastasiadis et al. (2011) found a decrease of void ratio for the increased tyre chips content up to 35% by dry mass. Further addition of chips decreases the void ratio. Reddy & Krishna (2015) observed a lowest void ratio at 30% by dry mass. Anvari et al. (2017) reported a decrease of void ratio for chips content up to 5% in sand while the density decreases for any inclusion of tyre chips. The increase in void ratio contributes directly to the increase of permeability and vice versa. The permeability of mixtures of steel furnace slag, coal wash and rubber crumbs reported by Indraratna et al. (2018) shows that increasing rubber content increases the hydraulic coefficient. It can be pointed out that the increase of permeability resulting from the increase of void ratio may be associated with the increase of rubber content.

2.1.1 Compressibility

Few studies were performed to evaluate the compressibility of sand tyre chips/shreds mixtures. The findings from the tests are reported by Hall (1991), Humphrey & Sandford (1993), Edil & Bosscher (1994), Masad et al. (1996), Warith & Rao (2006), Kowalska & Chemielewski (2017), Chenari et al. (2019).

Due to the compressibility of the individual shreds/chips and the larger void space between rubber particles, increasing the vertical stress yields to an increase of the vertical strain and a decrease of the void ratio. Pure tyre shreds/chips under vertical stress in the range of 20-700 kPa, exhibit vertical strains in the range of 21 - 47%. The associated Young's modulus is very small. This could be a discouraging finding for the possible use of the material alone in road construction. However, when mixed with sand, the compressibility characteristics of the mixture becomes tolerable for the application in civil engineering applications. Of course, the generated vertical strain in the mixture becomes higher than that exhibited by pure sand and increases to higher value for higher chips contents. The stiffness of the composite material decreases when the chips content increases.

2.1.2 Shear strength

The methodology of soil reinforcement mechanism addresses first the selection of the reinforcing material. Reinforcing material may consist of fibers, tyre shreds/chips or other particulate materials. To simulate the reality on site, reinforcing material should be randomly mixed with sand, thus enforcing various orientations of reinforcement. Shear strength enhancement can only be achieved for vertical and inclined orientation of the reinforcing elements. Impact of the reinforcements on the shear strength in sands can be evaluated in the laboratory through direct shear box or triaxial compression tests. The size of the equipment is dictated by the particle size of the reinforcement material.

Assuming that tyre chips/shreds are selected as reinforcing material, large scale direct shear box or triaxial devices should be adopted to avoid potential boundary/interactions effects caused by large particle sizes. The total shear strength of the mixtures S_{tot} equals the summation of soil shear strength S_s and shear strength induced by reinforcement S_T . A possible soil reinforcement mechanism was described by Gray & Ohashi, 1983 and is reproduced in Figure 1.

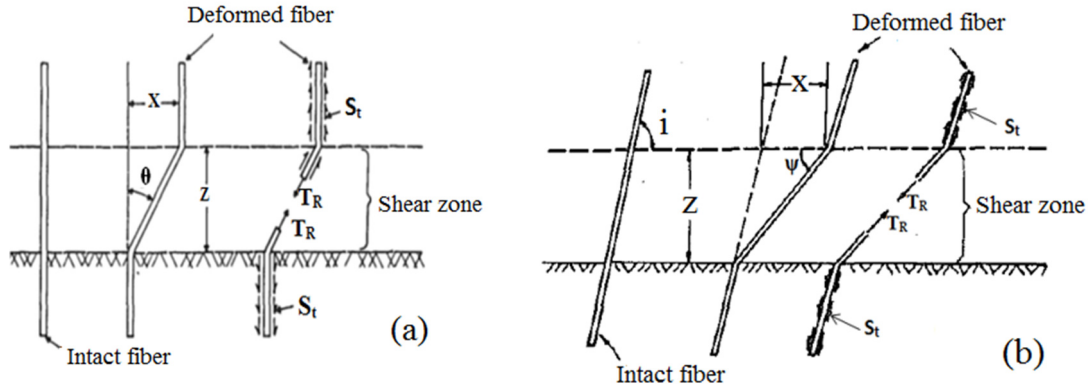


Figure 1: Fiber deformation during shearing (a) perpendicular to shear plane and (b) inclined at an angle (i) to the shear plane (Gray & Ohashi 1983)

The total shear strength of the reinforced soil is given by:

$$S_{tot} = S_S + S_T \quad (1)$$

where S_S is the shear strength of sand or sand with rubber chips in horizontal direction; $S_T = \Delta S_s + \Delta S_t$ the total increase of the shear strength induced by rubber chips in horizontal and vertical directions.

Practically, tyre chips are randomly distributed in soils during the preparation of the mixtures. Pure sand or sand mixed with tyre chips in horizontal direction derives their shear strength from friction resistance and cohesion from particle sticking, and can be expressed by:

$$S_S = c + \sigma_n \cdot \tan \varphi \quad (2)$$

where c the cohesion, σ_n the normal stress and φ the friction angle. Any additional strength increase may be derived from the reinforcement mechanism due to both vertical and inclined orientation of the chips in the mixtures and assuming that they are extended in both side of the shear plane, as depicted in Figure 1. During shearing, tyre chips deform in the shear zone and develop tensile resistance T_R . In tyre chips, T_R may be divided into two components. The first is normal to the shear plane and increases confining pressure at failure plane and mobilizes extra resistance to the induced shear force. The second is a tangential component which opposes directly to shear. For perpendicular direction of tyre chips, increase of shear strength can be estimated by:

$$\Delta S_s = F_R (\sin \theta + \cos \theta \cdot \tan \varphi) \quad (3)$$

$$\theta = \arctan \left(\frac{X}{Z} \right) \quad (4)$$

For inclined orientation of the tyre chips, additional increase of shear strength can be estimated by:

$$\Delta S_t = F_R [\sin(90 - \psi) + \cos(90 - \psi) \tan \varphi] \quad (5)$$

$$\psi = \tan^{-1} \left[\frac{1}{k + (\tan i)} \right] \quad (6)$$

where ΔS_s and ΔS_t denote the increase of shear strength due to reinforcement, T_R is the tensile strength developed in tyre chips per unit area of soil, φ is the internal friction angle of the composite material, θ is the shear distortion angle, i is the initial orientation angle of tyre shreds with respect to the shear plane; and k is the shear distortion ratio with $k = x/z$ where z is the thickness of the shear zone and x the horizontal shear displacement.

Note that the mobilized tensile strength F_R from tyre shreds/chips per unit area depends on the tensile stress of tyre chips and their concentration (area ratio) in the shear plane, and can be estimated by:

$$F_R = \left(\frac{A_R}{A_1} \right) \cdot T_R \quad (7)$$

where A_R is the area of the reinforcement, A_1 is the total area of the shear plane, T_R is the tensile stress in the tyre shreds within the shear plane.

Extensive researches have been concentrating on evaluating the shear strength of sand tyre chips mixtures as a key driving characteristic towards a novel ground improvement technology. Laboratory investigations were performed mainly using large direct shear box. The results for sand tyre chips/shreds mixtures at various rubber contents suggest a nonlinear stress-strain behaviour. A linear stress strain relation was observed for pure tyre chip samples. For chip sizes smaller than 50 mm, a friction angle in the range of 19 to 30° and cohesion of 3 to 11 kPa were obtained. Tyre shreds size in the range of 50 to 150 mm exhibited a friction angle of 30° with zero cohesion. Foose et al. (1996) used tyre shreds

smaller than 5cm, 5 to 10cm and 10 to 15cm containing metals. Tyre shreds content were 0/10/20/30/50% by dry mass. Normal stress in the range of 7 to 70 kPa were selected. Tests were performed using large direct shear device. Results from this study revealed an increase in shear strength for all shreds contents compared to that of pure sand. The maximum improvement was achieved at a shreds content of about 30%. Strain hardening behaviour and non-linearity of Mohr-Coulomb envelope were also obtained. Similar behaviour was reported by Edil & Bosscher (1994), Banzibaganye (2014).

Contradictory results were reported for sand mixed with rubber particles smaller than 5mm tested in a standard direct shear box. Cabalar (2011), Ehsani et al., (2015) observed a decrease of shear strength for all rubber contents. Anvari et al. (2017) reported a slight increase only up to 5% of granulated rubber content with subsequent decreased. The authors argued that the decreased strength was due to the inclusion of rubber granulate in sand which generates a poor interlocking compared to sand-to-sand particles contact.

A relatively small number of investigations was performed on sand tyre chips mixtures under triaxial testing conditions. In comparison to direct shear box, triaxial compression simulates better the stress loading conditions in the field. From this reason it is worth that the measurement of shear strength parameters from triaxial compression are accurate for design purposes. Studies conducted by Wu et al. (1997), Ghazavi (2004), Zornberg et al. (2004), Rao & Dutta (2006), Bałachowski & Gotteland (2007), Becker & Vrettos (2011), Vinot & Baleshwar (2013), Balunaini et al. (2014), Mashiri et al. (2014), Kowalska & Chemielewski (2017), Becker (2017), Madhusudhan et al. (2019), Tasalloti et al. (2021) for medium to larger shreds/chips included in sand or cohesive soils improved their strength. Excellent improvement was achieved for confining stress level of 100 kPa or less. Note that the soil used in these studies was essentially non-uniform. Generally, an optimum tyre chips content in the range of 20% for medium chips to 35% for larger chips by dry mass were reported. The opposite behaviour was reported by Ehsani et al. (2017) for rubber granulates embedded in sand. These findings indicated similar behaviour as those from direct shear tests.

During shearing in either direct shear or triaxial compression, the dilatancy behaviour is observed. Specimens with pure tyre chips only show pure compression. A small initial contraction is achieved followed by dilation for pure

sand samples regardless of the confining stress level. Sand tyre chips samples initially contract and then dilate. The contraction increases with increasing chips content in the mixture while the dilation decreases.

The contribution of tyre shreds/chips on the shear strength of the composite material is elucidated by Zornberg et al. (2004). Figure 2 shows the different strength contributions for similar/identical sand tyre chips samples. The curve shows strength contribution from the reinforcement mechanism, internal shear mechanism, and also the overall shear strength of the composite material. After a series of tests, the authors found that the strength contribution is high for lower confining stress and becomes less significant at higher confining stresses. Edil & Bosscher (1994) reported also a significant excellent contribution for larger tyre shreds under lower confining stress.

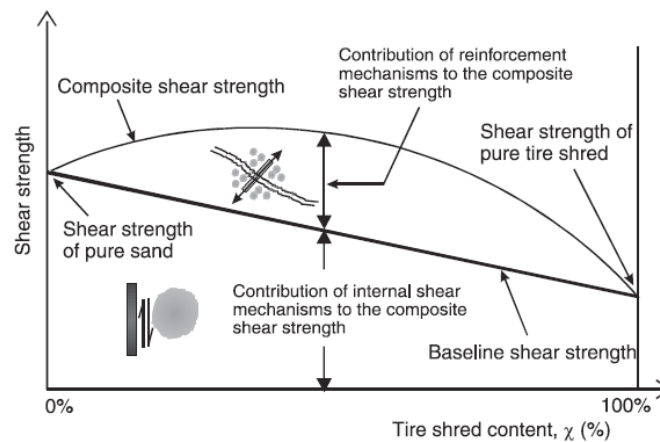


Figure 2: Schematic interpretation of the contribution of tyre shreds on the shear strength of sand tyre shreds mixtures under a constant soil matrix relative density (Zornberg et al., 2004).

2.2 Cyclic behaviour

Flexible tyre chips have been found to damp the energy applied during the compaction process. This behaviour motivated geotechnical engineers to explore the effect of tyre chips on the cyclic response of sand. In general, pure saturated sand may exhibit an earlier liquefaction failure at cycle numbers varying from 1 to 100. However, the cyclic resistance is influenced by the sand particle shape, the relative density, the applied stress or strain amplitude, the initial pre-cyclic static stress as well as the added artificial material, in this case the tyre chips.

A newly developed concept for stabilizing soils prone to liquefaction is through reinforcement using shredded tyre material in form of chips (Towhata, 2008; Hong et al., 2015). The resistance to liquefaction as well as shear modulus and damping of sand rubber chips mixtures were evaluated. One can mention Hazarika et al. (2008), Nakhaei et al. (2012), Kaneko et al. (2013), Mashiri (2014), Ehsani et al. (2015), Bahadori & Manafi (2015), Li et al. (2016), Bahadori & Farzalizadeh (2016), Madhusudhan et al. (2017), McCartney et al. (2017), Zhou & Wang (2019), Amuthan et al. (2020), Hazarika et al. (2020), Madhusudhan et al. (2020), Rios et al. (2021). The results indicate that increasing the chips content in the mixtures improves the resistance to liquefaction, decreases the shear modulus, increases the cyclic axial strain and increases the damping ratio. Hong et al. (2015) and Shariatmadari et al. (2018) observed the opposite behaviour. Their findings indicate that increasing tyre chips or ground rubber in sand decreases both the shear strength and the resistance to liquefaction. Mashiri (2014) noticed a decrease of liquefaction resistance of sand rubber mixtures at chips content of 40% by dry mass. This author asserts that in the mixture at this content, sand matrix void ratio becomes greater than the maximum void ratio of sand which leads to an increase in residual pore water pressure. The contradictory findings may also be attributed to type of sand, the relative density of the mixtures and the loading conditions. It should be noted that the soil used in these studies was essential non uniform sand.

2.3 Dynamic behaviour

Recently the resonant column device has been used to evaluate the dynamic behaviour of sand rubber mixtures. The investigations were limited to fine tyre chips or granulated rubber mixed with sand. This was due to the available testing facility whereby a maximum 70 mm diameter sample could be tested. The findings from these studies are summarized below.

Shear modulus and damping ratio of pure sand were first evaluated followed by those for sand or gravel rubber mixtures. The influence of confining stress, relative density, mean size ratio of soil to rubber ($d_{50,S}/d_{50,R}$) as well as the concentration of rubber on the dynamic behaviour of sand was evaluated (Zheng-Zheng-Yi & Sutter, 2000; Anastasiadis et al., 2009; Anastasiadis et al., 2011; Senetakis et al., 2011; Senetakis et al., 2012; Ehsani et al., 2015; Bernal-Sanchez et al., 2019). Granulated rubber particles with mean grain size in the range of 0.3

to 5 mm were used in these studies with the maximum of 6.35 mm. The concentration of the rubber granulates varied from 0 to 35%. Low amplitude shear modulus and damping ratio of sand rubber mixtures were investigated at confining stress levels starting from 25 kPa while high amplitude tests at 50 kPa. Dense to very dense samples were used in these studies.

It was generally reported that increasing the confining stress and the relative density increases the shear modulus, decreases the damping ratio and increases the shear strain amplitude (specify) of sand rubber mixtures. For the increased confining stress, a smoother decrease of the modulus reduction curve was observed (Anastasiadis et al., 2009). It was noted that the effect of confining stress on the linear behaviour of pure rubber granulates sample is negligible. Furthermore, increasing the rubber content decreases the shear modulus, increases the damping ratio and increases the shear strain amplitude of the mixtures. The opposite findings were derived by Das & Bhowmik (2020) where the increase of rubber content increases the shear modulus and decreases the damping ratio. The reason for this could be that the content of the rubber was limited to low values with a maximum of 6%.

Senetakis et al. (2011) evaluated the influence of confining stress, rubber content and $d_{50,s}/d_{50,r}$ on the shear modulus and the damping ratio of the composite material. They noticed that increasing the confining stress increases the shear modulus reduction and decreases the damping. While at the same confining stress increasing rubber granulate in the mixture increases shear strain amplitude, normalized shear modulus and damping ratio of the mixtures. At any given shearing strain, increasing the ratio of $d_{50,s}/d_{50,r}$ increases the modulus degradation and decreases the damping ratio. A high ratio $d_{50,s}/d_{50,r}$ implies a larger contact surface between rubber particles which turns the mixtures from sand-like to rubber-like. The rubber-like is likely to occur for fine rubber than for coarse rubber. Pistolas et al. (2018) argued that increasing the confining stress for the mixtures with $d_{50,s}/d_{50,r} < 1$ leads to soil inter-granular contact caused by the higher deformation of the rubber particles, and the response may be governed by soil fraction.

Esmaeili et al. (2013) conducted the laboratory tests on tyre shreds mixed with railway subgrade to obtain the shear strength and the deformability characteristics to be applied in subsequent numerical studies. A 2D numerical model of ballasted track was used. The authors reported that the vertical vibration

velocity at the ballast should increasing tyre shreds from 5 to 15% decreased the vertical vibration velocity by 44% at the ballast shoulder.

A large scale field test was performed to evaluate the effectiveness of soil rubber mixtures as possible geotechnical seismic isolation for structures (Pitilakis et al., 2021). Three similar tests were performed using gravel rubber mixtures at granulated rubber content of 0/10/30% by mass. The mixtures were placed in the test pit underneath the foundation structure and vibrations were applied from the top. Based on the results obtained, the authors conclude that the mixtures with 30% effectively cut- off all incoming waves, reduce the lateral movement and rocking stiffness of the geotechnical seismic isolation system. They pointed out that the effective compaction may not be achieved for the mixtures with rubber content beyond 30%.

Based on the evaluated behaviour of sand tyre shreds/chips mixture, various authors recommended the use of composite geomaterial rather than tyre chips alone as lightweight fill in road construction to prevent excessive pavement deflections and internal self-heating. The use of this novel composite material can also help to address the compressibility of softer foundations, liquefaction resistance, seismic isolation and the problems associated with shear failure. The technique may also contribute to the cleaning and saving environment. The decreased shear strength and liquefaction resistance for the added tyre crumbs or granulated rubber in sand could be an indication that tyre rubber particles of 5 mm diameter and smaller may not be suitable for soil reinforcement.

2.4 Effect of using tyre rubber on the environment

Various field studies were performed to evaluate the possible impact of civil engineering application of tyre shreds/chips on water quality. Few of them considered also the analysis of organic compounds and aquatic life. The quality of water leached from tyre shreds/chips layers was compared with the various United States standards for primary and secondary drinking water such as IDEM (Indiana Department of Environmental Management), EPA (Environmental Protection Agency), RAL (Regulatory Allowable Limit). It should be noted that all tyre shreds/chips used in these project trials contained steel belts.

Limited field studies were conducted to monitor the water quality effect of shreds/chips placed above ground water table mainly from the road project field

trials (Bosscher et al., 1993; Eldin & Senouci, 1992; Humphrey & Kartz, 2000; Hoppe 1998; Salgado et al., 2003; Brophy & Graney, 2004; Yoon et al., 2005). Water samples were collected directly from tyre shred/tyre chips or in the adjacent wells. For the water released directly from shreds/chips layers only the level of iron and manganese surpassed the secondary drinking water standards while other metal concentrations were well below the standards. It is further reported that the increase of the metal concentration does not exceed the primary drinking water standards. It is also reported that for water samples collected in wells located at a distance from tyre shred/chips layer, iron and manganese levels are about the same as in control levels. For other chemical concentrations no indication of tyre shreds/chips to affect the natural background levels.

Few studies analysed the water quality from the buried tyre shreds placed below ground water table (Twin City Testing, 1990; Humphrey & Kartz, 2001; Hoppe & Oman, 2013). It was reported that the metal released from tyre shreds does not exceed the limits specified by the primary drinking water standards. It was noticed that for water samples collected directly from tyre shreds the concentration of manganese, iron and zinc exceed the secondary drinking water standards. The concentration of these metals decreased for the leachate collected from wells installed at a distance from buried tyre shreds. Other chemicals showed no evidence of compromising the secondary drinking water standards.

Volatiles and semi-volatile organisms as well as aquatic toxicity were monitored in some of the above mentioned field trials. Regardless of where leachate water samples were collected, it was reported that tyre shreds/chips placed either above or below ground water table have a negligible increase of organic compound and do not affect the aquatic life.

A single road section trial was constructed in Europe (Sweden) considering tyre shreds layer (Edeskär & Westeberg, 2006). For the environmental point of view, the collected leaches from construction were analysed for the presence of metals, organic compound and other pollutants and compared with standard specified by Swedish Environmental Protection Agency. The authors reported that metals mainly zinc and organic compounds, PAH and phenols leached from the construction but their concentrations were minor. It was concluded that considering the low concentrations and dilution effects, tyre shreds used in construction have negligible effect on the surroundings.

3 Material investigated

3.1 Sands

Three types of clean sands S2, S3 and a mixture of the two named sand S4 (50%S2 + 50%S3) were selected for the present study. These are river sands collected from Bobenheim-Roxheim in Rheinland-Palatinate in Germany. Their particle size distribution through dry sieving is presented in Figure 3. They are classified as poorly graded uniform medium sand, uniform coarse sand and non-uniform sand, respectively. Properties are summarized in Table 1 and include particle density ρ_s , mean grain size d_{50} , uniformity coefficient C_u , coefficient of curvature C_c , coefficient of permeability k , minimum and maximum dry densities and the corresponding void ratios, $\rho_{d,\min}$, $\rho_{d,\max}$, and $e_{,\min}$ and e_{\max} , optimum water content, w_{opt} .

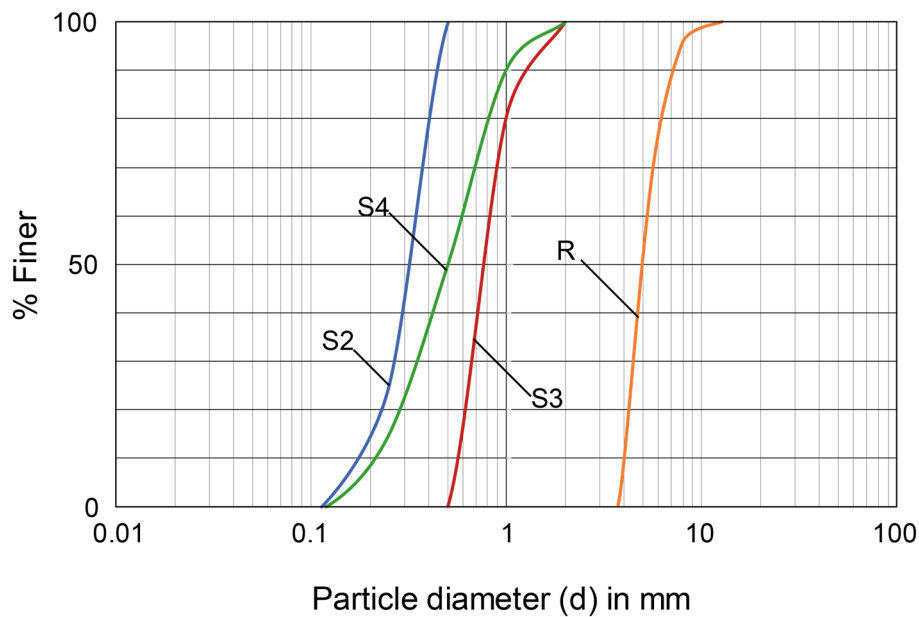


Figure 3: Particle size distribution of sands and rubber chips

Table 1: Properties of the sands used

Description	S2	S3	S4
ρ_s [g/cm ³]	2.65	2.65	2.65
d_{50} [mm]	0.32	0.77	0.5
C_u [-]	1.7	1.5	2.7
C_c [-]	1	0.9	1
$\rho_{d,\max}$ [g/cm ³]	1.591	1.663	1.798

$\rho_{d,\min}$ [g/cm ³]	1.388	1.466	1.466
e_{\min} [-]	0.665	0.594	0.474
e_{\max} [-]	0.909	0.807	0.807
$\rho_{d,\text{pr}}$ [g/cm ³]	1.579	1.575	1.685
w_{opt} [%]	15.9	10	13.3
k [m/s]	3.8×10^{-5}	4.5×10^{-5}	1.4×10^{-5}

3.2 Waste tyre rubber chips

Tyre particles have been obtained from a tyre recycling company Kurz Karkassenhandel GmbH. Tyre cutting process involves primary shredding where by 12 cm long shreds free of steel belts and fibres are produced. These pieces enter in a secondary shredding phase named milling which has two parts. The first milling phase uses the milling machine that shreds the material from primary shredding process to 40 to 0.8 mm long chips. The second milling phase involves grounding these rubber particles to smaller than 1 mm. The material from this stage is sieved to ensure that all rubber particles produced are finer than 1 mm, after which the larger return to the last milling machine for further grounding. Tyre particles from primary shredding process were collected. Their chemical composition as provided by manufacturer include carbon black of 25-40%, polymer content >40%, natural rubber content 10-35%, acetone extract 10-20%, ignition residue <10%, free metal content <0.1%, free fiber content < 0.5%. Other data include particle density between 1 and 1.1 g/cm³, bulk density in the range of 0.250 to 0.55g/cm³, moisture content < 1%.

In the laboratory, the long tyre pieces were first manually sorted out. The rest was dry sieved and the rubber size in the range of 4 to 14mm remained. In this study, tyre particles are described as rubber chips R with their sieve results shown in Figure 3. The median grain diameter of the chips d_{50} is 5 mm. Water absorption capacity of the chips was evaluated. Rubber chips have been immersed in water for 24 hours and water absorption capacity w_{ac} was determined as follows:

$$w_{ac} = \frac{M_w - M_R}{M_R} \quad (8)$$

where M_w : is the mass of rubber chips, M_R is the dry mass of rubber chips.

After several trials, the results showed that the water absorption capacity of the rubber chips averages to 2.8%. This value is within the range reported in the literature. It was concluded that there is no correlation between tyre chips size and water absorption capacity.

The particle density of rubber chips was determined. The weighed material was poured into the graduated cylindrical tube filled with water up to a certain level. ASTM D 6270-2020 provides guidelines for the use of waste tyres but due to the low specific weight of rubber, the procedure may yield unreliable results. The displaced volume of water is measured by taking into account the absorption capacity of rubber chips, and the particle density ρ_R is determined. Several attempts were performed to evaluate ρ_R and an average value of 1.05 g/cm³ was obtained. This value is within the range of 1 to 1.10 reported in literature.

$$\rho_R = \frac{M_R}{V_{dw} + V_{aw}} \quad (9)$$

where M_R is the mass of dry rubber (g), V_{dw} the volume of the displaced water (cm³) and V_{aw} the volume of absorbed water (cm³).

Hardness of rubber chips was determined using Shore durometer scale (Shore A). The results from the tested 15 smoothed surface rubber pieces showed a hardness value in the range of 64 to 67 with an average value of 66. The range of hardness values indicates that the rubber chips used are of the same hardness and can be classified according to hardness scale as medium hard material.

3.3 Sand rubber chips mixtures

To produce the mixtures, the three types of sand S2, S3 and S4 mentioned above were separately dry mixed with rubber chips. The mixtures were prepared in dependence of rubber chips content χ in percentage by dry mass. The contents used were 0/10/20/30/100%. The mixture formed were named medium sand rubber chips mixture S2RM, coarse sand rubber chips mixture S3RM and sand mixture rubber chips mixture S4RM. An example of the mixture is shown in Figure 4. The segregation of the individual particles was likely to occur for dry mixture with chips content beyond 20%. To prevent this problem, the appropriate mitigation measures were applied. Furthermore, the ratio of d_{50R}/d_{50S} was calculated for the mixtures. Values of 15.6, 10 and 6.5 were obtained for S2RM,

S4RM and S3RM, respectively. The particle density of the composite material, $\rho_{s,SRM}$ was calculated using equation (10).

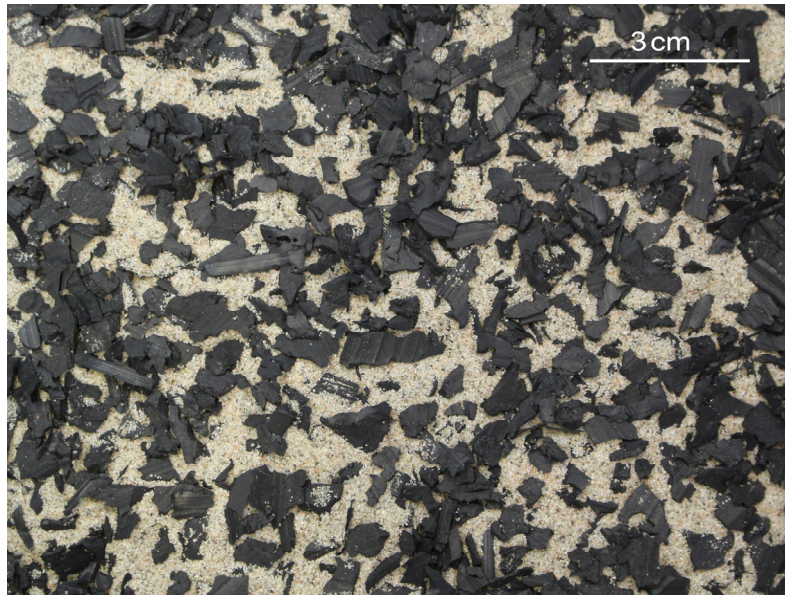


Figure 4: Sand S2 mixed with rubber chips at 20% by dry mass

$$\rho_{s,SRM} = \frac{1}{\frac{\chi}{\rho_{s,R}} + \frac{(1-\chi)}{\rho_{s,S}}} \quad (10)$$

where $\rho_{s,S}$ is the particle density of sand, χ the rubber chips content and $\rho_{s,R}$ is the particle density of rubber chips.

3.3.1 Densities

- Proctor test

Proctor tests were performed to evaluate the effect of rubber chips on the optimal density of sand. Standard proctor methods described in detail in DIN 18127 were adopted to evaluate the compaction characteristics of the composite material. These methods involve the use of a compaction mould having 100 mm diameter, 120 mm height and a 2.5 kg compaction hammer. The choice of the methods was based on the fact that the material tested have particle size smaller than 19 mm. The compaction characteristics could not be affected by the effort and the mould used because of the energy damping capacity of rubber chips (Edil & Bosscher, 1994). The maximum dry density and the optimum water content from these tests

can be used during the placement and compaction of fills for geotechnical engineering projects.

The Proctor density and the corresponding water content are provided in Table 1. Sands S2 and S3 exhibited almost similar maximum dry density but at different optimum water content. Sand S4, a mixture of the two, has higher dry density at an optimum water content between S2 and S3. Figure 5 presents the selected results for sand S2RM. It is inferred in the figure that increasing rubber chips content decreases the density and water content of the mixtures. Additional rubber chips in the mixture reduces the curve peaking effect. Density vs. moisture content relationship for the mixtures formed by sands S3 and S4, exhibited the same behaviour (not shown herein).

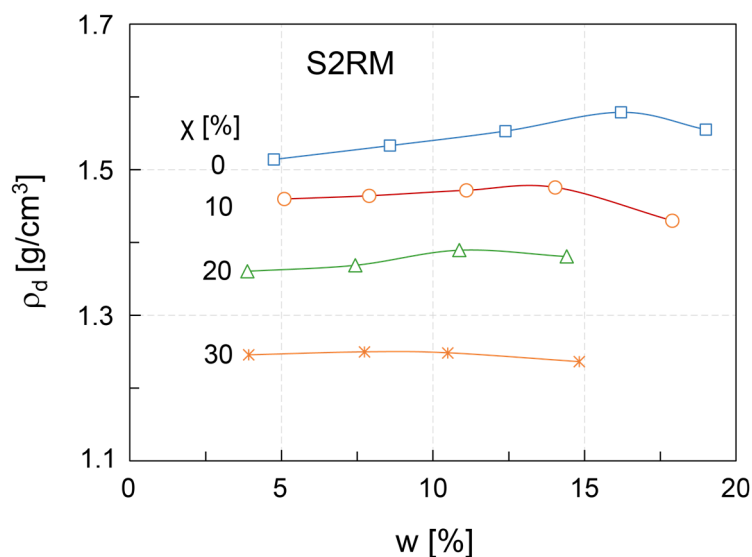


Figure 5: Density-moisture content relationship for S2RM mixtures.

Figure 6 presents the data comparing the results for S2RM, S3RM and S4RM. The influence of rubber chips on the maximum dry density and optimum water content is pronounced. It is clear from figure that increasing rubber chips in sand decreases drastically the maximum dry density of the mixtures. This is due to the inclusion of the lightweight rubber material in sand. It is also clear that the rubber chips content influences the optimum water content. Increasing the rubber content decreases the optimum water content. S2RM requires a large amount of water content to ease move grains into a denser state (stronger soil structure). This amount is reduced for the increased sand grain size. Consequently, S3RM results in smaller optimum water content compared to S4RM and S2RM. Due to

their low capacity to absorb water, rubber chips were found to decrease the optimum water content of the mixtures.

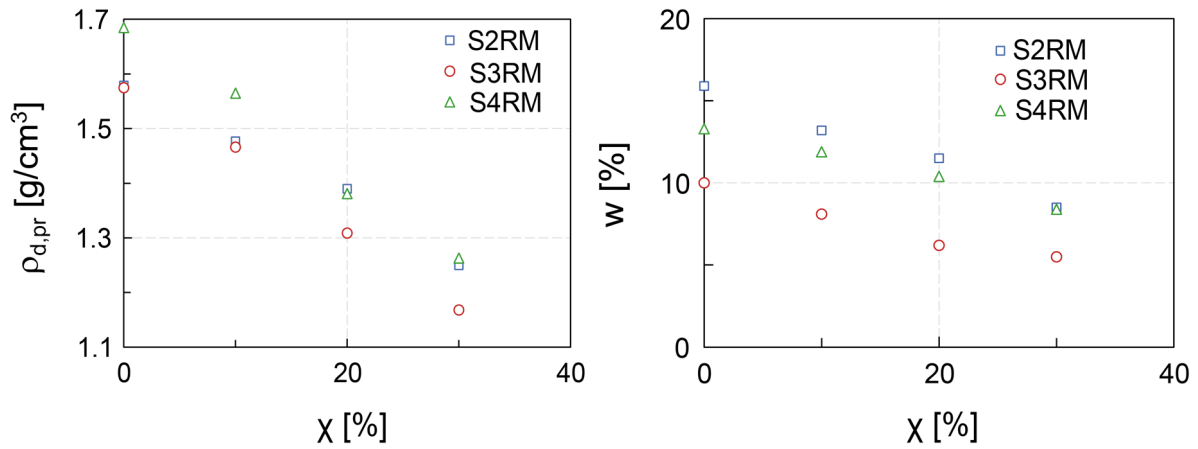


Figure 6: (a) Maximum Proctor dry density and (b) optimum water content for different sand rubber mixtures

- Minimum and maximum dry density tests

Controlled vibration tests were performed to determine the maximum and minimum dry densities of the granular soil. These tests were conducted in this study to evaluate these quantities for sand rubber chips mixtures. A 7.1 cm diameter and 11.22 cm high mould was used to determine the minimum densities, while 9.92 cm diameter and 11.1cm high mould was used for the maximum densities. The details of the devices used and testing procedure are fully described in DIN 18127-100X. The minimum and maximum dry densities $\rho_{dmin,SRM}$ and $\rho_{dmax,SRM}$ are determined in the tests.

Typical results are presented in Figure 7 and Table 2: Minimum and maximum dry densities for sand rubber mixtures. The maximum dry density value of 1.588, 1.663 and 1.798g/cm³ was achieved for pure S2, S3 and S4. It can be observed in the figure that increasing the rubber chips decreased both maximum and minimum dry densities for S2RM, S3RM and S4RM mixtures. Sand S2 exhibits a better interaction with rubber chips compared to other two sand types. The lower value of the minimum dry density was obtained for pure S2 while S3 and S4 exhibit almost the same value. Adding chips in all sands reduces the minimum dry density of the mixtures. A strong degradation can be observed for S3RM.

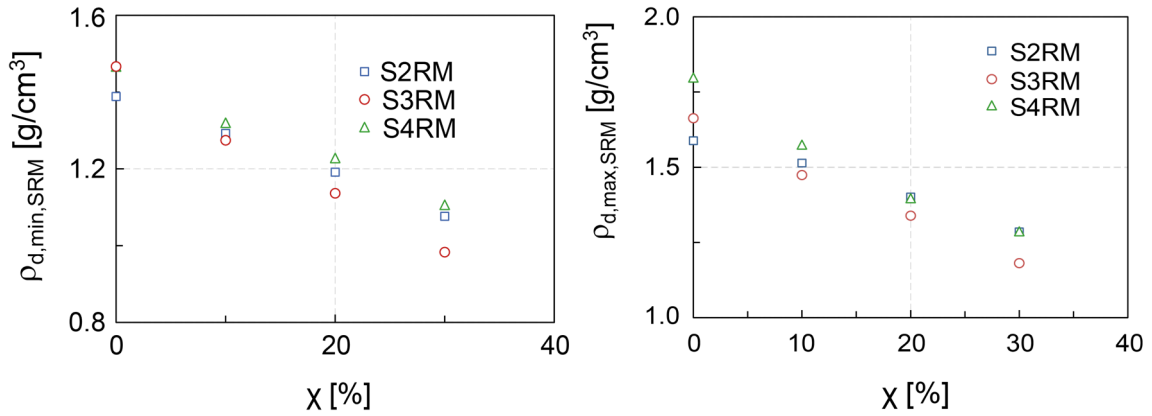


Figure 7: Minimum and maximum dry densities for sand rubber chips mixtures

Table 2: Minimum and maximum dry densities for sand rubber mixtures

	S2RM		S3RM		S4RM	
χ	$\rho_{d,min}$	$\rho_{d,max}$	$\rho_{d,min}$	$\rho_{d,max}$	$\rho_{d,min}$	$\rho_{d,max}$
%	g/cm ³	g/cm ³	g/cm ³	g/cm ³	g/cm ³	g/cm ³
0	1.388	1.588	1.466	1.663	1.466	1.798
10	1.292	1.514	1.274	1.474	1.32	1.575
20	1.191	1.401	1.136	1.339	1.228	1.397
30	1.076	1.285	0.983	1.181	1.106	1.287

3.3.2 Permeability

The material suggested to serve as road fill, backfill behind retaining walls or bridge abutment fill should be evaluated for its permeability. In this regard, a series of laboratory tests were performed to analyse the hydraulic conductivity of sand rubber chip mixtures. Standard proctor was performed prior to the specimen retrieval. However, a sample size of 10 cm diameter and 12 cm high on each type of mixture was produced and sealed in a latex membrane, fixed on the base of the equipment and enveloped in the permeameter cell. A constant head laboratory permeability equipment was used. Instead of gravity water falling, a constant pressure of about 36 kPa was used to press water through the specimen. The test was performed under a confining stress of 50 kPa. The full description of the laboratory equipment, sample preparation and testing procedure can be found in DIN EN ISO 17892-11.

The dependence of the permeability on rubber chips is presented in Figure 8. These data indicate the lower coefficient of permeability for sand S4 compared to sands S2 and S3. This is evidenced by the grain size distribution of the

material, density and the associated void spaces for each sand type. Initially adding 10% rubber chips in sand S2 reduces its hydraulic conductivity. Further increase yields an increased permeability coefficient. For S3RM and S4RM, increasing rubber chips definitely increases the hydraulic conductivity.

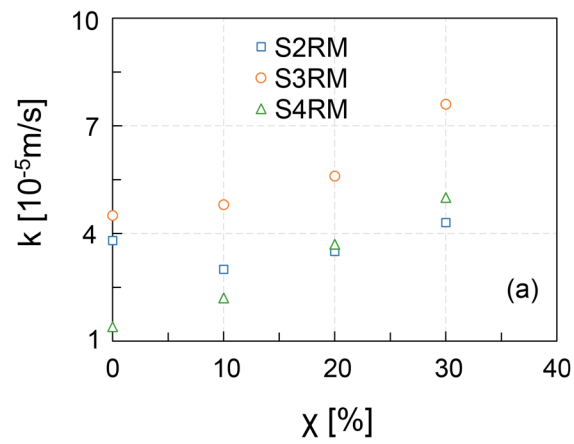


Figure 8: (a) Permeability vs. rubber content for different sand rubber mixtures

4 Static tests

4.1 Oedometer tests

The compressibility of any construction material is a key parameter to be considered in the design and construction of earth structures. The proposed composite material for this study, i.e. sand rubber chip mixtures, was subjected to loading-unloading-reloading cycles to evaluate its behaviour under compression. A series of tests were performed using standard oedometer equipment on a ring of 100 mm and 20 mm diameter and height respectively. The tests were carried out in accordance with DIN EN ISO 17892-5. The parameters from these tests can be used to estimate the settlement of fills during the service life of the structure.

As mentioned earlier, segregation of the individual particles was likely to occur during dry sample preparation. To mitigate this problem, the calculated sand and rubber chips amount forming each layer was measured separately. The materials were mixed and placed in the oedometer ring in two layers and compacted to achieve the desired density. This method ensured that each layer contains the same amount of rubber chips. Pure sand and pure rubber chips were first subjected to loading-unloading-reloading cycles. Their mixture with 10/20/30% chips contents by dry mass followed. The specimens were subjected to vertical stresses varying from 50 to 300 kPa. Stress was doubled for each increment up to 200 kPa. In the last stage, an increment of 100 kPa was applied.

The vertical strain ε (%) resulted from the compression tests is affected by the vertical stress, σ'_v (kPa) and the chips content χ (%). The compression of pure dry sands S2, S3 and S4 under a vertical stress of 300kPa yielded vertical strains of 2.17%, 2.73% and 1.42%, respectively. These specimens were prepared at a relative density I_D of 65.6%. Pure rubber chips under the same vertical stress yield a vertical strain of about 39% at stress 300kPa. The typical results obtained from various mixtures are presented from Figure 9 to Figure 11. The data plotted in Figure 9 for S2RM show that at any stress level, as expected the vertical strain increases with increasing vertical stress and rubber chips content. It can also be seen that major compression takes place in the first loading cycle, a portion of which is irrecoverable but with significant rebound upon unloading. The subsequent loading cycles follow the same trend but with small rebound

compared with the first loading cycle. The evolution of the vertical strain for S3RM and S4RM mixtures (not shown here) follows the same trend.

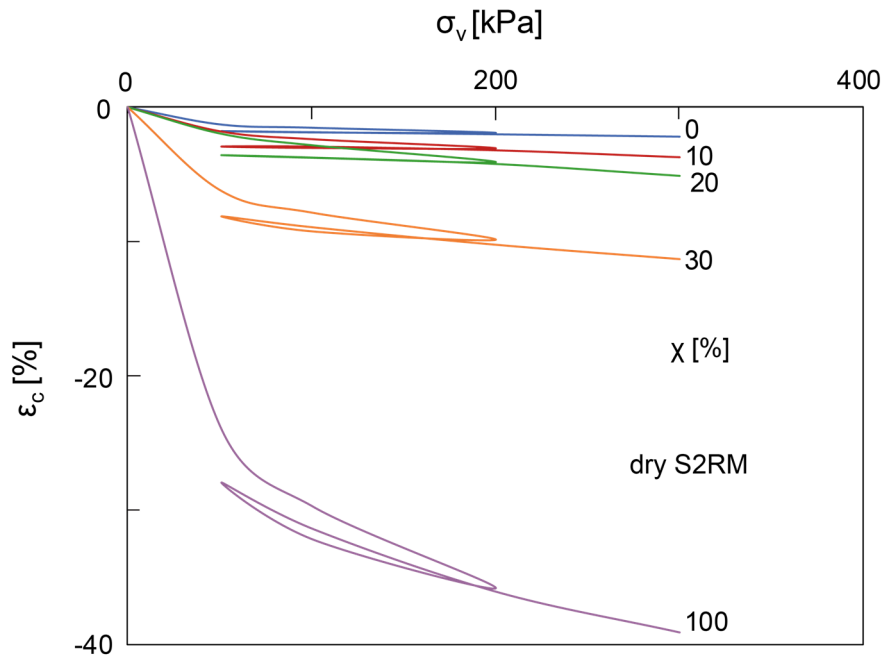


Figure 9: Stress-strain data for (a) dry S2RM mixtures

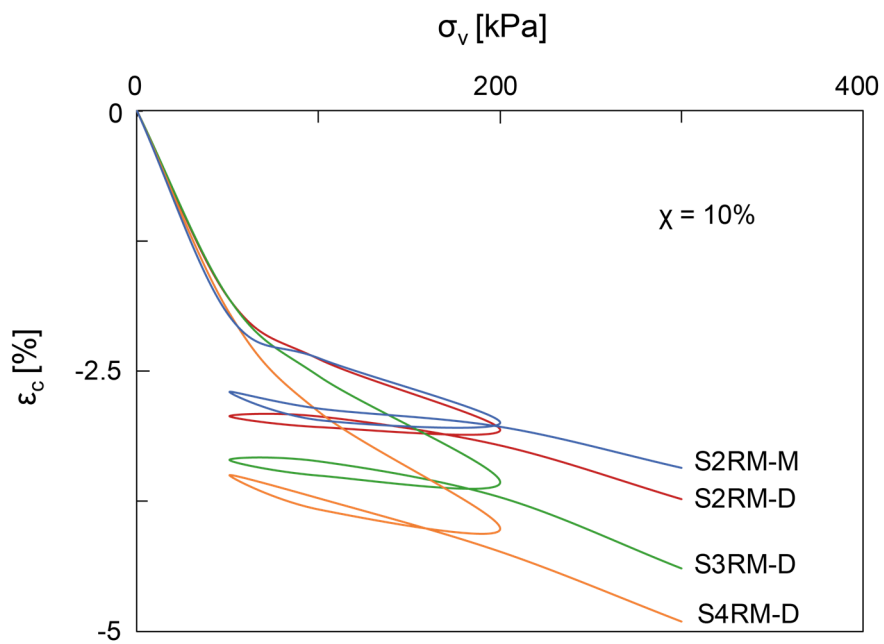


Figure 10: Stress-strain data from three types of sand mixed with rubber chips at 10%

S2RM-D is the dry medium sand rubber chips mixture; S2RM-M the moist medium sand rubber mixture; S3RM-D the dry coarse sand rubber chips mixture; S4RM-D the dry sand mixture rubber chips mixture.

A comparison of the stress-strain curves for different mixture types at 10% chips content is displayed in Figure 10. These data indicate almost similar compression behaviour for both dry and moist S2RM. Dry S2RM yields smaller vertical strains whereby the S4RM yields the higher one. At 20% and 30% chips contents S2RM still develop smaller strains under a vertical stress of 300 kPa while S3RM yields larger ones. Note that all mixtures at $\chi = 10, 20$ and 30% were prepared at relative densities of 83.4%, 88.6% and 97.4% respectively. The increase of the vertical strains can be attributed to the compression of the void space in the mixtures and the compressibility of the individual chips. These results suggest that there is a better interaction between sand S2 and rubber chips compared to that in sands S3 and S4. A stress dependent relationship suggested in equation (10) can be used to estimate the compression strain.

$$\varepsilon_c[\%] = a_1(\sigma'_v / P_a)^{0.3} \quad (10)$$

$$a_1 = a_2 \cdot \chi^2 + a_3 \cdot \chi + 1.056 \quad (11)$$

where χ is rubber chips content in percentage.

Table 3: Constants for equation (11)

Mixture	a_2	a_3
S2RM	0.0012	0.158
S3RM	-0.0005	0.325
S4RM	0.0002	0.259

The constrained modulus E_s was determined from the tests and the values obtained for example for S2RM and S3RM are plotted against the normal stress in Figure 11. As expected, increasing the vertical stress increases the constrained modulus. Furthermore increasing the rubber chips content reduces the modulus of the composite material.

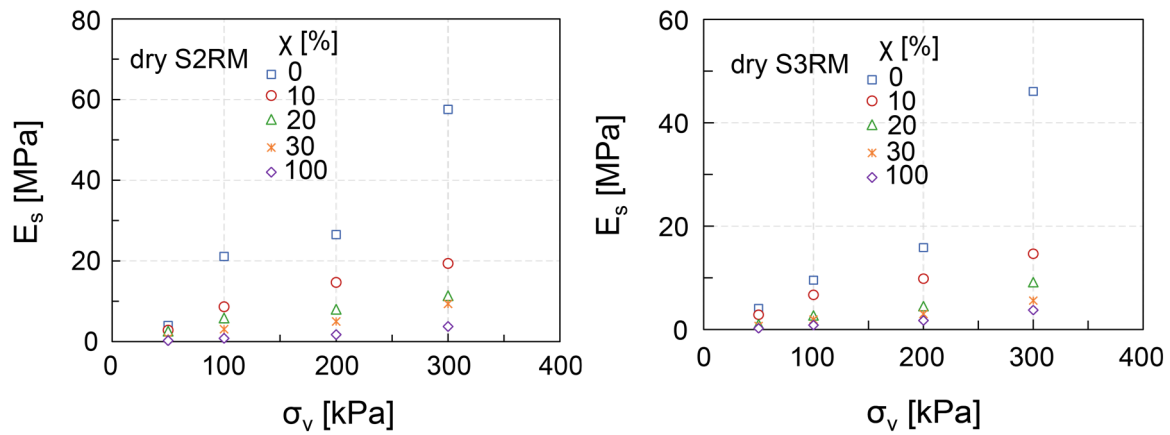


Figure 11: Constrained modulus vs normal stress for S2RC and S3RM

4.2 Direct shear tests

4.2.1 Equipment and testing procedure

Direct shear tests constitute a convenient laboratory method for measuring the shear strength of soils. This method was used to evaluate the shear strength of sand tuber chips mixtures. The rubber particle size used exceeded the limit of one tenth of the specimen diameter for standard direct shear box as specified in DIN EN ISO 17892-5. However, a direct shear device with box 300 x 300mm was utilized. The equipment was manufactured and supplied by InfraTest and has been upgraded. This device has a vertical loading unity capable to apply a force of up to 50 kN. The shear box is horizontally divided into two halves boxes assembled accurately together by alignment screws passed vertically through the walls of the top half and screwed into the bottom. The assembled box is placed in the rectangular brass container prior to sample preparation.

Sample preparation followed the procedures described in DIN EN ISO 17892-5. The weight of sand rubber mixtures was determined in dependence of the rubber chips contents by dry weight. Dry mixtures were prepared and significant particle segregation was only noticed for the mixtures with rubber content beyond 20%. To avoid this problem, a total mass of material was divided into equal three portions and the quantity of sand and rubber chips was calculated separately for each portion. The materials were then mixed and placed into the box and compacted until the target dry density was achieved. The dry density in the direct shear tests corresponds to the value of standard proctor curve at 5% water content

and the calculated relative density was for S2RM was applied to S3RM and S4RM.

Particular attention was paid to avoid shearing between layers. It was ensured that the second compacted layer covers and extends an equal portion beyond the top and bottom of the shear plane. A variable gravimetric rubber content by dry mass $\chi = 0/10/20/30/100\%$ was used. After sample preparation a rectangular brass container was pushed in the rigid frame and the top half of the box was tightly connected and prevented from moving laterally so that when the horizontal force is applied on the carriage the bottom half of the shear box can move. The direct shear test set up is shown in Figure 12. Samples were prepared under dry conditions and their properties are given in Table 4



Figure 12: Direct shear test set up

Table 4: Properties of the tested material, normal stresses and test number

Soil	χ [%]	ρ_d [g/cm ³]	I_D [-]	σ_n [kPa]	Test No.
S2	0	1.515	0.65	50	DS01
				100	DS02
				200	DS03
	10	1.480	0.86	50	DS04

				100	DS05		
				200	DS06		
	20	1.374	0.88	50	DS07		
				100	DS08		
				200	DS09		
	30	1.281	0.98	50	DS10		
				100	DS11		
				200	DS12		
S3	0	1.591	0.65	50	DS13		
					100	DS14	
					200	DS15	
	10	1.437	0.83		50	DS16	
						100	DS17
						200	DS18
	20	1.312	0.88		50	DS19	
						100	DS20
						200	DS21
	30	1.175	0.97		50	DS22	
						100	DS23
						200	DS24
S4	0	1.669	0.65	50	DS25		
					100	DS26	
					200	DS27	
	10	1.532	0.85		50	DS28	
						100	DS29
						200	DS30
	20	1.377	0.89		50	DS31	
						100	DS32
						200	DS33
	30	1.273	0.93		50	DS34	
						100	DS35
						200	DS36
R	100	0.64	-	50	DS37		
					100	DS38	
					200	DS39	

Direct shear tests were performed according to DIN EN ISO 17892-5. Three similar specimens were prepared for each type of mixture and tested under three normal stresses of 50, 100 and 200 kPa. Specimens were sheared under a strain rate of 0.1mm/min as specified later for triaxial tests. Note that the equipment applies a maximum horizontal displacement of 50 mm. During testing, the shear force and horizontal deformation were recorded prior to computing the shear stress τ and shear strain γ . Sand rubber chips mixtures mobilize higher strengths at larger shear deformations. Some tests showed even strain hardening behaviour with no explicit peak. However, the stress at failure was taken to correspond to peak shear stress or maximum value at 15% shear strain whichever comes the first.

4.2.2 Results

Selected results are presented in form of stress strain and volumetric strain curves from Figure 13 to Figure 15 for sands S2RM and S3RM at a normal stress of 100kPa.

Figure 13 plots the shear stress vs. shear strain and volumetric strain vs. shear strain curves for sand S2 at $\chi = 10\%$ under different normal stresses. As usual, increasing normal stress increases the shear stress in the composite material. It can also be observed that increasing normal stress increases the contraction and decreases the dilative behaviour. The same trend was observed for S2 at $\chi = 0, 20, 30\%$ and all the mixtures formed by sands S3 and S4. An exception was observed for pure sand S2 at 50 kPa that yielded lower dilation and higher contraction compared to the ones at 100 kPa. This might be caused by the applied compaction from which a medium dense specimen was achieved that yielded a higher contraction during shearing.

The influence of rubber chips content on shear strength of sand was investigated. It has been observed from the results that increasing chips contents in the mixtures increases the shear strength of all types of sand for the range of normal stressed investigated. Figure 14 plots the typical examples of shear strength vs. shear strain curves for S2RM and S3RM at a normal stress of 100 kPa. An exception was observed for sand S3 at normal stress of 200 kPa not shown herein whereby the increased chips content decreased the shear strength. It can also be seen in the plot that the shear strain at failure increases with increasing rubber chips content. This may result from the increased ductility of the composite

material and the tensional stress developed within the individual chip in the region of shear plane. It can also be noted that the increase of shear strength could be attributed to the reinforcement mechanism that occurred within the shear plane whereby individual chips develop the tensile resistance. The dilatancy behaviour plotted in Figure 15 shows that increasing chips content increases the contraction and decreases the dilation.

By adopting a Mohr-Coulomb failure criterion as shown in Figure 16 the internal angle of friction and cohesion at peak or maximum stress are obtained as compiled in Table 5. Increasing the chips content in the mixtures increases the cohesion in all types of sands. A marginal increase of the internal friction angle ϕ was observed for sand S2 at 10% chips content that decreased for more added rubber chips. For sands S3 and S4 the increased chips content increased the cohesion and reduced the internal angle of friction. The shear strength of sand is increased by adding rubber chips. The shear parameters for pure rubber chips are $c = 7.9 \text{ kPa}$ and $\phi = 25.2^\circ$. With reference to the test data obtained from small direct shear box on pure sand S2, the results generated from large direct shear box tests are conservative.

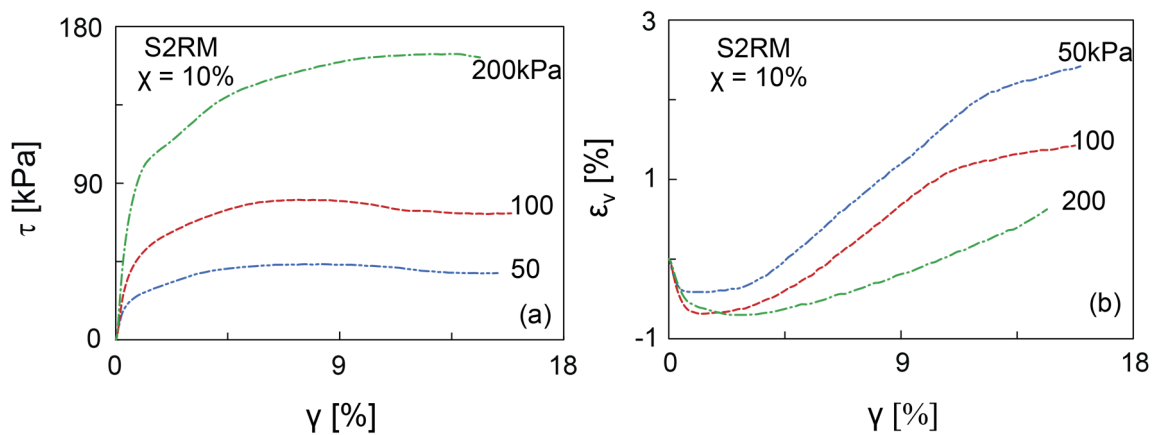


Figure 13: a) Shear stress vs. shear strain and (b) vertical strain vs. shear strain for sand S2 at 10% chip content at $\sigma_n = 50/100/200 \text{ kPa}$

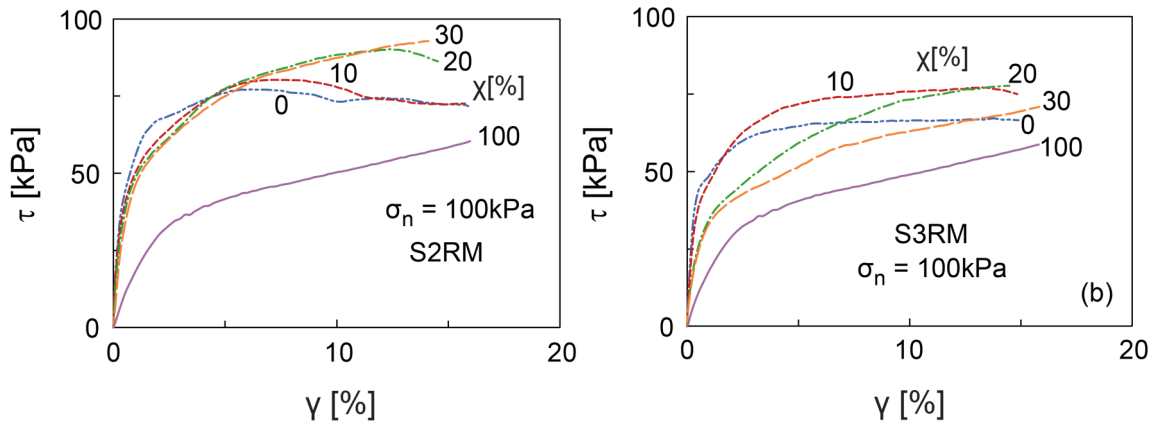


Figure 14: Shear stress vs. shear strain for (a) sand S2RM and (b) sand S3RM at various chips contents; $\sigma_n = 100$ kPa

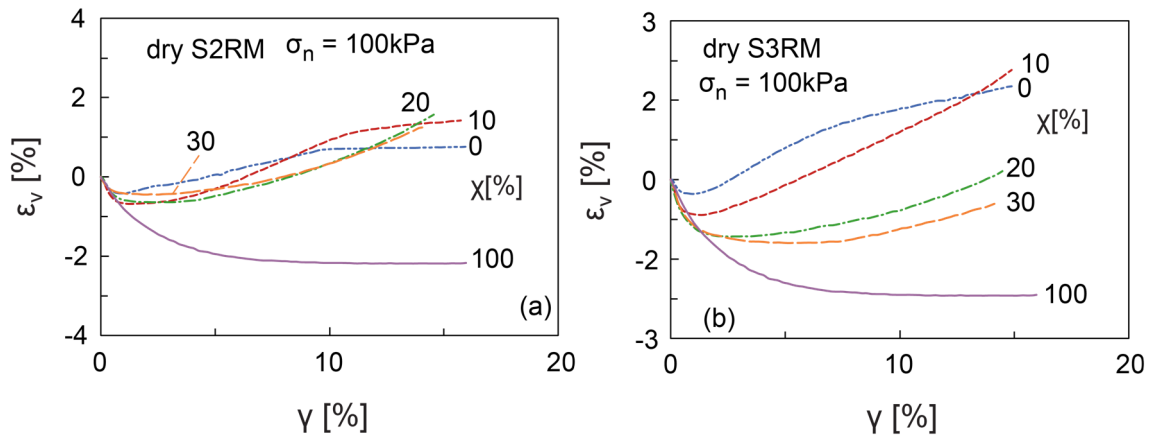


Figure 15: Vertical strain vs. shear strain for (a) sand S2RM and (b) sand S3RM at $\chi = 0/10/20/30/100\%$, $\sigma_n = 100$ kPa

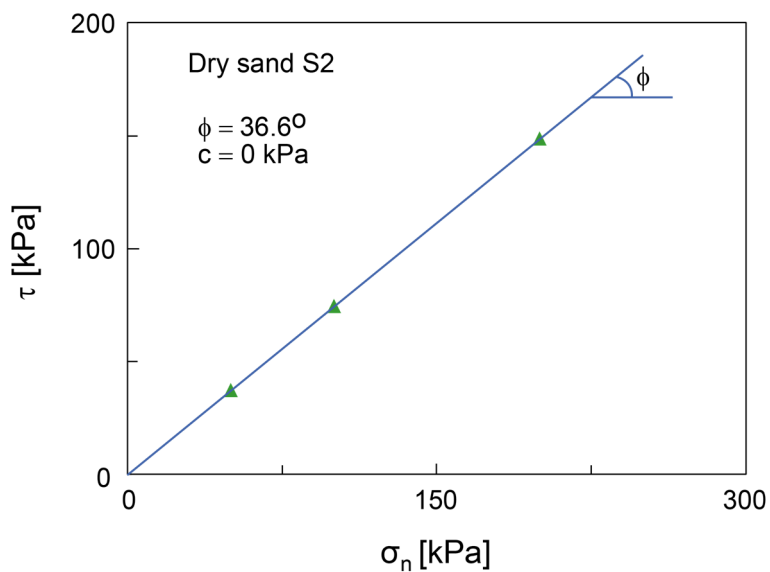


Figure 16: Normal stress vs. shear stress for pure dry sand S2

Table 5: Shear strength parameters for dry mixtures

Mixtures	dry S2RM		dry S3RM		dry S4RM	
	c [kPa]	φ [°]	c [kPa]	φ [°]	c [kPa]	φ [°]
0	0	36.6	0	38.2	0	38.6
10	1.6	39	4.8	35	4.4	37.6
20	7.8	37.8	9.2	33.2	14.9	34.1
30	14	37.1	9.3	30.8	15.8	33.8

4.3 Triaxial tests

4.3.1 Equipment and testing procedure

The dynamic cyclic triaxial testing system was used to perform both static and cyclic triaxial tests. The system with the commercial name ELDYN was manufactured and supplied by GDS and is shown in Figure 17. It comprises a velocity-controlled load frame capable to apply an axial load of up 10 kN at a frequency of up to 10 Hz through a servo-controlled actuator. A static load at a constant rate or cyclic load can be applied to the specimen through an axial movement. The axial load is measured by an internal submersible load cell while the induced deformation by high accuracy external linear displacement transducer (strain gauge). The triaxial cell can accommodate a cell pressure up to 2 MPa. The drainage ports are on the top cap and the base pedestal. Pore pressure in the specimen can be measured at the top and the bottom. The confining stress is applied by a pneumatic cell pressure controller.

For saturation, a 2 MPa back pressure/volume controller is used. It also measures the change in volume of the sample during saturation, consolidation, static triaxial compression and subsequent cyclic loading stages. The entire system is controlled by a GDS dynamic controller which provides a 4-channel dynamic data logger with 16 bits from which various transducers are connected. The system is shown.

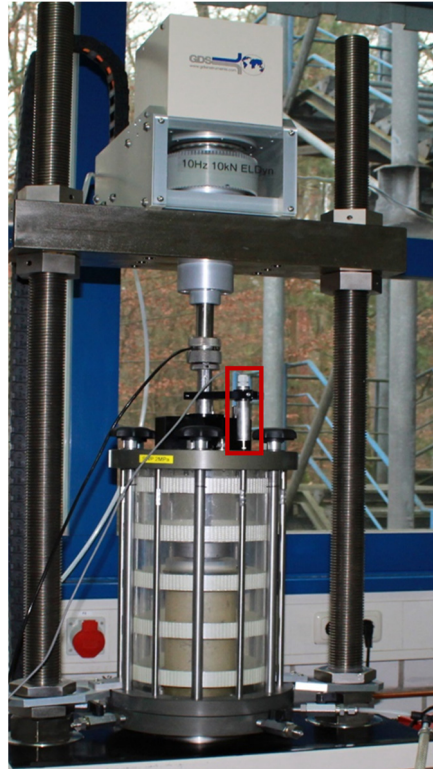


Figure 17: Dynamic triaxial device and

Prior to the sample preparation, the two halves metal split mould were first assembled together. Then the latex membrane was placed to cover the inner surface of the wall. The assembled mould with the porous plate at the bottom was placed on the rigid platen pedestal. To ensure the clinging of the latex membrane to the wall of the mould, a vacuum pressure was applied between them. The specimens were 100 mm in diameter and 150 mm in height. The selection of a large diameter was dictated by the rubber chip size. It is stated in ASTM 3999-2003 that the maximum particle size should not exceed 1/6 of the specimen's diameter. In this study the maximum particle size was 14 mm.

Sample preparation followed the same procedure applied for direct shear tests with an exception of the number of layers the increased to five for the triaxial tests. The calculated weight for each layer were mixed then placed into the mould and compacted until a thickness equal to one fifth of the specimen height is obtained. For the purpose of stabilizing the sample, a small vacuum pressure of 15 kPa was applied immediately after sample preparation. For S2RM, dry densities for triaxial test corresponded to the value of the standard Proctor curve at 5% water content. The corresponding relative densities were reproduced for the S3RM and S4RM specimens.

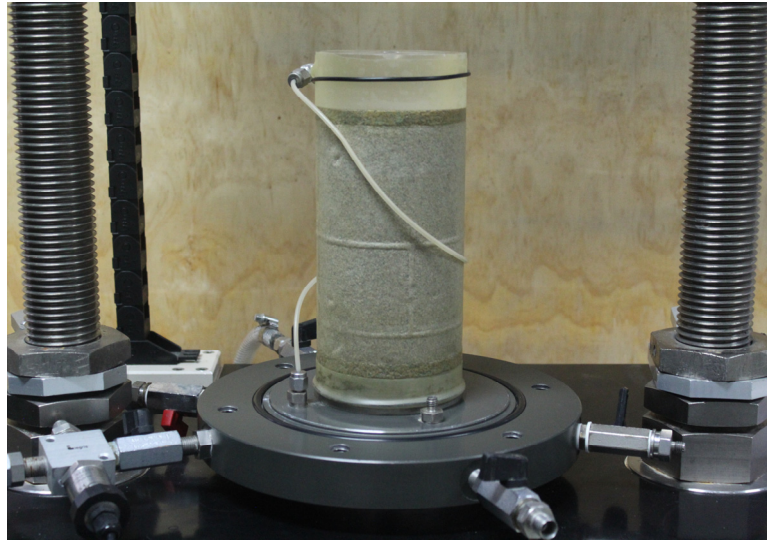


Figure 18: Specimen for medium sand S2

To account for the effect of water content on shear strength behaviour, a small water content of 5% was selected. Moist samples were produced by adding the necessary amount of water to the pre-mixed sand rubber chips. It should be pointed out that for the moist mixtures at all rubber contents used no segregation of sand-rubber grains occurred even if the sample was compacted in one portion. The procedure described above was followed for all samples.

Samples were prepared for sands S2, S3 and S4 at $\chi = 0/10/20/30/100\%$ by dry mass. Saturated samples were also prepared but only for pure medium sand (sand S2) at a relative density of 50%. Saturation procedure is fully described in Chapter 5. The properties of the tested samples are summarized in Table 6 where ρ_d is the dry density of the composite material, I_D the relative density, DD stands for dry drained test, MD for moist drained test, SU for saturated undrained test and SD for saturated drained test.

Table 6: Properties of the tested specimens, normal stresses and test number

Soil	χ [%]	ρ_d [g/cm ³]	I_D [-]	Condition	σ'_3 [kPa]	Test No.
S2	0	1.484	0.5	SU	50	ST01
					100	ST02
					200	ST03
	0	1.484	0.5	SD	50	ST04
					100	ST05

				200	ST06
0	1.515	0.65	DD	50	ST07
				100	ST08
				200	ST09
10	1.480	0.86	DD	50	ST10
				100	ST11
				200	ST12
20	1.374	0.88	DD	50	ST13
				100	ST14
				200	ST15
30	1.281	0.98	DD	50	ST16
				100	ST17
				200	ST18
0	1.514	0.65	MD	50	ST19
				100	ST20
				200	ST21
10	1.477	0.86	MD	50	ST22
				100	ST23
				200	ST24
20	1.371	0.88	MD	50	ST25
				100	ST26
				200	ST27
30	1.275	0.98	MD	50	ST28
				100	ST29
				200	ST30
0	1.444	0.31	DD	50	ST31
				100	ST32
				200	ST33
10	1.355	0.32	DD	50	ST34
				100	ST35
				200	ST36
20	1.250	0.32	DD	50	ST37
				100	ST38
				200	ST39
30	1.133	0.32	DD	50	ST40
				100	ST41

					200	ST42
S3	0	1.591	0.65	DD	50	ST43
					100	ST44
					200	ST45
					50	ST46
	10	1.437	0.83	DD	100	ST47
					200	ST48
					50	ST49
	20	1.312	0.88	DD	100	ST50
					200	ST51
					50	ST52
	30	1.175	0.97	DD	100	ST53
					200	ST54
50					ST55	
S4	0	1.669	0.65	DD	100	ST56
					200	ST57
					50	ST58
	10	1.532	0.85	DD	100	ST59
					200	ST60
					50	ST61
	20	1.377	0.89	DD	100	ST62
					200	ST63
					50	ST64
	30	1.273	0.93	DD	100	ST65
					200	ST66
					50	ST67
R	100	0.504	-	DD	100	ST68
					200	ST69
					50	ST67

Tests were performed under strain-controlled conditions according to ASTM D7181-11. Three similar specimens were prepared for dry, wet and saturated material and consolidated under three different confining stresses of 50 kPa, 100 kPa and 200 kPa. The applied vacuum pressure was slowly released immediately after the application of a confining stress of 30 kPa. A strain rate of 0.1mm/min was applied. In some tests, a strain hardening behaviour with no explicit peak was observed. Due to the elasticity of rubber chips, sand rubber chips mixtures can mobilize the maximum shear strength at higher deformation.

In this study the stress at failure was taken equal to peak deviatoric stress or maximum value at axial strain of 15% whichever comes first.

The axial deformation and the force during test were measured by high accuracy external linear displacement transducer and load cell respectively. The triaxial testing system was not able to measure the volume change of dry and moist samples (unsaturated condition). To enable the volume change measurement, a cylindrical pressure tube was introduced (Figure 17). During dilation backpressure controller compressed the pressurized water into the tube. The volume compression of the specimen was measured through the compressed water back to back pressure controller. The compressed volume of water to and from the tube was measured as dilation and contraction of the specimen by a build in pressure volume transducer. Calculations were performed following the equations given in the pertinent DIN EN ISO 17892-9.

4.3.2 Results for saturated sand

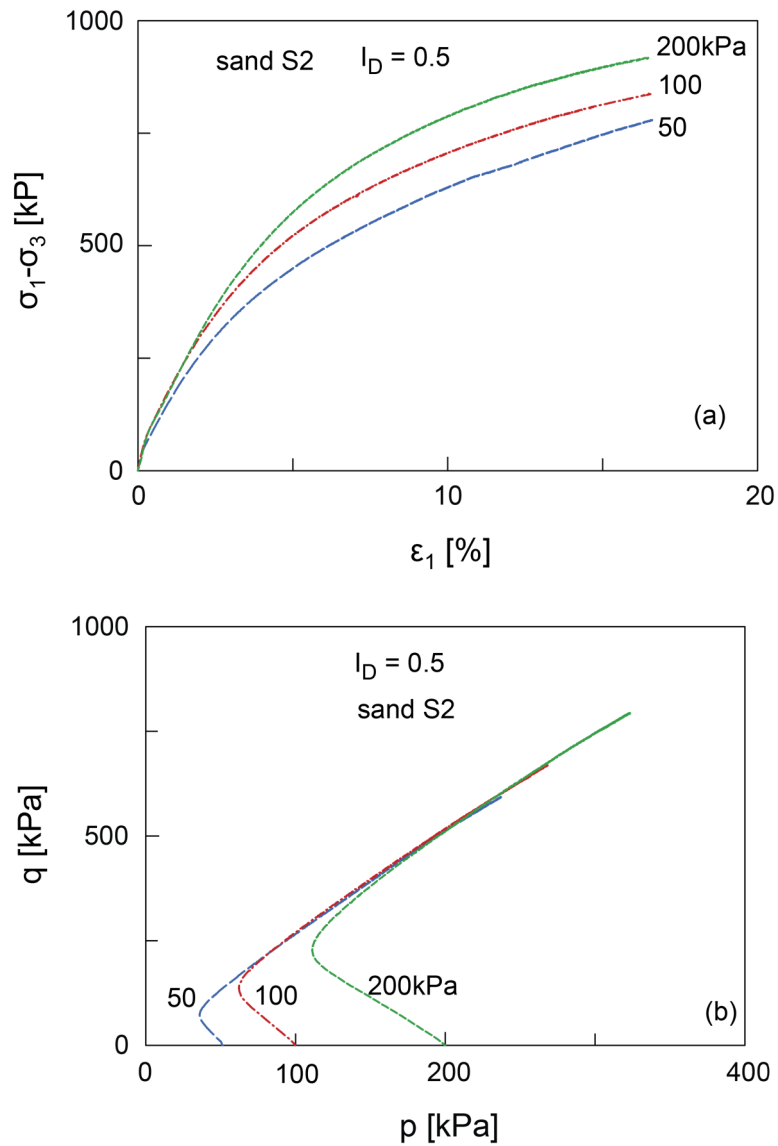
The results described herein are for undrained and drained static triaxial compression tests on saturated medium sand. These tests were performed at confining stresses of 50, 100 and 200 kPa for samples prepared at a relative density $I_D = 0.5$.

The evolution of the stress-strain, effective stress path in p - q plane and excess pore water pressure in undrained tests are presented Figure 19. As expected increasing confining stress increases the deviatoric stress and excess pore water pressure. For all confining stresses the excess pore water pressure initially increased followed by its dissipation up to zero and even below. This results in the initial decrease of the effective confining stress then increases while the deviatoric stress increases. The decrease of the excess pore water pressure could be caused by an initial contraction followed by the dilation during testing. It can also be seen in p - q plane that all curves follows the same line.

$$p = (\sigma'_1 + 2\sigma'_3) / 3; q = \sigma'_1 - \sigma'_3$$

Figure 20 displays typical results from saturated drained tests. As expected the deviatoric stress increases with increasing confining stress and the tests exhibit an initial volume contractive behaviour followed by expansion (dilation). The contraction increases with increasing confining stress while the dilation

decreases. To find shear strength parameters Mohr stress circles were first constructed by plotting principal stresses at failure against the measured shear strength. Then a failure envelope was drawn. By adopting the Mohr-Coulomb failure criterion shown in Figure 21 the internal friction angle of 32.7° and cohesion of 3.2 kPa were obtained.



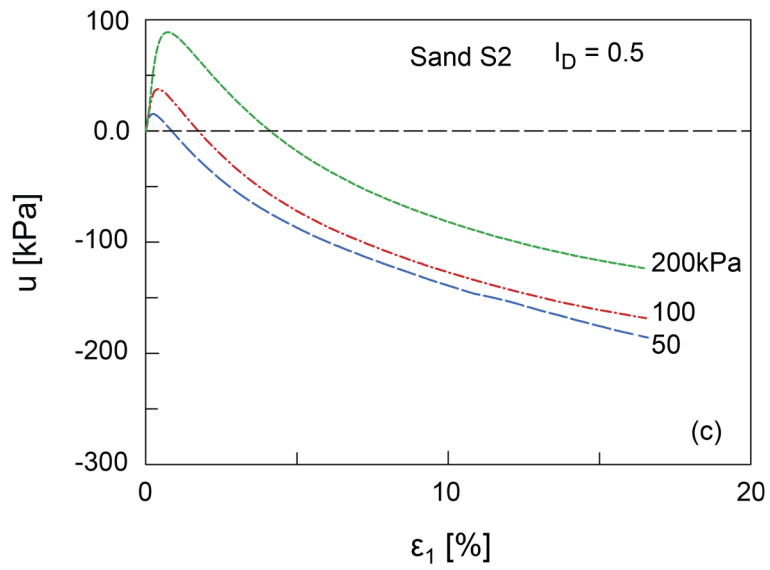
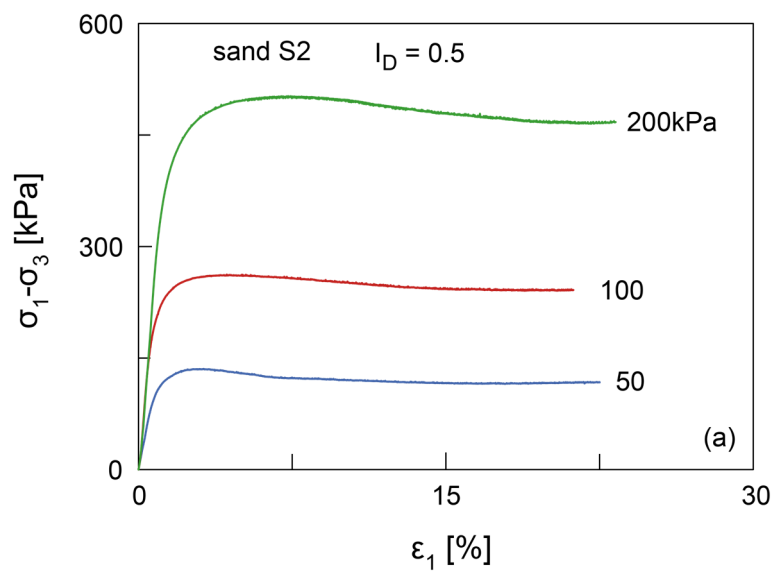


Figure 19: Undrained triaxial tests on saturated medium sand S2 (a) stress strain curves, (b) stress path and (c) excess pore water pressure.



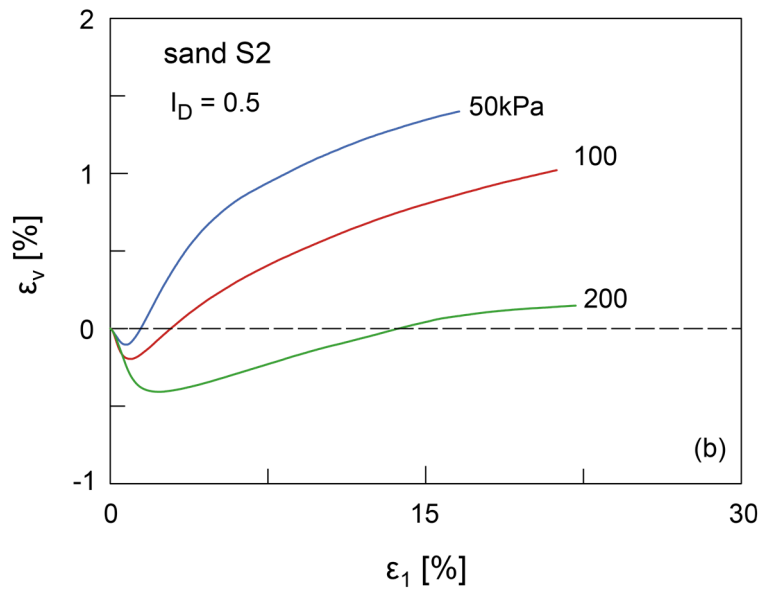


Figure 20: Stress-strain and volumetric strain from drained triaxial tests on saturated medium sand S2

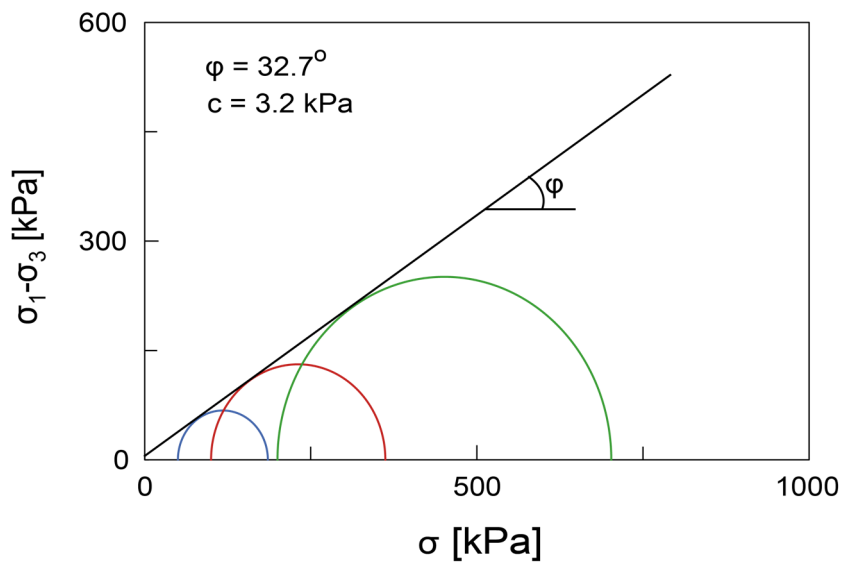


Figure 21: Results from triaxial tests for saturated sand S2

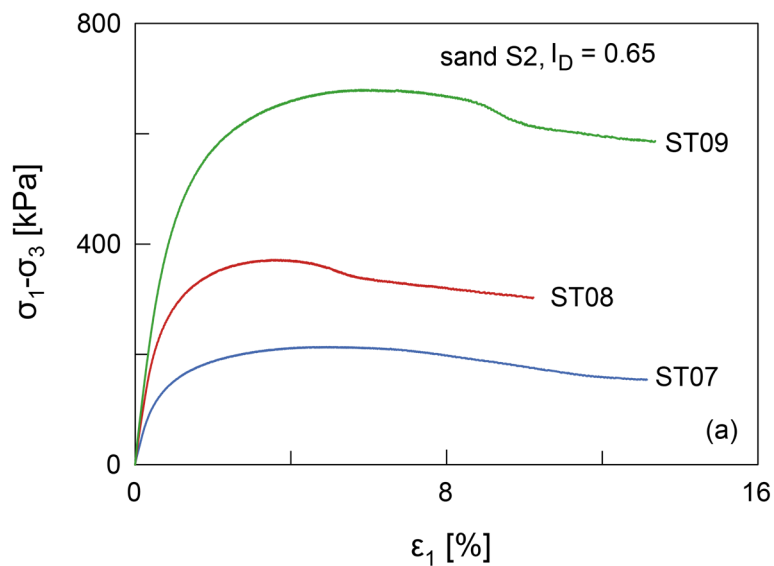
4.3.2 Results of drained test on dry and wet sand

The results presented herein are for pure sand specimens prepared at a relative density of 0.65 (medium dense sample). Three type of sand i.e. medium sand (S2), coarse sand (S3) and sand mixture (S4). The tests were conducted at the effective confining stresses of 50, 100 and 200 kPa.

Figure 22 presents the evolution of the deviatoric stress and dilatancy with axial strain for tests at different confining stresses. As expected it can be seen from

sands S2 and S3 at 50/100/200 kPa that increasing confining stress increases the deviatoric stress and contraction while the dilation decreases. It is clear that the tests at all confining stresses peaked. Loose sand S2 samples prepared at $I_D = 0.31$ and tested at the same confining stresses displayed in Figure 23 exhibit small deviatoric stress compared to the medium dense samples. These tests did not peak and the dilatant behaviour showed a full contraction. The same trend was observed for the tests on dry sand S4 and wet sand S2.

A comparison of the development of the stresses and strains for various types of dry sand specimens is shown in Figure 24. Medium sand S2 specimens at confining stresses of 50 and 100 kPa exhibit higher shear strength compared to coarse sand S3 specimens. The contraction show the opposite trend. Sand S4 (50% S2 + 50% S3) specimens demonstrate almost the same peak shear strength as that of sand S2 but with dilatant behaviour almost the same as that for sand S3.



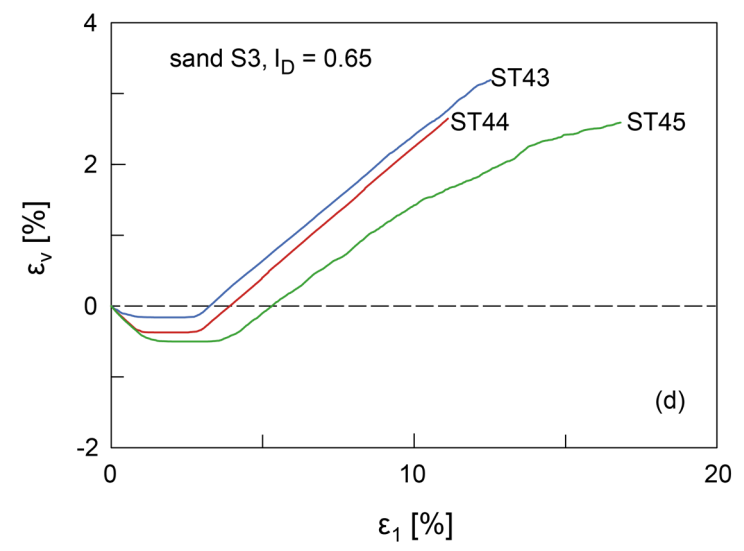
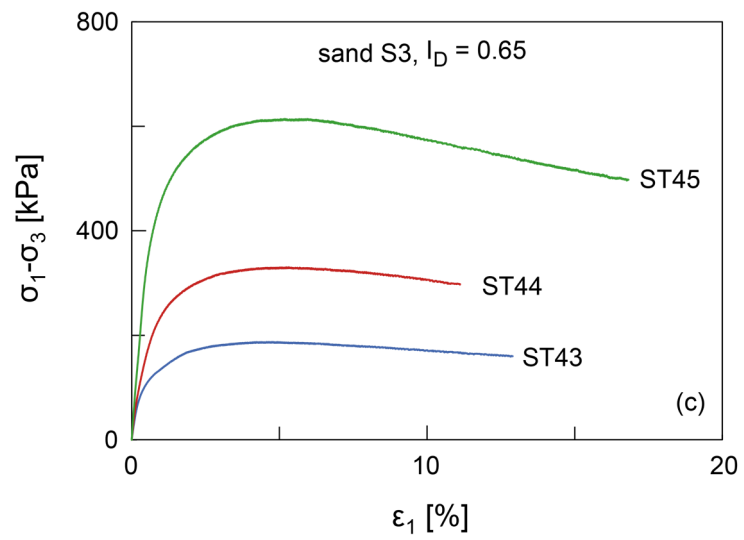
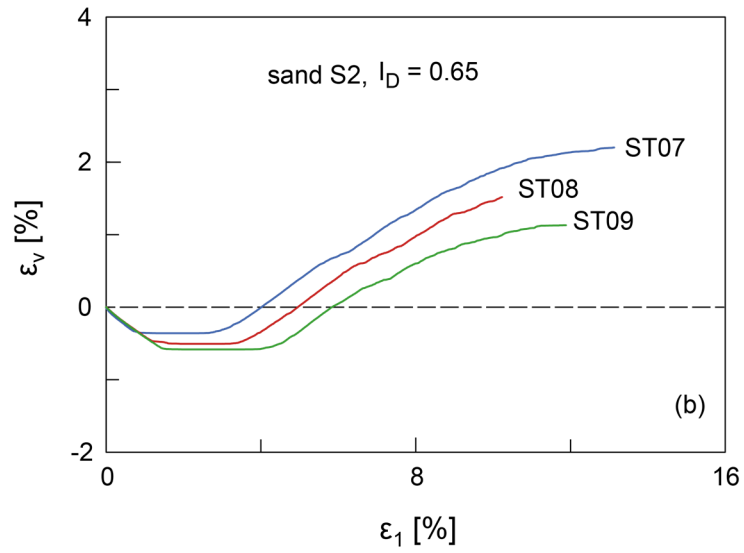


Figure 22: Stress vs. stain and volumetric strain vs axial strain curves for dry sand samples

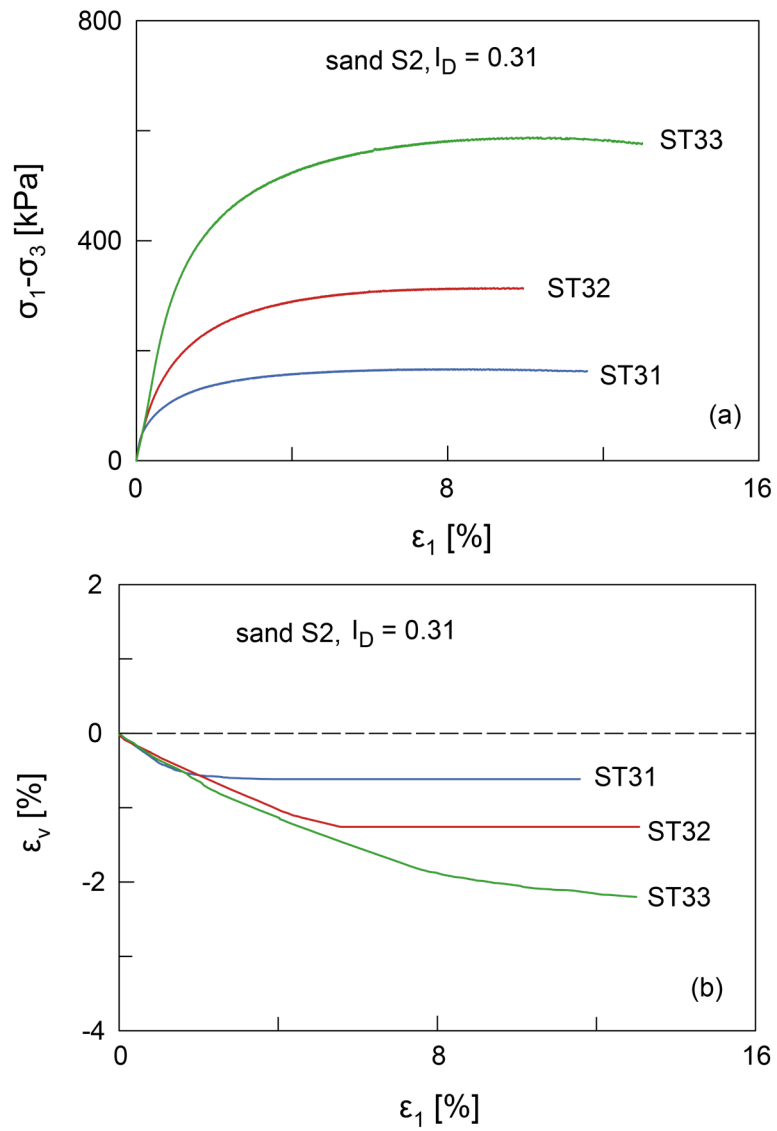
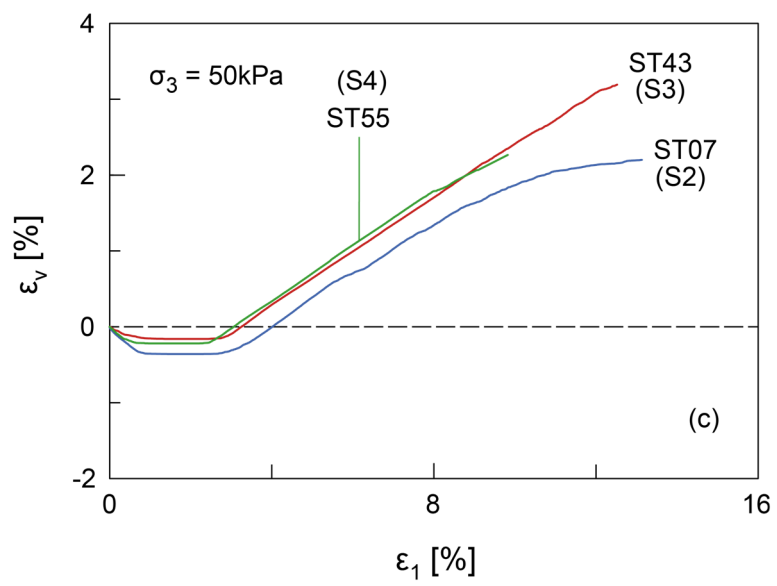
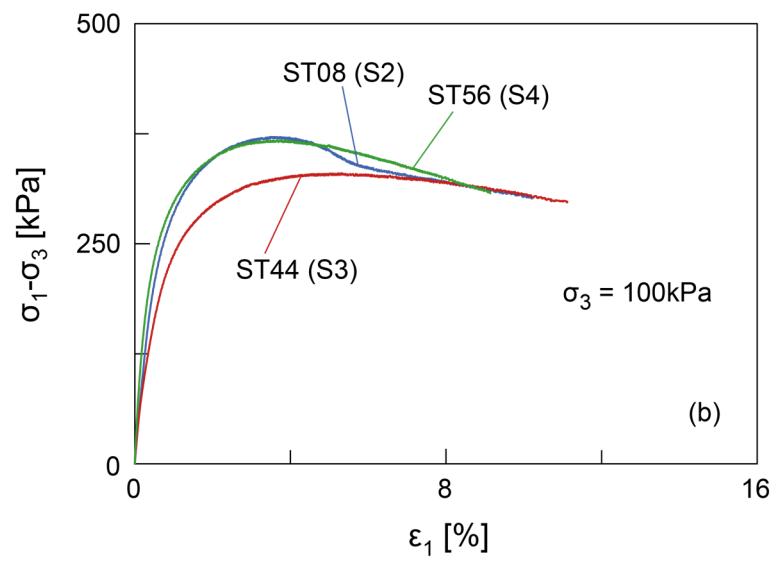
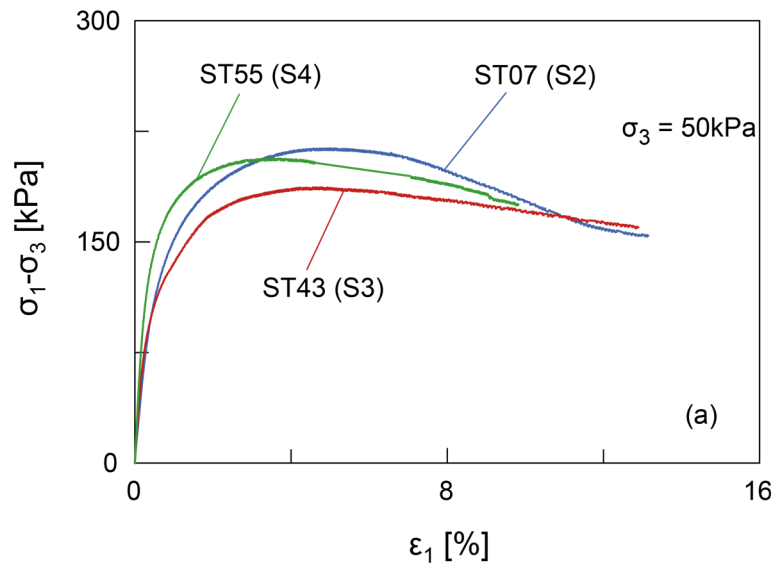


Figure 23: Stress-strain curve and volumetric strain curves for loose sand S2 samples at various confining stresses



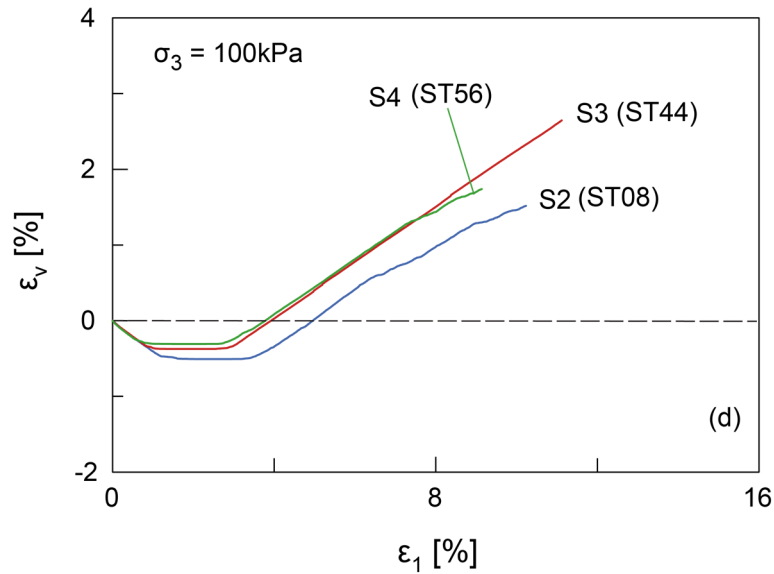


Figure 24: Deviatoric stress vs. axial strain and volumetric strain vs. axial strain for sands S2, S3 and S4

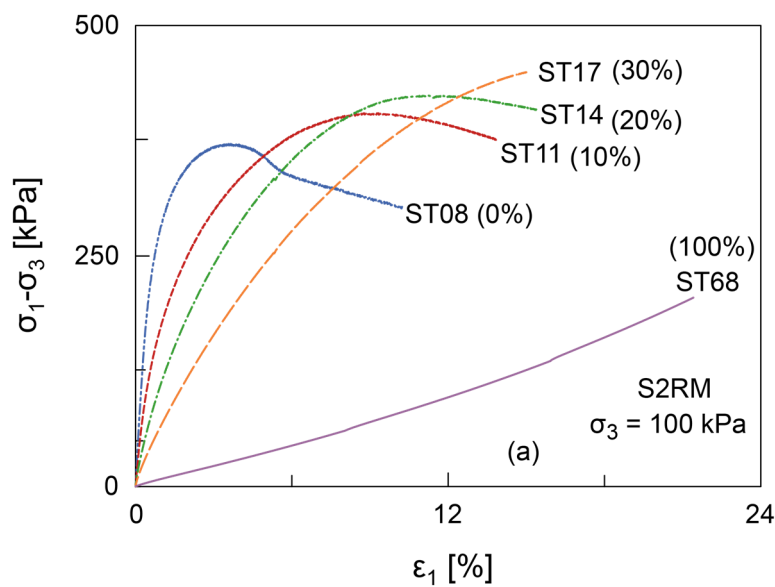
4.3.3 Results for unsaturated sand rubber mixtures

The selected results for 100 kPa are presented in form of stress vs. strain and volumetric change in Figure 25 and Figure 26. These results show that the shear strength increases with increasing chips content in the mixtures. It can be seen in Figure 25 that pure sand and the mixtures containing 10 and 20% rubber exhibit a clearly defined peak in the stress-strain curves, whereas samples with 30% and 100% chips did not peak. The same trend is observed in the results at confining stress of 50 kPa and 200 kPa that are not shown herein. For all specimens at all three confining stresses an increase in chips content yielded an increase in the axial strain at failure.

Results for dry and wet S2RM specimens at 0% and 10% chips content are plotted in Figure 27. Both pure dry sand (test ST08) and wet sand (test ST20) specimens have almost similar shear strength. Dry and wet mixture specimens (test ST11 and test ST23) at 10% chips content behave in the same way. The mixtures containing other chips contents show the same trend. However a small amount of water content can not alter the shear strength of sand rubber chips mixtures. As can be seen in Figure 27 a small difference can only be observed for the stiffness after a certain deformation. Wet specimens are slightly stiffer than dry ones for the chips content up to 20%. At 30% chips content the opposite trend is observed. A small amount of water added to sand rubber chips mixtures

helps to prevent the particle segregation during sample preparation. Sand rubber chips mixtures in their loose state have also been tested. The densities for these mixtures can be seen in Table 6. Stress-strain curves not shown herein indicate a stress-hardening behaviour. The influence of rubber chips content on the shear behaviour follows the same trend as previously described. Lower values of shear strength are obtained compared to medium dense or dense mixtures. In general, the contribution of rubber chips to the shear strength of the composite soil was achieved. This can be observed for example in Figure 28 for dry sand S2 at various chips contents under a confining stress of 50 kPa. Up to the maximum percentage of rubber chips investigated (30%) the shear strength increases continuously for the range of confining stresses used (50 to 200 kPa).

The dilatant behaviour of sand rubber chips mixtures is certainly influenced by confining stress and chips content. It can be seen in Figure 26 that pure sand exhibits small initial compression followed by dilation. Increasing rubber chips content increases the contraction and decreases the dilation. From some specimens, a higher axial strain is required for dilation to occur. No dilation is observed for the specimens with 20% chips content and higher. The same trend was observed for other tests not shown herein. The results for all loose S2RM (not presented herein) show only contraction behaviour.



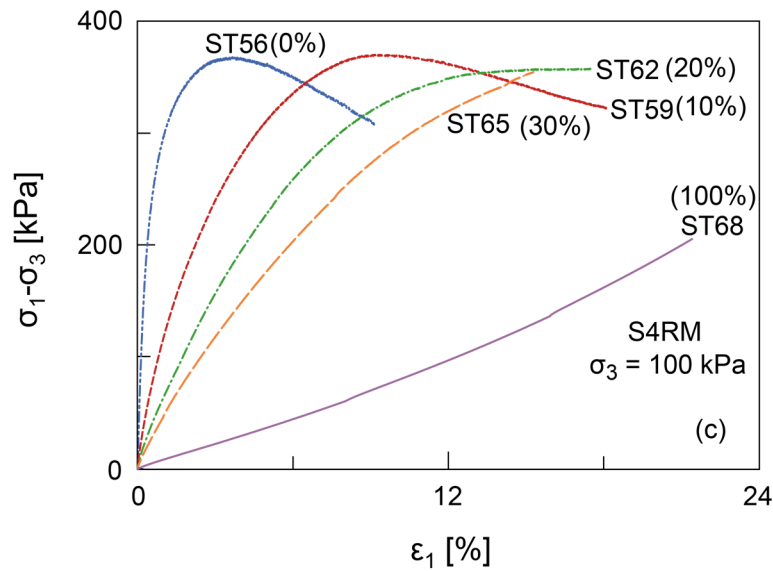
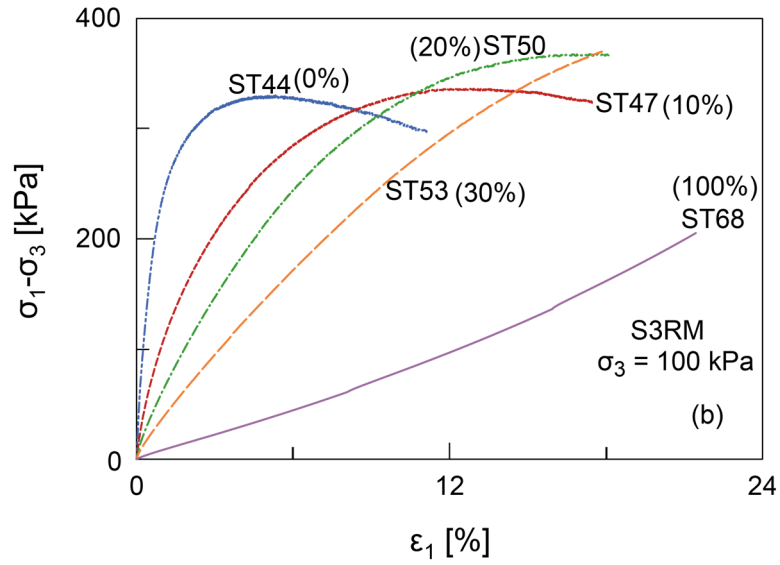
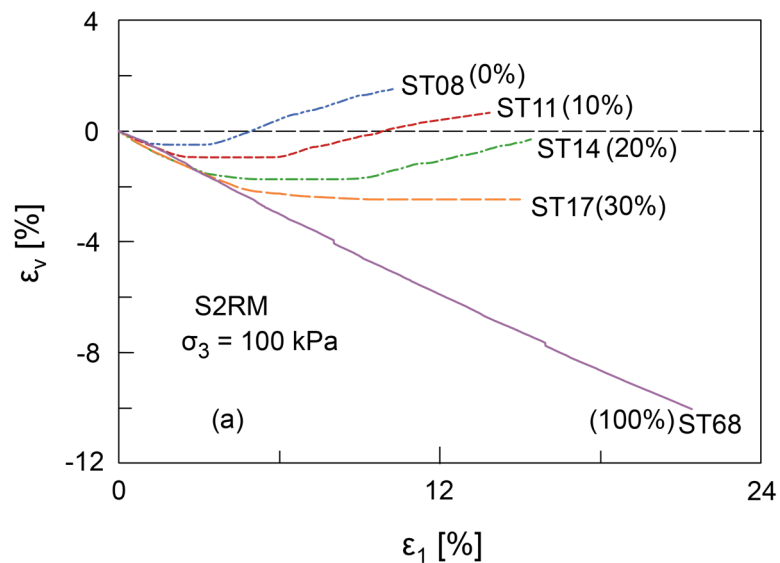


Figure 25: Stress-strain curves for dry sands (a) S2RM, (b) S3RM and (c) S4RM



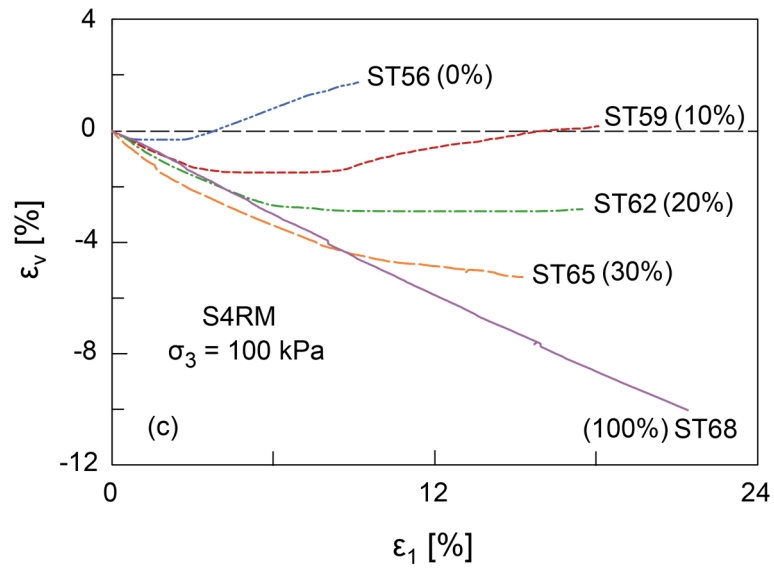
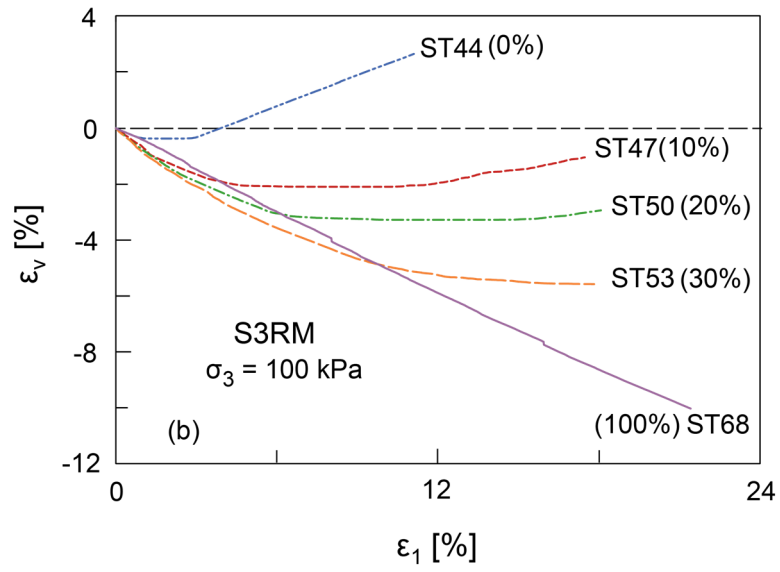
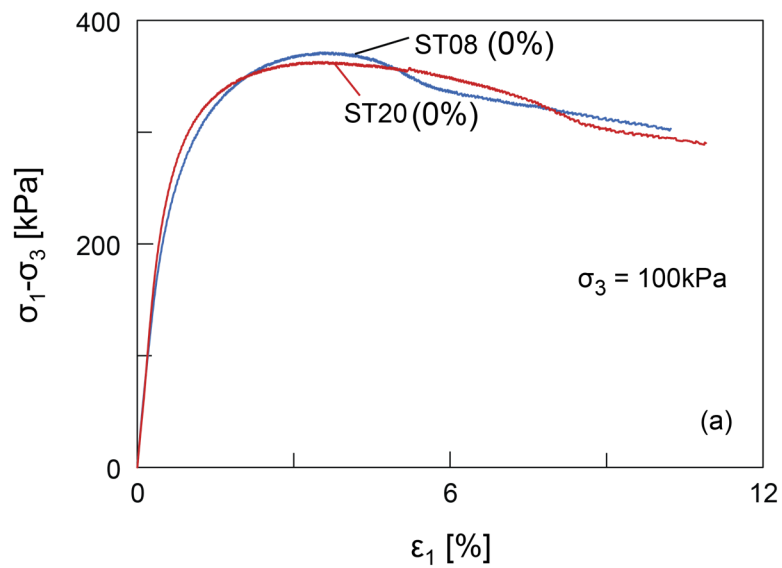


Figure 26: Dilatancy behaviour for dry sand (a) S2RM, (b) S3RM and (c) S4RM



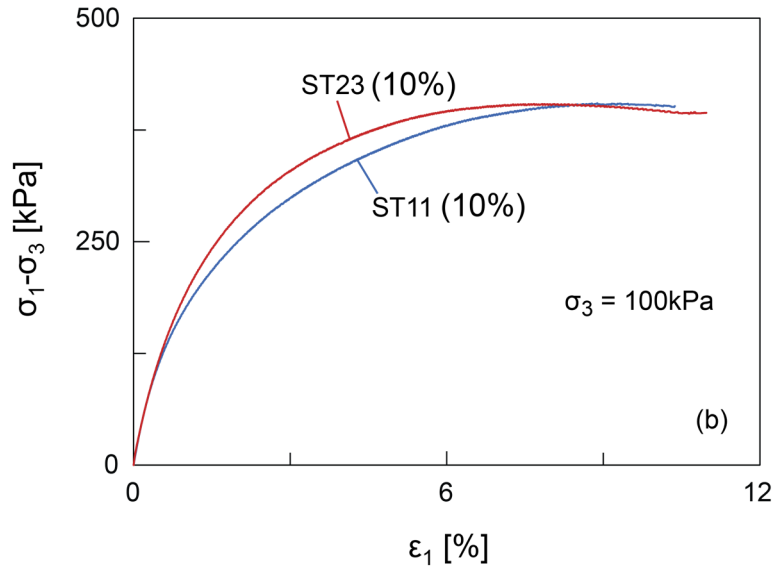


Figure 27: Comparison of shear strength from dry and wet sand S2 at (a) 0% and (b) 10% chips contents

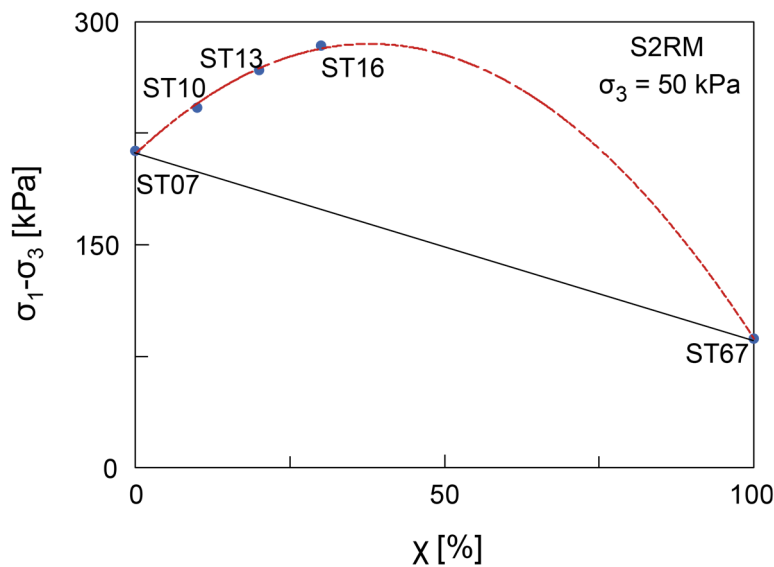


Figure 28: Effect of rubber chips on peak shear strength of sand rubber chips mixture

Further results are presented in terms of shear strength parameters derived at peak strength. The internal angle of friction and cohesion at peak or the maximum stress at failure are summarized in Table 7. Increasing the rubber chips content in the mixtures increases the cohesion for all types of sand. The internal angle of friction decreases with an exception of wet sand S2RM whereby a small increase is noticed at 10% chips content then decreases.

Table 7: Shear strength parameters for dry and wet sand rubber chips mixtures

Soil type	dry S2		wet S2RM		dry S3RM		dry S4RM	
	c [kPa]	φ [°]	c [kPa]	φ [°]	c [kPa]	φ [°]	c [kPa]	φ [°]
0	9.5	37.5	16.8	35.4	8.7	35.4	10.3	37
10	21.1	36.5	20	36.8	14.5	34	20	35
20	26.3	35.9	22.4	36.5	29.3	32.1	26.5	32.8
30	36.8	33.8	32.1	35	39.2	28.8	31.5	31.6
100	20.3	13.2	-	-	20.3	13.2	20.3	13.2

Figure 29 plots the data comparing the maximum shear strength for different confining stress levels. The data reported by Youwai & Bergado (2003) for sand at 30% rubber by dry mass show small values of peak shear strength compared to other values. This could be attributed to the tyre crumbs instead of rubber chips. The data from Zonberg et al. (2004), Mashiri et al. (2015) and the present study for sand S2 at 30%, 35% and 30% rubber chips contents show higher values. The sand used in these studies is dominated by the smaller grains that may interact better with rubber chips. Sands S3 and S4, on the other hand, yield slightly lower values of shear strength. They contain larger particles and their interaction with rubber chips may be poor compared to that with sand S2.

The influence of the sand mean particle size on the shear strength of the composite material is displayed in Figure 30. It is inferred from that figure that S2RM samples with higher d_{50R}/d_{50S} value at a confining stress of 50 kPa exhibit higher shear strength, while S3RM with lower ratio yield lower values. The same trend is observed for confining stresses of 100 kPa and 200 kPa.

The static stiffness in terms of Young's modulus of the mixture was calculated as secant modulus at a deviatoric stress equals 50% of its peak or maximum values from triaxial tests and is denoted by E_{50} . Data for dry S2RM are exemplarily plotted in Figure 31. As expected, adding rubber chips to sand reduces significantly the overall stiffness of the composite material in both dry and wet conditions. Similar behaviour is obtained for S3RM and S4RM. The cause of the decreased stiffness can be attributed to the increased elasticity and the associated reduced density of the mixtures.

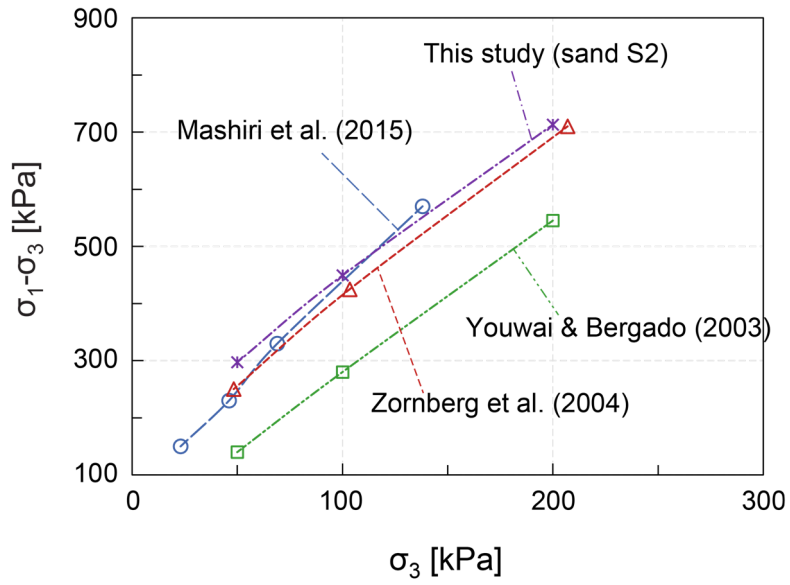


Figure 29: Peak deviatoric stress vs. confining stress for the experimental data and previous studies

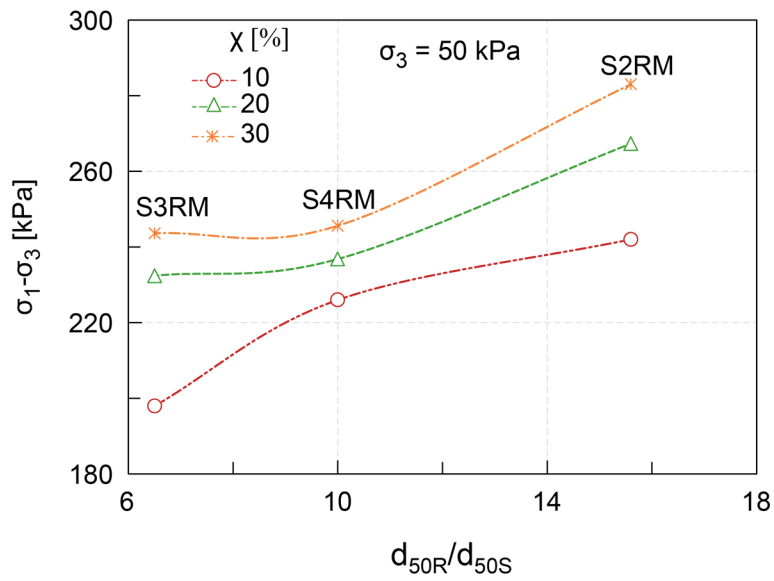


Figure 30: Influence of d_{50R}/d_{50S} on peak shear strength of sand rubber chip mixtures

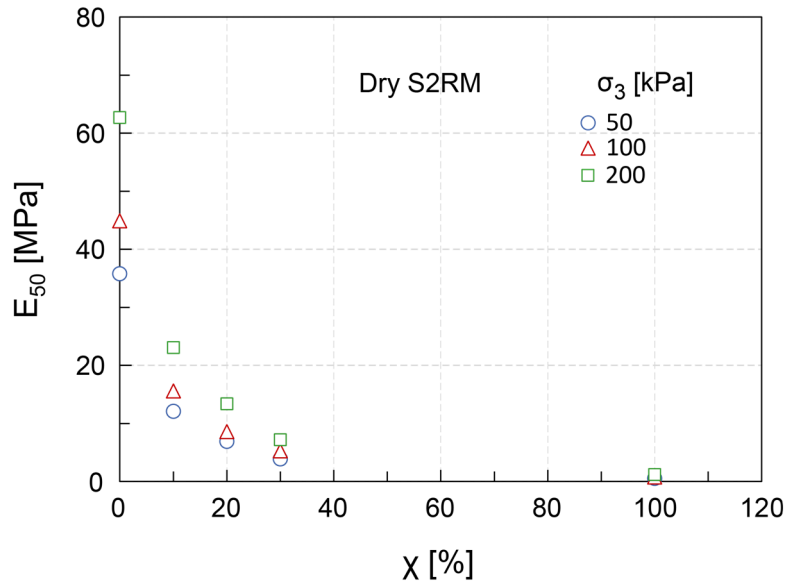


Figure 31: Effect of rubber chips on static stiffness of the composite soil.

4.4 Discussion

Whatever amount of rubber chips that can be added to sand negatively affects its compressibility characteristics i.e. increases the vertical strain and decreases the compression modulus. This is attributed mostly to the compressibility of individual chips in sand tyre chips mixtures for the increased chips contents. The results suggest that there is a better interaction between sand S2 and rubber chips compared to sands S3 and S4.

The shear strength was determined from both direct shear and triaxial tests. From both techniques the increased chips contents in sand S2, S3 and S4 increased an overall shear strength. A decrease of internal angle of friction and increase of cohesion were observed. A marginal difference in shear strength parameters was noticed from triaxial and direct shear tests. This is obvious because the two testing techniques are different. A slightly higher friction angle from direct shear may be due to the fact that, a shear plane is defined in direct shear while in triaxial compression, a shear plane is formed itself in the sliding region upon sample failure. Sand rubber chips mixture derives its improved shear strength from the combined friction resistance between sand and tyre chips and the tensile resistance developed in tyre chips. The higher improvement achieved for smaller sand grains sand S2 ($d_{50} = 0.32\text{mm}$) at various chips contents may indicate a good interaction with rubber chips compared to sand with larger grains, sand S3 ($d_{50} = 0.77\text{mm}$) and sand S4 ($d_{50} = 0.5\text{mm}$). In all mixture types the failure axial strain

becomes larger or strain hardening behaviour (no defined peak) is pronounced. This may result from the increased ductility in the composite material, reinforcement effect and the tensional stress developed in the individual chip in the region of the shear plane. It was observed from the results that increasing rubber chips content decreases dilation and increases the contraction. This can be due to the compressibility nature of the rubber chips particles. For sand to sand contact, the sand particles tend to move on one another resulting in the dilative behaviour. For sand to rubber or rubber to rubber contact, the decreased dilation and the increased contraction may result from the compressibility of the rubber chips.

As described in section 2.1.2 sand rubber mixture derives its improved shear strength from the interaction between rubber and sand particles and the reinforcement effect along the shear failure plane. The tensile strength developed in rubber chips contributed to the increased shear strength of the composite material. Increasing the content of rubber chips result in a more ductile behaviour of the composite material. An optimum chips content around 30% by dry mass in wet condition (low water content) is recommended to reinforce the uniform medium sand (sand S2) and coarse sand (sand S3) as well as their mixtures (sand S4) for engineering applications considering the fact that the higher concentrations in dry condition may lead to particle segregation.

5 Cyclic triaxial tests

5.1 Equipment and testing procedure

Cyclic response of sand rubber chips mixtures was evaluated in laboratory using a dynamic cyclic triaxial testing system. This system with the commercial name ELDYN was manufactured and supplied by GDS. The equipment and procedure for sample preparation are described in section 4.3.

Saturated specimens with 100 mm diameter and 150 mm in height were produced at the selected relative densities I_D of 30 and 50%. They were prepared for sands S2, S3 and S4 at rubber chips contents of 0/10/20/30% by dry mass under wet condition to prevent segregation of particles. Saturation was accomplished following the procedure described in ASTM D 5311-2004 using the back pressure technique. B -values obtained were all above 0.95 at back-pressure levels of around 800 kPa for pure sand and around 200 kPa for sand rubber chips mixtures. All specimens were first isotropically consolidated under an effective confining stress σ'_3 of 100 kPa. To obtain anisotropically consolidated samples, a stress controlled drained pre-cyclic static deviator stress $\sigma'_{1,st} = 45$ kPa was imposed in all tests. Cyclic tests were performed stress controlled according to ASTM D 3999-2003. A defined stress amplitude $\sigma_{1,cy}$ equal to 50 kPa was applied at a frequency of 1 Hz. The application of this static stress induces an anisotropic loading condition which simulates the field condition. Isotropically consolidated undrained cyclic tests were only performed on pure medium sand S2 for comparison with samples under anisotropic conditions.

Two types of stress-controlled cyclic triaxial test were conducted: i) consolidated undrained single stage dynamic cyclic triaxial tests to evaluate the development of accumulated excess pore water pressure, and ii) consolidated drained single stage dynamic cyclic triaxial tests with the measurement of volume change evolution with cycle number. It should be noted that no post cyclic static test was performed for the tests under saturated condition. The properties of the tested samples are summarized in Table 8 where ρ_d is the dry density of the composite material, I_D the relative density. That table contains also test type, i.e. drained

(D) or undrained (U), as well as results in terms of number of cycles to initial liquefaction N_f that are discussed later.

Table 8: Sample properties and test conditions for saturated cyclic tests, $\sigma'_3 = 100$ kPa

Soil	χ [%]	ρ_d [g/cm ³]	I_D [-]	$\sigma'_{1,st}$ [kPa]	$\sigma_{1,cy}$ [kPa]	CSR	N_f [-]	Test type	Test No.
S2	0	1.442	0.3	45	50	0.25	24	U	CY01
							no	D	CY02
	0	1.484	0.5	45	50	0.25	43	U	CY03
							no	D	CY04
	10	1.351	0.3	45	50	0.25	14	U	CY05
							20	D	CY06
	10	1.393	0.5	45	50	0.25	30	U	CY07
							30	D	CY08
	20	1.246	0.3	45	50	0.25	22	U	CY09
							35	D	CY10
	20	1.287	0.5	45	50	0.25	24	U	CY11
							34	D	CY12
	30	1.132	0.3	45	50	0.25	32	U	CY13
							40	D	CY14
	30	1.171	0.5	45	50	0.25	40	U	CY15
							no	D	CY16
S3	0	1.520	0.3	45	50	0.25	no	U	CY17
							no	D	CY18
	0	1.558	0.5	45	50	0.25	no	U	CY19
							no	D	CY20
	10	1.328	0.3	45	50	0.25	66	U	CY21
							no	D	CY22
	10	1.365	0.5	45	50	0.25	178	U	CY23
							no	D	CY24
	20	1.188	0.3	45	50	0.25	202	U	CY25
							no	D	CY26
	20	1.228	0.5	45	50	0.25	321	U	CY27
							no	D	CY28

	30	1.070	0.3	45	50	0.25	272	U	CY29
							no	D	CY30
	30	1.108	0.5	45	50	0.25	no	U	CY31
							no	D	CY32
S4	0	1.553	0.3	45	50	0.25	7	U	CY33
							25	D	CY34
	0	1.615	0.5	45	50	0.25	26	U	CY35
							no	D	CY36
	10	1.388	0.3	45	50	0.25	4	U	CY37
							7	D	CY38
	10	1.436	0.5	45	50	0.25	5	U	CY39
							10	D	CY40
	20	1.274	0.3	45	50	0.25	20	U	CY41
							34	D	CY42
	20	1.307	0.5	45	50	0.25	23	U	CY43
							30	D	CY44
	30	1.155	0.3	45	50	0.25	39	U	CY45
							no	D	CY46
	30	1.189	0.5	45	50	0.25	44	U	CY47
							no	D	CY48
S2	0	1.442	0.3	0	50	0.25	5	U	CY49
					40	0.20	11	U	CY50
					30	0.15	83	U	CY51
					20	0.10	312	U	CY52
	0	1.484	0.5	0	50	0.25	12	U	CY53
					40	0.20	25	U	CY54
					30	0.15	143	U	CY55
					20	0.10	949	U	CY56
	0	1.484	0.5	45	40	0.20	729	U	CY57
					30	0.15	no	U	CY58
					20	0.10	no	U	CY59

S2/S3/S4 denote medium sand/coarse sand/ sand mixture

U/D stand for undrained/drained

no stands for no-liquefaction

The cyclic stress ratio CSR is defined as follows:

$$CSR = \frac{\sigma_{1,cy}}{2\sigma'_3} \quad (12)$$

For dry mixtures, specimens were prepared for sands S2, S3 and S4 at rubber chips contents of 0/10/ 20/30/100% by dry mass. To include the effect of water content on cyclic strength, samples were prepared for sand S2 with the same chips contents at 5% water content. The procedures described in Section 4.3 were followed during sample preparation. The initial relative densities used were the same as those used for static triaxial tests. The properties of the tested samples are summarized in Table 9.

All specimens were first isotropically consolidated under the selected effective confining stress σ'_3 of 100 kPa. To obtain anisotropic consolidated specimens, a defined stress controlled pre-cyclic static deviator stress $\sigma'_{1,st}$ was imposed. The obtained maximum shear strength from the static monotonic tests was utilized to define the loading level for cyclic triaxial tests. The datum stress prior to the cyclic loading was set equal to one-half of the peak or maximum deviatoric stress determined by the static test. Tests were performed stress controlled according to ASTM D 3999-2003. The stress amplitude $\sigma_{1,cy}$ was set equal to 20% of the datum stress level. Each specimen was cyclically loaded in two successive steps of 50 and 1000 cycles under a frequency of 1Hz. Strain controlled post cyclic monotonic static tests were performed to evaluate the shear strength after the cyclic loading. In this stage a strain rate of 0.1mm/min was applied. Due to the compressibility of rubber chips, the mixtures can mobilize the maximum shear strength at larger deformation. However, stress at failure was taken to correspond either to peak deviatoric stress or to the maximum value at 15% axial strain whichever comes first.

Table 9: Sample properties and test conditions for dry and wet specimens (CAD cyclic tests), $\sigma'_3 = 100$ kPa

Material	χ [%]	ρ_d [g/cm ³]	I_D [-]	Sample Condition	$\sigma'_{1,st}$ [kPa]	$\sigma_{1,cy}$ [kPa]	CSR	Test No.
S2	0	1.515	0.65	D	187.2	37.5	0.182	CY60
	10	1.480	0.86		220.3	44	0.214	CY61
	20	1.374	0.88		233.8	46.8	0.227	CY62
	30	1.281	0.98		251	50.2	0.244	CY63
R	100	0.64	-	D	67.5	13.5	0.066	CY64
S2	0	1.514	0.65	M	192.3	38.3	1.184	CY65
	10	1.477	0.86		216.6	43.3	0.21	CY66
	20	1.371	0.88		226.7	45.5	0.221	CY67
	30	1.275	0.98		248.4	49.6	0.241	CY68
	0	1.444	0.31	D	159.2	31.8	0.154	CY69
	10	1.355	0.32		178.3	35.6	0.173	CY70
	20	1.250	0.32		205	41	0.199	CY71
	30	1.133	0.32		197.4	39.5	0.192	CY72
S3	0	1.591	0.65	D	174.5	34.9	0.169	CY73
	10	1.437	0.83		183.4	36.7	0.178	CY74
	20	1.312	0.88		238.8	40.1	0.195	CY75
	30	1.175	0.97		184	36.8	0.179	CY76
S4	0	1.669	0.65	D	187.9	37.6	0.183	CY77
	10	1.532	0.85		200.6	40.1	0.195	CY78
	20	1.377	0.89		217.8	43.6	0.212	CY79
	30	1.273	0.93		191.1	38.2	0.185	CY80

D/M stand for dry/moist

The measurement of the axial load and deformation were performed in the way similar to that used for static triaxial tests using load cell and a high accuracy external linear displacement transducer (LVDT), respectively. During the undrained tests, the excess pore water pressure was recorded by a high accuracy pore water pressure transducer. The equivalent volume change in drained test was measured in terms of discharged water directly by the volume change controller without any other assistance. Pore water pressure ratio r_u , dynamic

Young's modulus E_d and shear modulus G_d (secant modulus), shear strain γ and damping ratio D were calculated as follows:

$$r_u = \frac{\Delta u}{\sigma'_3} \quad (13)$$

$$E_d = \frac{\sigma'_{1,cy}}{\varepsilon_{1,cy}} \quad (14)$$

$$\gamma = (1 + \nu)\varepsilon_{1,cy} \quad (15)$$

$$G_d = \frac{E_d}{2(1 + \nu)} \quad (16)$$

$$D = \frac{\Delta E}{4\pi E} \quad (17)$$

where $\sigma'_{1,cy}$ is the stress amplitude per each cycle, $\varepsilon_{1,cy}$ the corresponding axial strain, ν the Poisson's ratio, E the area of a dashed triangle which is a stored energy in elastic material and ΔE the enclosed area of the entire loop which is a dissipated strain energy per unit volume in the loading cycle as shown in Figure 32.

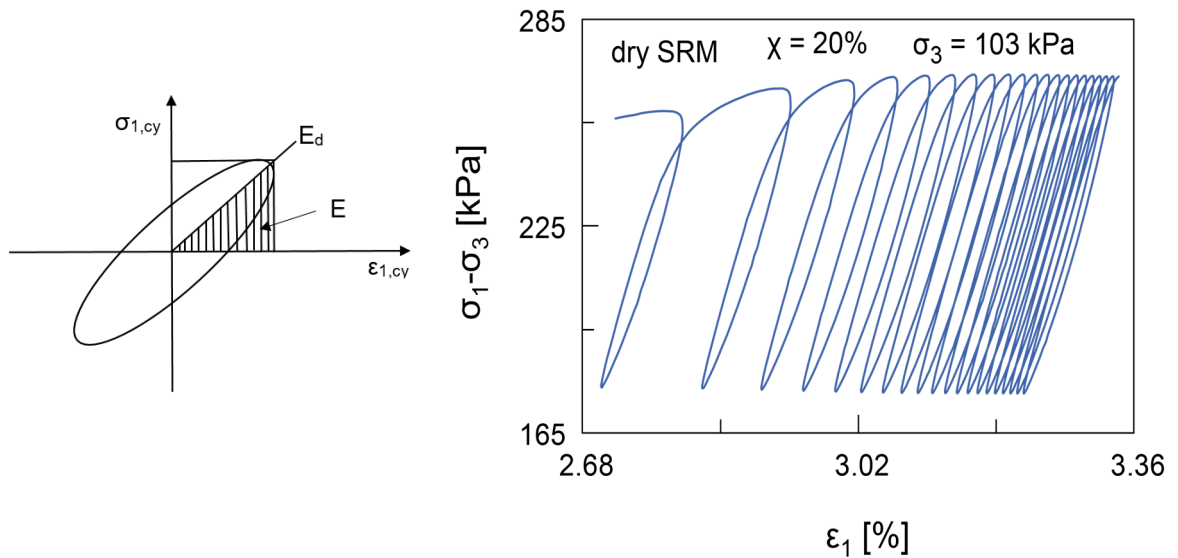


Figure 32: Stress-strain loops in cyclic triaxial test

5.2 Results of undrained tests on saturated material

5.2.1 Cyclic resistance of pure sand

The results presented herein were generated from undrained cyclic triaxial tests for pure medium sand S2 specimens prepared at $I_D = 0.3$ and 0.5 . Saturated specimens were consolidated by a minor initial effective consolidation stress σ'_3 of 100 kPa. For isotropically consolidated undrained (CIU) specimens the major principal stress, $\sigma'_1 = \sigma'_3$ while for anisotropic consolidated undrained (CAU) specimens $\sigma'_1 > \sigma'_3$. Specimens were cyclically loaded stress controlled at various cyclic stress ratio (CSR). Soil resistance depends also on relative density and confining stress level, and becomes significantly weaker when loading conditions lead to a stress reversal. For the test set up used herein the combined shear stress was always positive for anisotropic consolidated undrained tests (CAU). The cyclic loading in isotropic consolidated undrained tests (CIU) is always accompanied by stress reversal (compression and extension). The specimen properties, loading conditions and test numbers can be seen in Table 8.

Failure in saturated specimens due to cyclic loading is defined either in terms of excess pore water pressure Δu or in terms of deformations. For the former, the pore water pressure ratio r_u is introduced by relating Δu to the minor effective consolidation stress σ'_3 and the onset of initial liquefaction is defined when r_u attains a value of 1. For the later a threshold value of double amplitude axial strain of 5% for isotropic consolidated undrained tests CIU or an accumulated axial strain e.g. 5% or more for anisotropic consolidated undrained tests (CAU) can be used to indicate the onset of failure (Hyodo et al., 2002; Chen et al. 2019).

The development of the excess pore water pressure has been evaluated. For validating the testing procedure results for excess pore water pressure are compared with the predictive equations for fine sand suggested by Egglezos & Bouckovalas (1998) for a large number of cyclic triaxial tests. The evolution of pore water pressure with number of cycles is expressed by means of a power law functions:

$$\Delta u(N) = \Delta u(1) \cdot N^c \quad (18)$$

$$\Delta u(N) = \left(\frac{2}{\pi} \right) \sigma'_3 \arcsin \left(N^{(1/2b)} \sin \left(\frac{\pi \cdot \Delta u(1)}{2 \cdot \sigma'_3} \right) \right) \quad (19)$$

where $\Delta u(1)$ denotes the excess pore water pressure after the first loading cycle and N_f is the number of cycles required to cause initial liquefaction. These equations have been derived for fine sand with uniformity coefficient C_u approximately 1.5. A comparison is made herein for medium sand S2 that is coarser but exhibits a similar behaviour. In equation (18) the cyclic stress amplitude and the confining stress and the void ratio are incorporated in $\Delta u(1)$ making these values the decisive parameters for the quality of the prediction. The parameters c and b are set equal to 0.48 and 1.03, respectively, Egglezos & Bouckovalas (1998). Figure 33 compares the test data and the prediction for anisotropic consolidated specimens and Figure 34 for isotropic consolidated specimens. Both show a good agreement. The other two sands tested (S3 and S4) were either much coarser or less uniform and deviated from the validity range of equations.

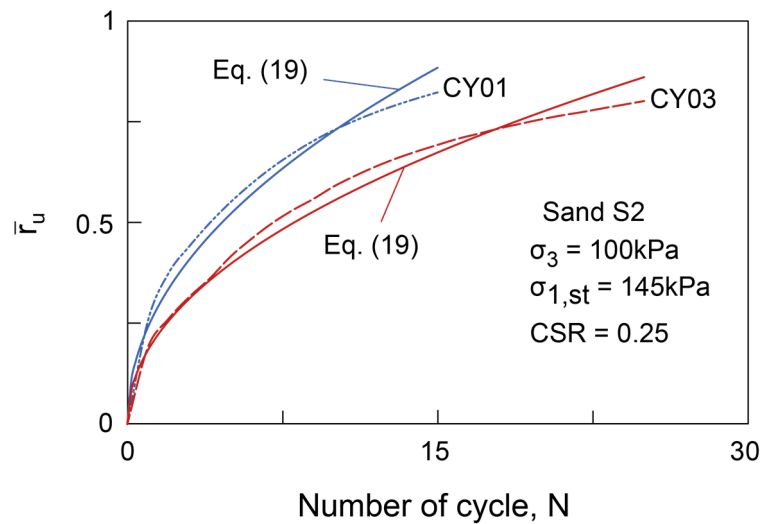


Figure 33: Comparison of test data for Sand S2 with predictive equation (18) (CAU)

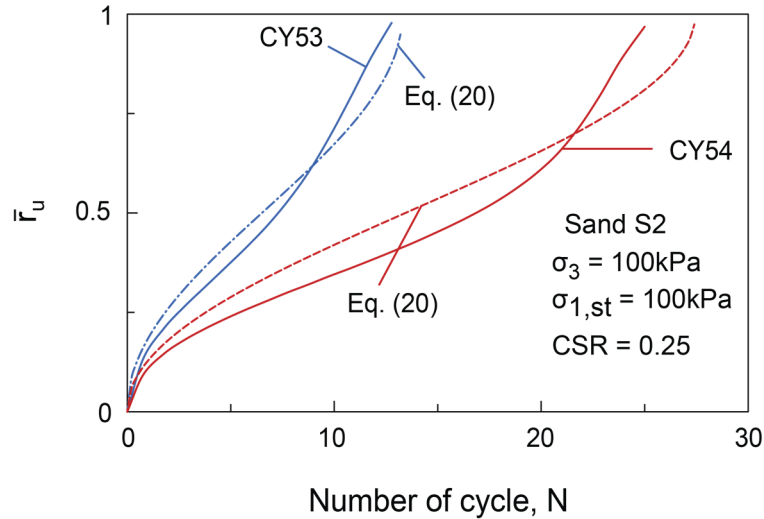


Figure 34 Comparison of test data for sand S2 with predictive equation (19) (CIU)

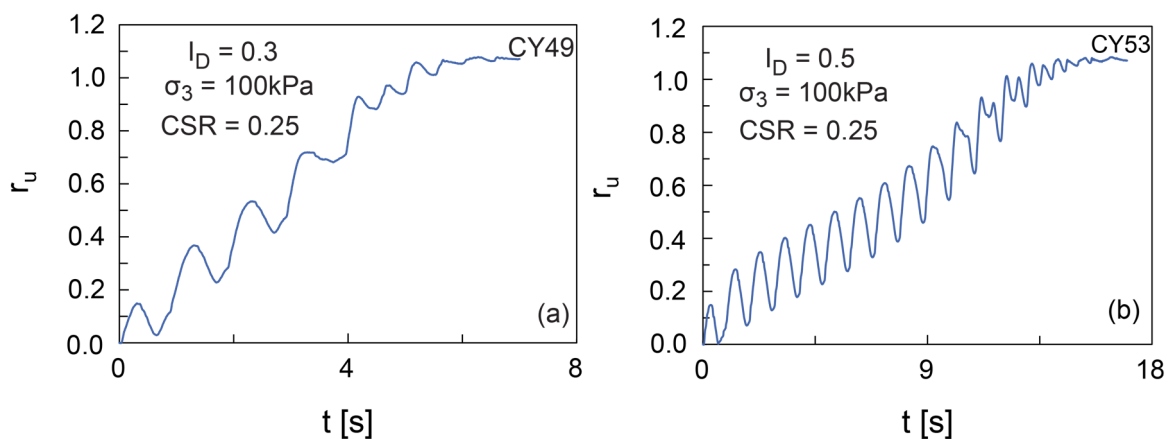
Figure 35 displays a typical time history of the excess pore water pressure and axial strain as well as stress paths in the p - q plane data recorded during cyclic triaxial tests under isotropic consolidation condition for sand S2. Specimens prepared at $I_D = 0.3$ and 0.5 , isotropically consolidated and cyclically loaded at $CSR = 0.25$ liquefied after 5 and 12 cycles respectively. The strain diagram in Figure 35 shows that the double amplitude axial strain at failure fulfil the failure criterion ($\varepsilon_1 \leq 5\%$) when the mean effective consolidation stress reaches zero. After an initial liquefaction is reached ($\sigma'_3 = 0$) for both loose and medium dense sand specimens cyclic strain increases sharply with almost no mobilized shear resistance. Similar response was observed for all liquefied sand specimens loaded at various CSR, see Table 8.

For data recorded from anisotropic consolidation specimen prepared for example at $I_D = 0.5$ (Figure 36), the rate of excess pore water pressure increases rapidly up to r_u approximately 0.65 beyond which a slow increase is observed until r_u reaches unit. The accumulated axial strain increases continuously with a slow rate up to a value of $r_u = 0.65$ with a rapid increase afterwards. This specimen liquefied at accumulated axial strain higher than 5%. It should be noted that from this test cyclic resistance is apparent even after the occurrence of initial liquefaction. The same response was obtained for the liquefied specimens loaded under various CSR.

The development of excess pore water pressure (average \bar{r}_u) is visualised in Figure 37 for isotropically consolidated specimen loaded under various *CSR*. It can be seen that the rate of the development is considerable up to $\bar{r}_u = 0.2$ already from the first cycle followed by a slower increase up to a value of 0.5. After this level the increase is again fast indicating the induced instability of the specimen.

The effect of initial static stress on cyclic strength was identified. Specimen prepared at $I_D = 0.3$ and loaded with $CSR = 0.25$, test CY49, with no initial static stress liquefied only after 5 cycles, whereas test CY03 with static stress of 45 kPa prior to cycling liquefied after 24 cycles. Specimen prepared at $I_D = 0.5$ and loaded with $CSR = 0.25$, test CY53, with no initial static stress liquefied after 12 cycles and the duplicate specimen in test CY03 with initial static stress of 45 kPa liquefied after 43 cycles. The same behaviour was obtained for $CSR = 0.2, 0.15$ and 0.1. Note that some specimens did not liquefy even after 2000 cycles (see Table 8).

The *CSR* value causing initial liquefaction after 10cycles is a criterion commonly adopted for the cyclic resistance of the specimen. Recorded data for isotropically consolidated specimens are presented in Figure 38. It is inferred that the cyclic resistance (*CSR*) for the specimens at $I_D = 0.5$ is higher than that of those at $I_D = 0.3$ which is obvious. Data not presented herein indicate that the cyclic resistance is higher for CAU tests compared to CIU tests.



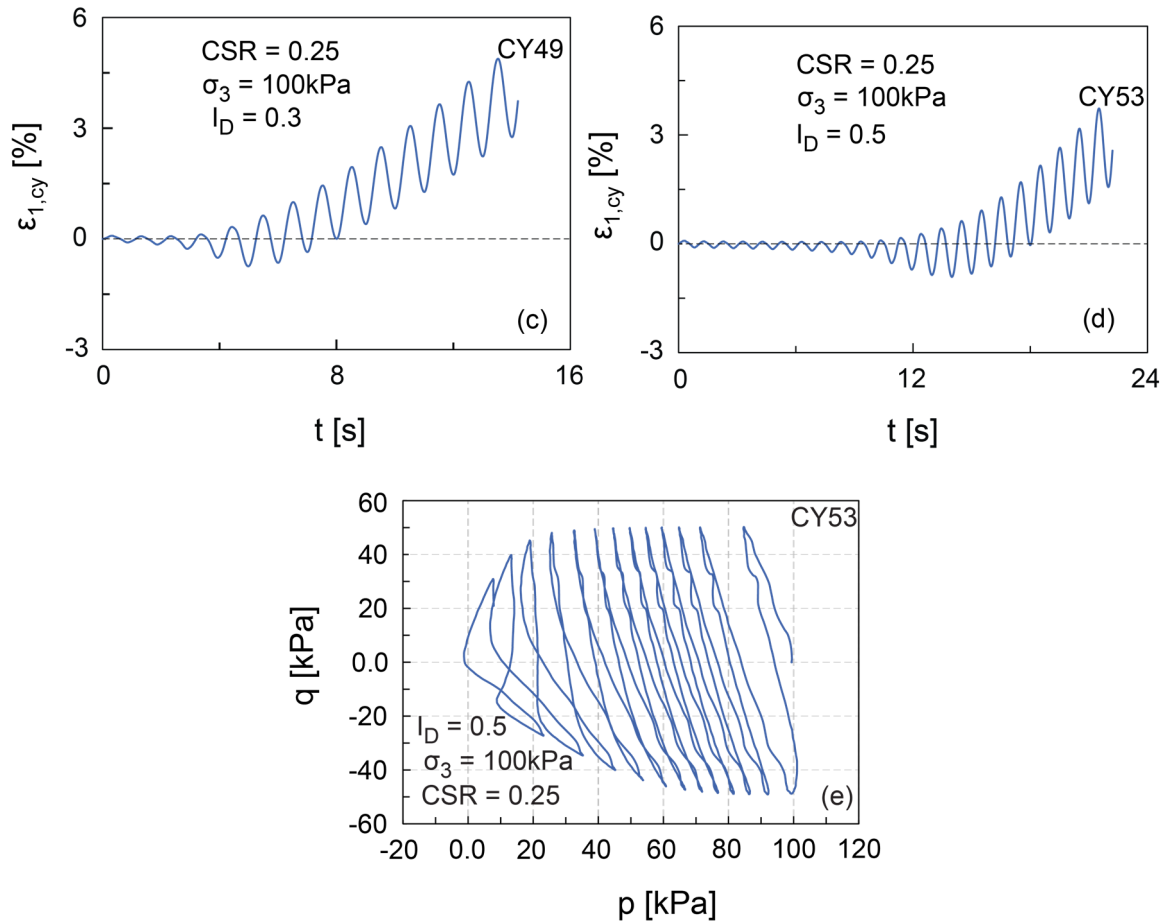
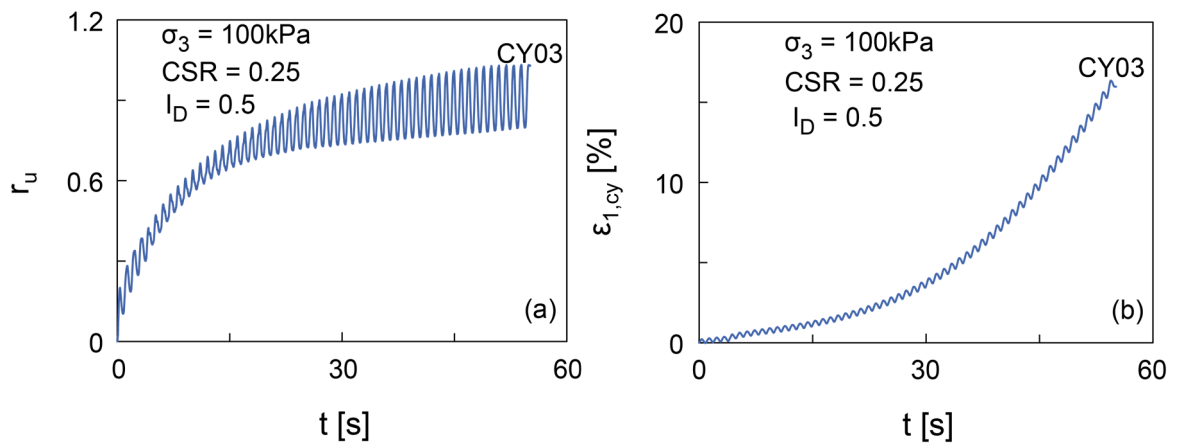


Figure 35: Evolution of excess pore water pressure ratio, axial strain and stress path for pure sand S2, CIU tests



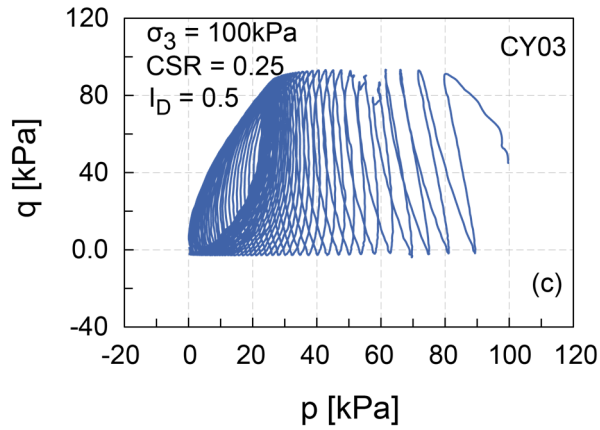


Figure 36: Evolution of undrained excess pore water pressure ratio, cyclic axial strain and stress path for pure sand S2, CAU test

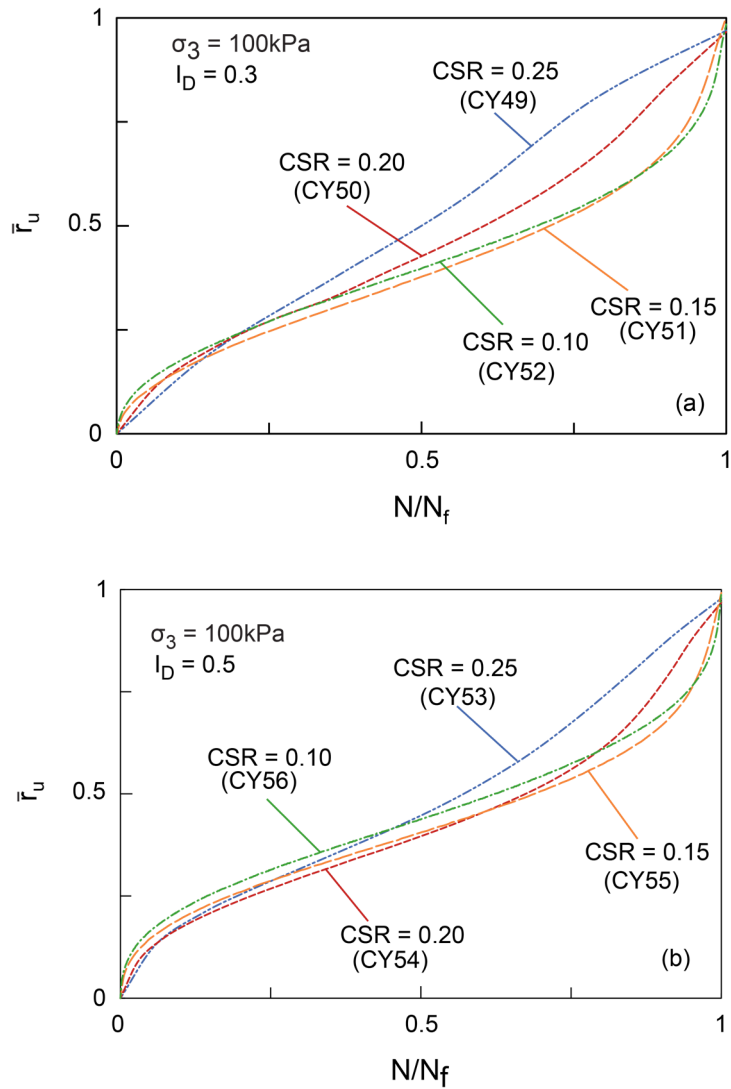


Figure 37: Average excess pore water pressure ratio vs normalized cycles at various CSR, CIU tests

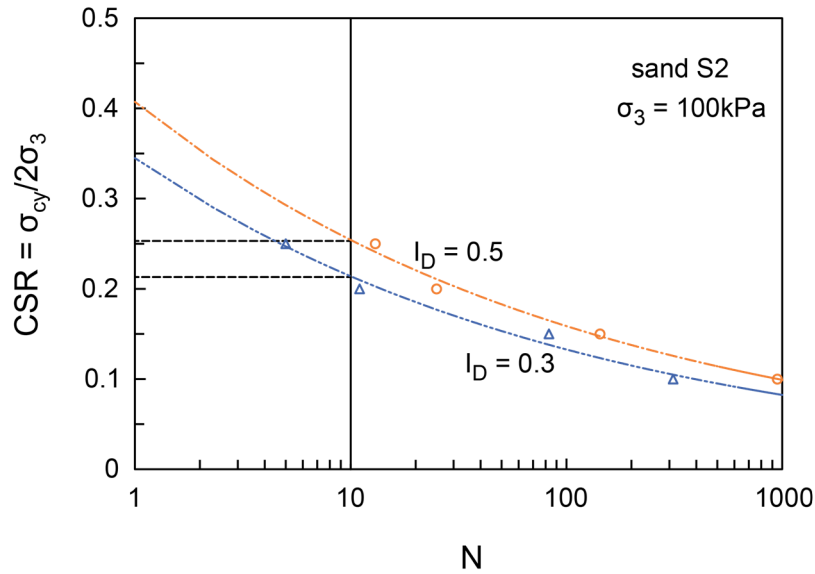


Figure 38: Cyclic resistance for medium sand S2, CIU tests

5.2.2 Cyclic resistance of sand rubber chips mixtures from CAU tests

- **Excess pore water pressure and resistance to liquefaction**

Figure 39 displays typical time histories of the development of excess pore water pressure for S2RM, S3RM and S4RM specimens at 0% rubber content (pure sand) prepared at $I_D = 0.3$. Figure 40 shows the corresponding curves for S2RM at 20 and 30% rubber chips content and $I_D = 0.3$. As shown in Figure 39 S2RM and S4RM specimens exhibited liquefaction, whereas for S3RM liquefaction did not occur. S4RM specimens liquefied and exhibited an abrupt failure already after few cycles. Adding 10% rubber chips to sands increases the accumulated excess pore water pressure compared to pure sand. Further increase of rubber chips has the opposite effect and decreases excess pore water pressure.

24 cycles were required to cause initial liquefaction for S2RM specimen at 0% chips prepared at $I_D = 0.3$ while S2RM at 30% chips content necessitated 32 cycles. The results for the composite material compacted at $I_D = 0.5$ show that pure sand is stronger against liquefaction than all other mixtures. Initial liquefaction for S2RM at 0% chips was achieved after 43 cycles compared to that of the specimen with 30% chips content initiated after 40 cycles (see Table 9). It can be suggested that the rubber chips contents beyond those used in this study may yield higher resistances compared to pure sand at $I_D = 0.5$.

A comparison for S2RM and S4RM not shown herein showed that S4RM at 0% and at 10% chips content at $I_D = 0.3$ exhibit rapid development of excess pore water pressure compared to S2RM at 0% and 10% chips contents. The rate of excess pore water pressure generation decreases remarkably from a gravimetric content of 20% and higher for sand S4RM and moderate for sand S2RM. The excess pore water pressure for S2RM and S4RM becomes almost similar at 30% rubber chips content.

A direct comparison among tests for S2RM is visualized in Figure 41 that displays the computed average pore pressure ratio \bar{r}_u against number of cycles. Note that, as mentioned before, \bar{r}_u is always smaller than r_u by definition and its highest value remains slightly below 1 at initial liquefaction. Similar trend, not presented herein (see electronic supplement), was observed in the test series for S3RM and S4RM at $I_D = 0.3$ and 0.5. Further comparison of the pore water pressure from three types of mixtures is presented in Figure 42. It can be observed from the curves for the mixtures at 10% rubber chips that the rate of excess pore water pressure development in sand S3 (test CY21) is lower compared to that in S2RM (test CY05) and S4RM (test CY37). It was noticed that the excess pore water pressure build-up in S2RM and S4RM at 30% rubber chips follows almost the same lines.

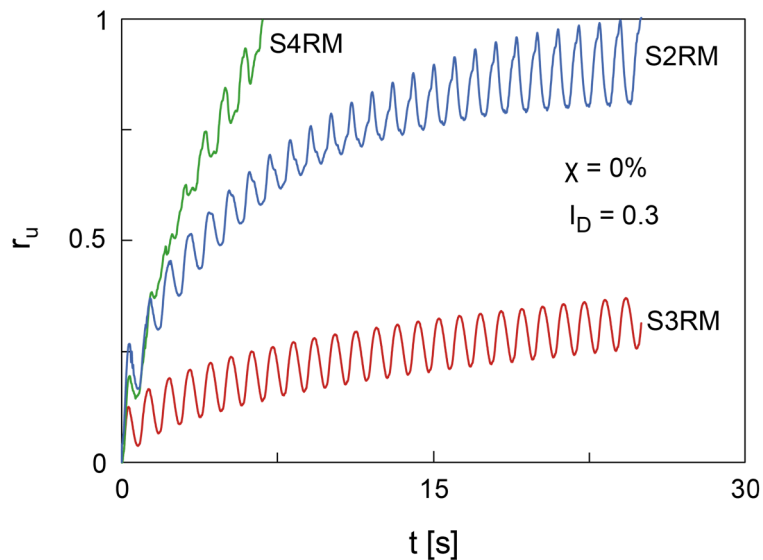


Figure 39: Evolution with time of the excess pore water pressure ratio for S2RM, S3RM and S4RM at $I_D = 0.3$, CAU tests

As shown in Table 8 all S3RM specimens required a higher number of cycles to initiate liquefaction compared to the S2RM and S4RM specimens. Note that tests on S3RM at 0% chips content, $I_D = 0.3$ and 0.5 and at 30% chips content, $I_D = 0.5$ did not liquefy even after 500 cycles.

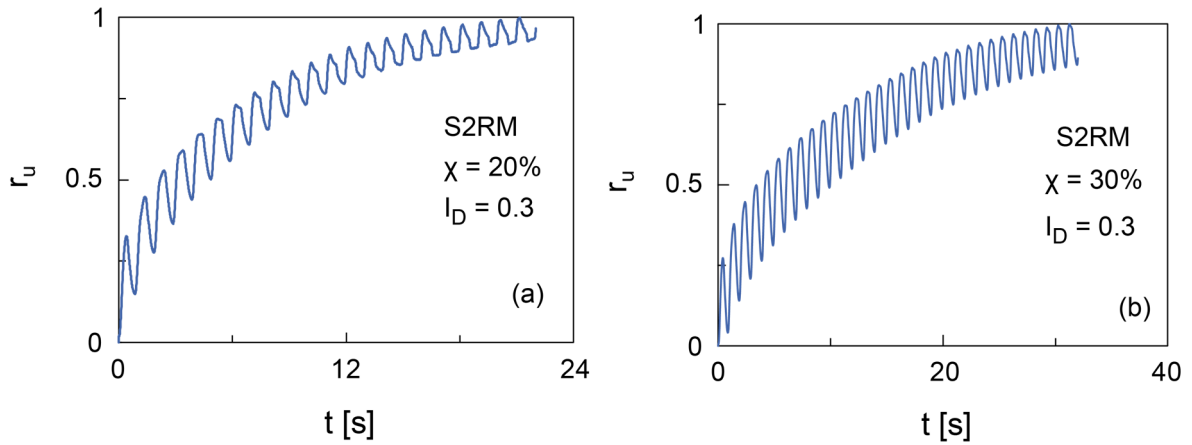
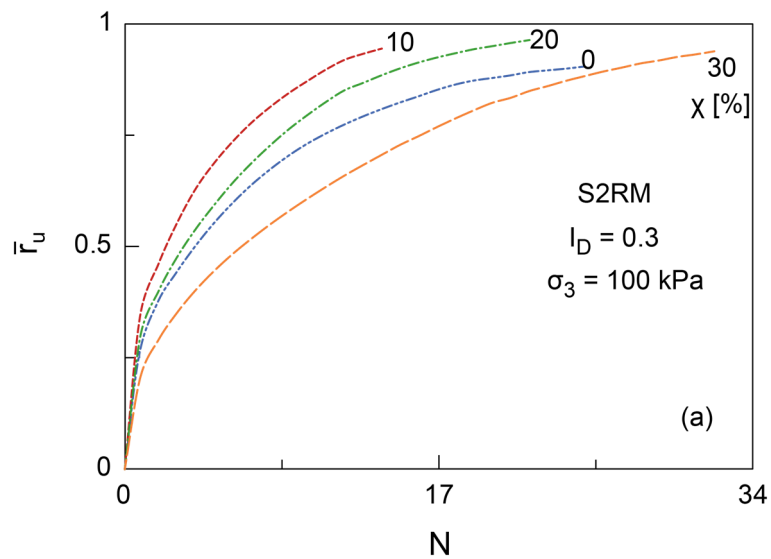


Figure 40: Evolution with time of excess pore water pressure ratio for S2RM at 20 and 30% rubber chips content at $I_D = 0.3$, CAU tests



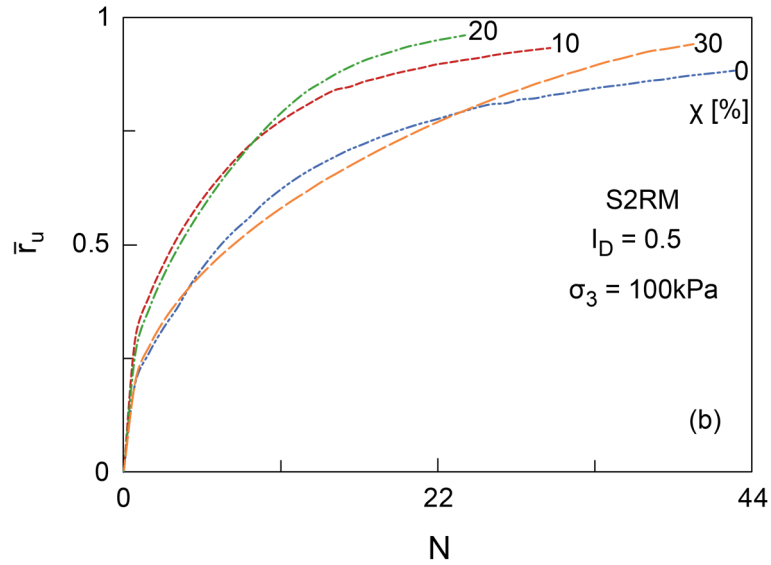


Figure 41: Average excess pore water pressure ratio vs. number of cycles for S2RM at various rubber chips contents for $I_D = 0.3$ and $I_D = 0.5$; CAU tests

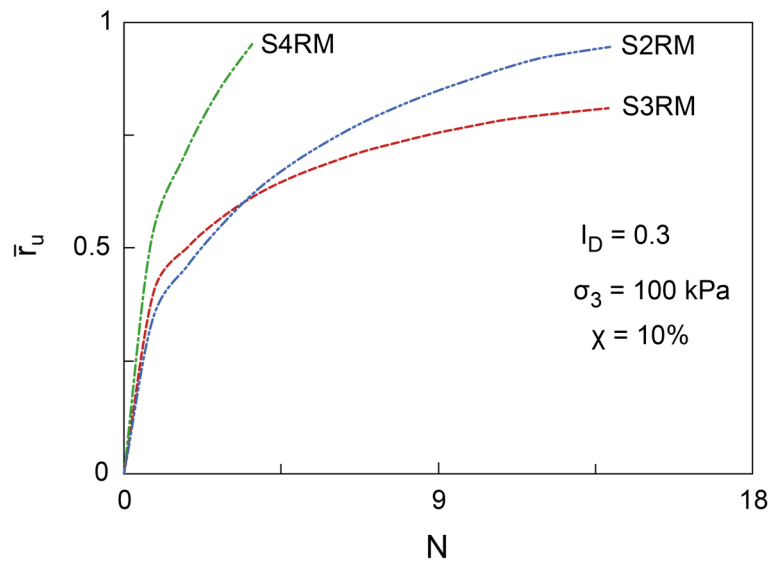


Figure 42: Average excess pore water pressure ratio vs. number of cycles for S2RM, S3RM and S4RM at 10% chips contents for $I_D = 0.3$; CAU tests

Figure 43 plots the average pore pressure ratio \bar{r}_u versus the normalized cycles number N/N_f . It can be seen that curves from different tests are close to each other. This is independent on the soil type for all sands investigated. The relationship \bar{r}_u vs. N/N_f may be approximated by the following equation (20). Thus, a unique \bar{r}_u vs. N/N_f relationship is established, roughly independent of the relative density and the rubber chips content but still strongly dependent on the soil types.

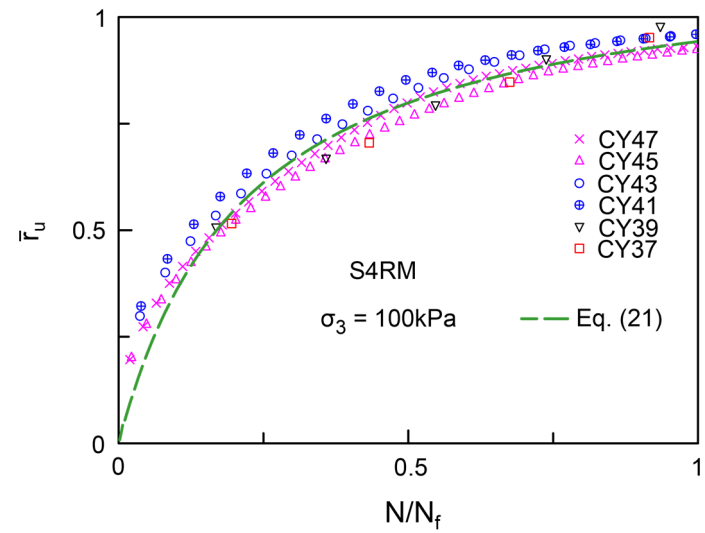
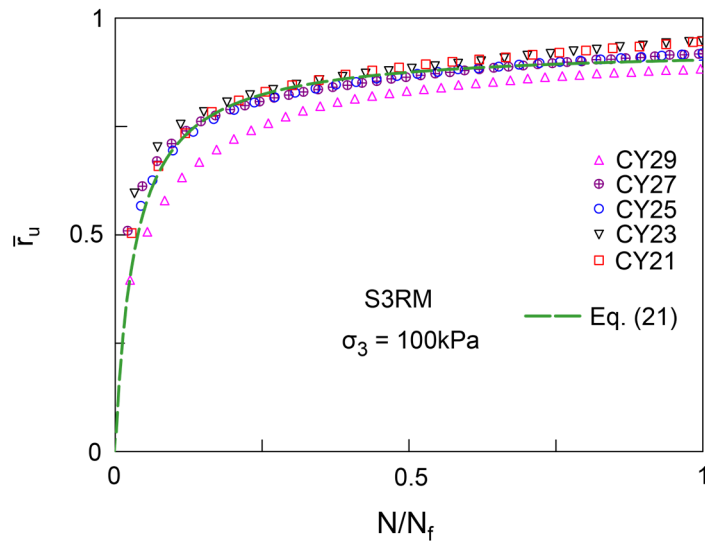
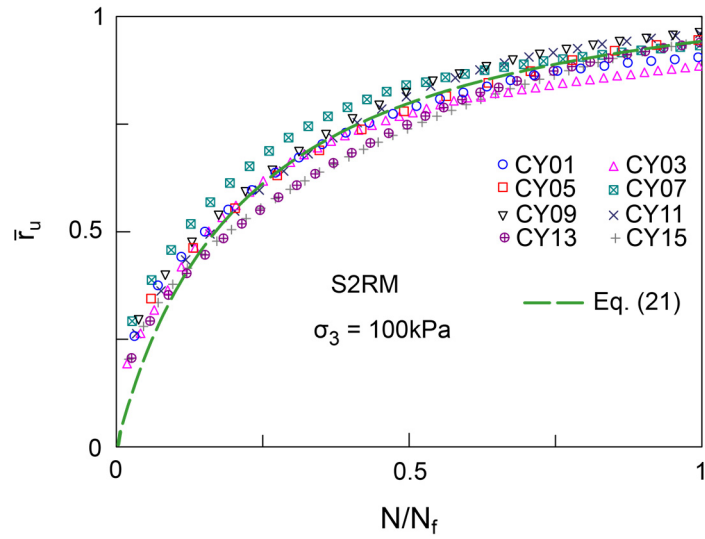


Figure 43: Average excess pore pressure ratio vs normalized cycle number for S2RM, S3RM and S4RM

$$\bar{r}_u = \frac{b_1 \cdot N / N_f}{b_2 + b_3 \cdot N / N_f} \quad (20)$$

with the following fitting parameter sets: $b_1 = 2.3$, $b_2 = 0.44$, $b_3 = 2$ for S2RM and S4RM; $b_1 = 28$, $b_2 = 1$, $b_3 = 20$ for sand S3RM. This equation is valid for rubber chips contents up to 30%.

- **Accumulated axial strains**

Settlements induced by earthquake shaking in saturated sands is relevant for the assessment of liquefaction hazard. This is the consequence of the rapid generation of the excess pore water pressure causing the soil to liquefy. Settlements may also be generated in loose or medium dense sands. Excessive settlements may lead to collapse of constructed buildings or infrastructures. Cyclic tests under anisotropic pre-cyclic stress condition were conducted to assess the impact of rubber chips on the deformations in saturated sand. Tests were also performed for dry or wet mixtures for which results are discussed later.

Figure 44 exemplarily plots time histories of axial strain recorded during undrained cyclic tests for S2RM, S3RM and S4RM specimens at 0% chips content prepared at $I_D = 0.3$. For S2RM specimen, test CY01, the axial strain increases slowly with the cycles number at the beginning, then increases rapidly when the test ends-up in liquefaction failure. S3RM specimen, test CY17 did not liquefy, however the accumulated axial strain increases continuously at the same rate. For S4RM specimen, test CY33, the instability starts at the beginning of the tests. This means the axial strain increased rapidly at the start of the test. The same behaviour was observed for specimens prepared at $I_D = 0.5$.

Cyclic deformation is affected by rubber chips added to sand. This can be clearly shown by the average data plotted in Figure 45 and Figure 46. It can be seen in Figure 45 that a sample containing 10% rubber chips exhibits higher deformation compared to that of pure sand. Further increase of rubber chips content generally increases the resistance to axial deformation of the saturated composite material. The results for the S3RM mixtures not shown herein follow the same trend. The cyclic deformation of sand rubber chips mixtures is also affected by the relative density. As expected, the test data from various mixtures revealed that the cyclic axial strain from the mixtures at $I_D = 0.5$ is lower than that of the mixtures at $I_D = 0.3$. For S4RM at 0 and 10% rubber content the occurrence of initial

liquefaction after few cycles was immediately followed by a flow failure. Further addition of rubber chips rendered the composite material more ductile, in particular at rubber chips content of 20% and higher, see Figure 45.

Comparison of the cyclic deformation for S2RM and S4RM showed that non-uniform sand S4 at 0 and 10% rubber chips content exhibited earlier abrupt failure with higher deformation compared to the uniform sand S4. A drastic reduction of axial strain was observed at 20% and higher chips contents for sand S4RM. Further comparisons for the mixtures are presented in Figure 46. It is observed that the rate of the development of cyclic strain for the mixtures at 10 and 30% rubber chips in S3RM is lower compared to that in sand S2RM and S4RM. The deformation of S2RM and S4RM at 30% rubber chips follows nearly the same lines. This may be an indication that at higher rubber chips content S2RM and S4RM may exhibit almost similar dynamic response. The same was observed for sand tyre chips mixtures at $I_D = 0.5$.

As previously mentioned, adding a small amount of lightweight rubber chips in sands (up to approx. 10%) increases the cyclic axial strains. This increase may be attributed to the reduced density of the mixture, the compressibility of the individual rubber chips as well as insufficient ductility. Further density reduction for the increased chips content in the mixtures may be compensated by the improved ductility which in turn increases the resistance to cyclic deformation.

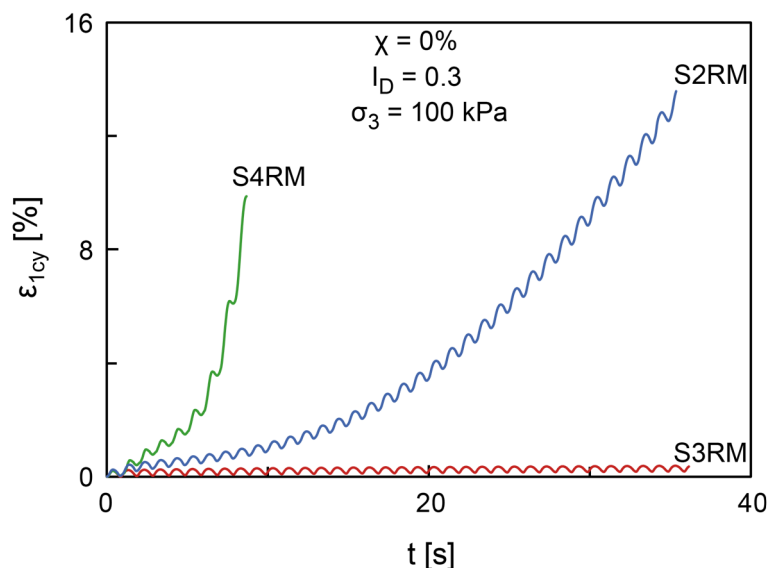


Figure 44: Evolution with time of the undrained cyclic axial strain for S2RM, S3RM and S4RM at 0% chips content at $I_D = 0.3$; CAU tests

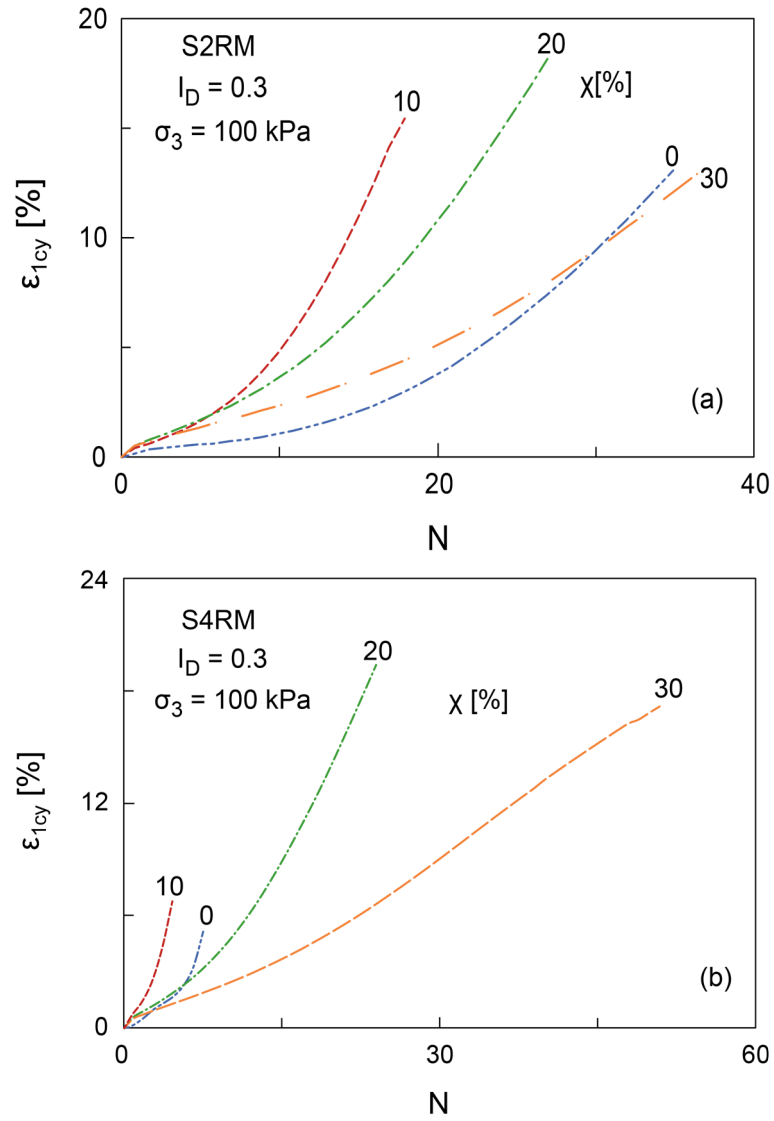
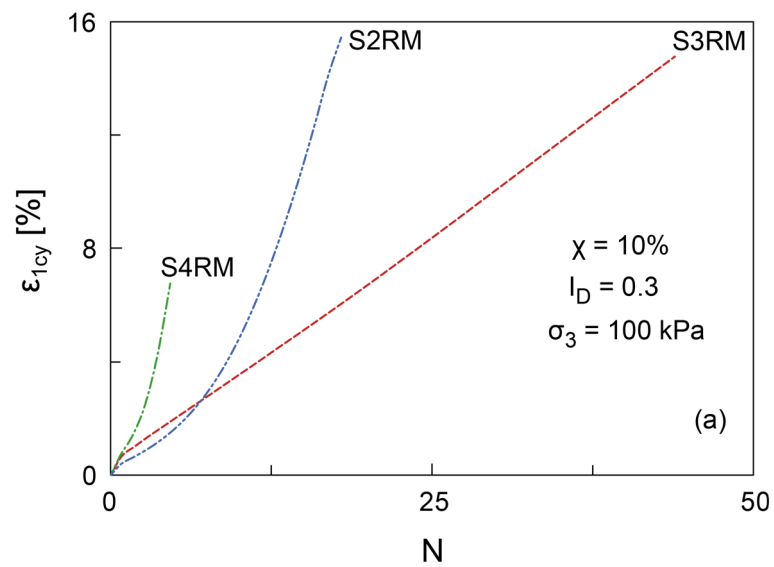


Figure 45: Average axial strain vs. number of cycles for S2RM and S4RM at various rubber chips contents at $I_D = 0.3$; CAU tests



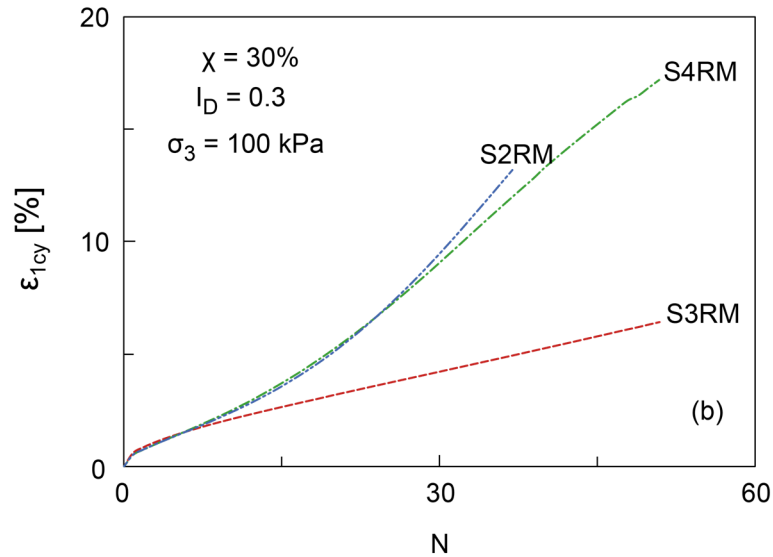


Figure 46: Comparison of undrained axial strain for mixture from sands S2RM, S3RM and S4RM at 10% and 30% chips content at $I_D = 0.3$; CAU tests

5.3 Results of drained tests on saturated material

For cyclic tests under drained condition, drainage improves the material stiffness. It was noticed that the fast loading during cyclic prevents full drainage. Therefore, some excess pore water pressure may be generated leading to liquefaction particularly for S2RM and S4RM specimens with low rigidity and ductility (cf. Table 8). This contributes to the stiffness degradation already after some cycles. For the specimen with enhanced ductility (increased rubber chips content) excess pore water pressure initiated at the beginning of cycling dissipated after a sufficient number of cycles. This contributes to the increased resistance to liquefaction and stabilizes the stiffness value at larger number of cycles.

5.3.1 Volume change

The change in volume in the drained tests may depend on soil grain size distribution, rubber chips content and the cyclic stress amplitude. Figure 47 exemplarily plots the time history of the volume change as recorded during drained cyclic test on pure sands at $I_D = 0.3$. It can be seen that at 0% rubber chips content S3RM exhibits lower change in volume than S2RM and S4RM. Due to larger mean particle in sand S3, it would be hard for the external load to force water in the voids to flow out. For sands S2 and S4 a state of particle

parking may occur resulting from combined repeated loading and drainage. The change in volume in these sands follows nearly the same lines.

The effect of rubber chips on volume can be clearly described by the calculated average data displayed in Figure 48 for S2RM. Regardless of sand type and relative density, increasing the amount of rubber chips in sand up to 20% yields a higher volume change. A decrease was noticed for chips content larger than 20% that can be attributed to the increased overall compressibility due to particle re-arrangement and the ductility due to the increased rubber content. Note that for specimens that did not liquefy the volume change increased slightly or became almost stable around 70 to 120 cycles. The same trend was obtained for other mixtures not shown herein.

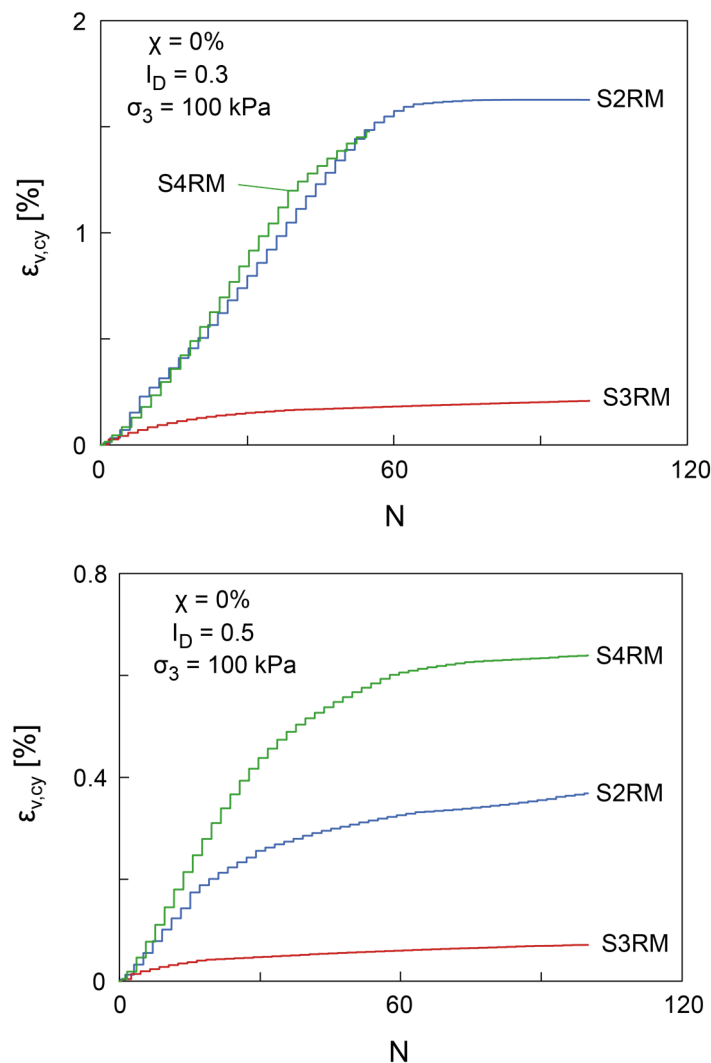


Figure 47: Time histories of the volume change in drained tests for S2RM, S3RM and S4RM at 0% rubber chips content, CAD tests

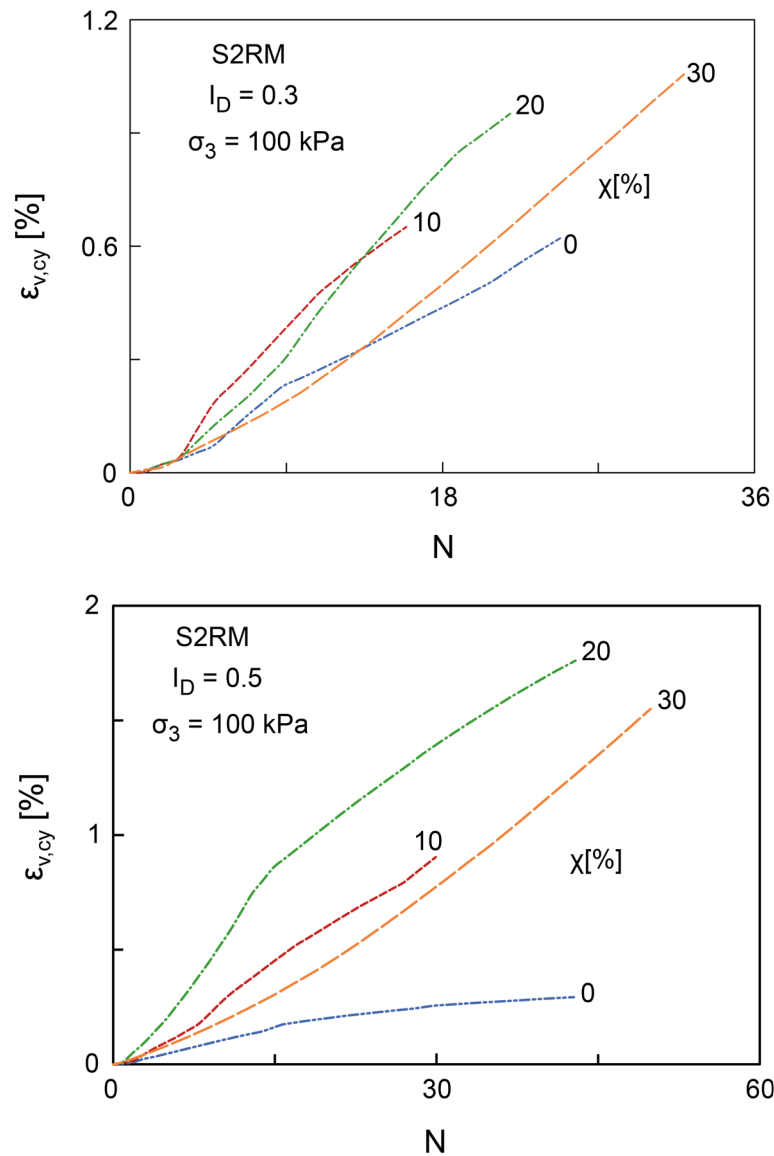
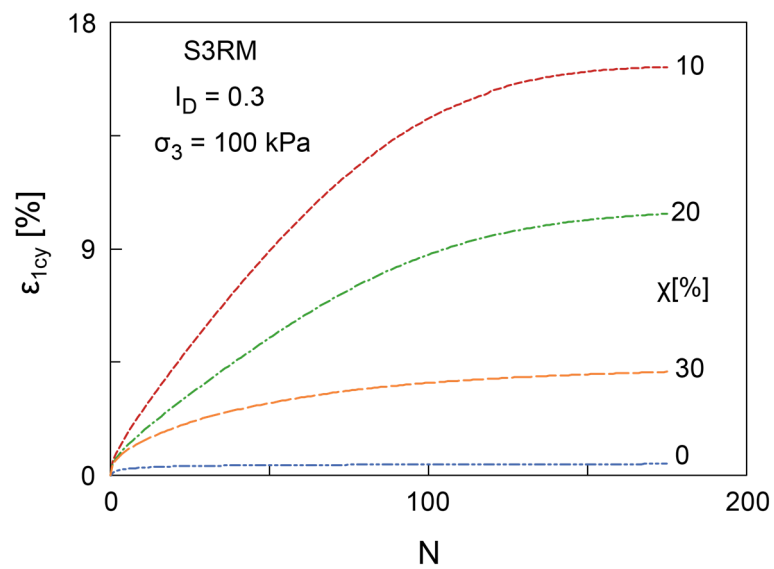
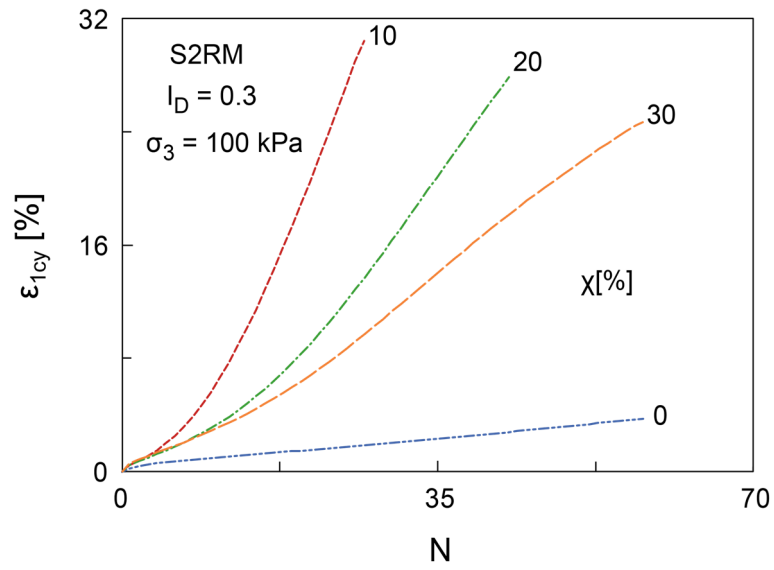


Figure 48: Average volumetric strain vs. number of cycles in drained tests for sand S2RM at various chips content, CAD tests

5.3.1 Accumulated axial strain

Figure 49 plots the average axial deformation vs. the number of loading cycles for saturated drained cyclic tests on sand rubber mixtures at $I_D = 0.3$. It can be seen that the axial strains increases with cycles number but at slow rate and with an increased cyclic resistance compared to undrained tests. The same as undrained tests, adding a small amount of rubber chips (10%) to sand decreases the cyclic resistance and increases the axial strain. Further increase of rubber chips slow down the development of the axial strain. The results demonstrate a continuous development of the axial strains in all S2RM and S4RM specimens while in

S3RM they become stable at $N \approx 150$. This behaviour was observed for the mixtures at $I_D = 0.5$ not shown herein but with an improved cyclic resistance.



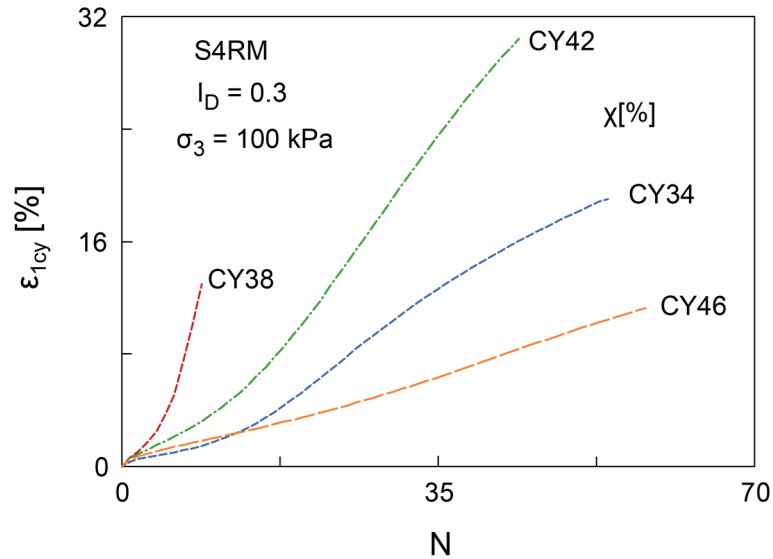


Figure 49: Cyclic axial strain vs. number of cycles for saturated drained sand rubber mixtures, CAD tests

5.4 Link between undrained and drained test results

In the drained cyclic tests, the volume change data were recorded. During these tests, a complete cycle of stress loading causes grain slipping followed by volume compaction and water discharge through the drainage line. A relationship between excess pore water pressure in undrained tests and volume change in drained tests can now be established. This relationship is presented by the curves \bar{r}_u vs. $\varepsilon_{v,cy}$ in Figure 50 and can be approximated through curve fitting by the following equation:

$$\bar{r}_u = \frac{\varepsilon_{v,cy}}{0.07 + \varepsilon_{v,cy}^{0.9}} \quad (21)$$

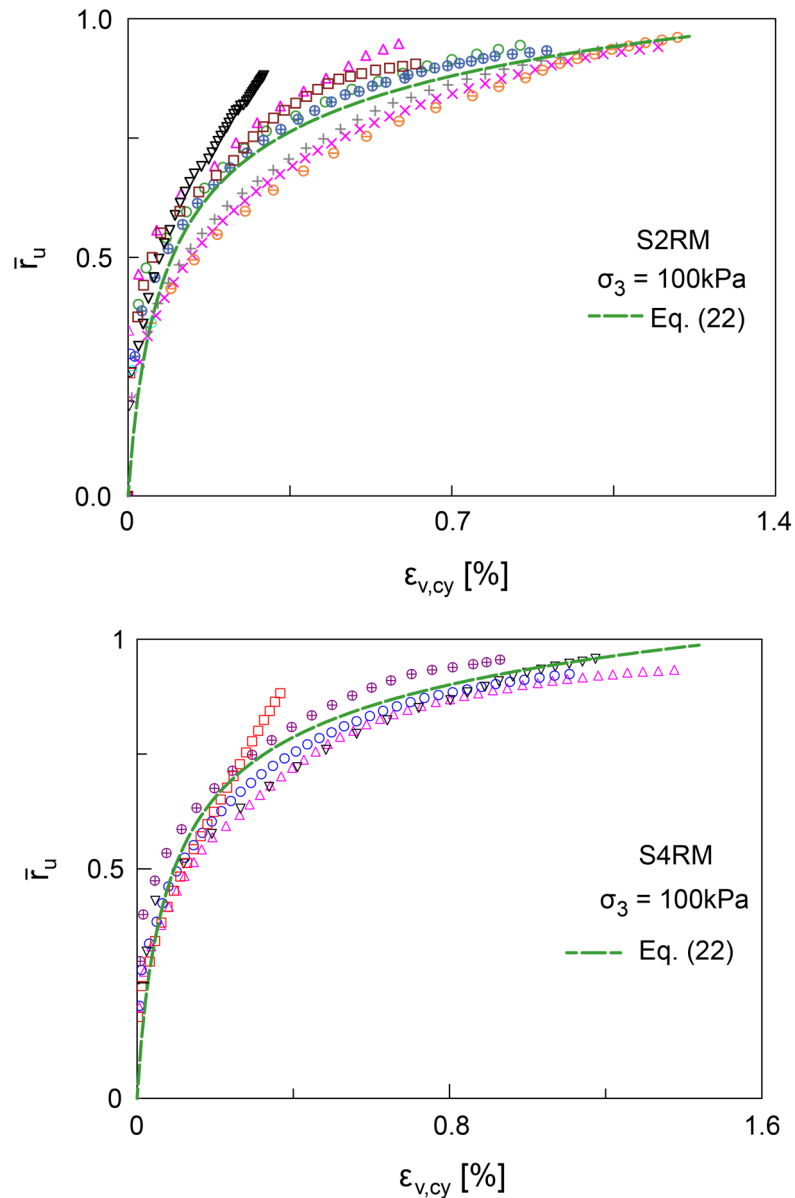


Figure 50: Excess pore water pressure ratio vs volumetric strain for S2RM and S4RM at various rubber chips contents, $I_D = 0.3$ and 0.5

Tests with no liquefaction or sudden failure just after a few cycles are not included in the regression analysis. Also not included are results from S3RM since in the majority of the tests on this type of mixture only minor excess pore water pressures was observed.

5.5 Long term cyclic response of unsaturated material

5.5.1 Stress-strain curves and accumulated strain

Series of cyclic tests were performed on various sand rubber chips mixtures under dry and wet conditions. The relative density I_D varied and was the same as in the standard monotonic triaxial tests. In the cyclic tests, a static deviatoric stress was applied prior to cyclic loading. Post cyclic monotonic tests were performed to evaluate the effect of cyclic loading on shear strength. The stress-strain curves for the entire test is presented in Figure 51. The developed strain vs. time curves are plotted together with average values in Figure 52. It can be seen in Figure 51 for S2RM specimens that the static strain level above which the cyclic phase starts is different in the various individual tests. This strain level mainly depends on the rubber chips content. The same was observed for S3RM and S4RM.

Figure 52 plots the accumulated cyclic axial strain vs. cycles number for pure dry sand S2 during the first 50 cycles. The average strain values at the end of each cycle are also plotted. For ease of discussing the effect of rubber chips on the developed axial strain, values at the end of each cycle (average value) are plotted in Figure 53 for S2RM, S3RM and S4RM. Generally, increasing the rubber chips content increases the accumulated axial strain of the composite material. This is obvious, because rubber chips are compressible and may lead the composite material to be more deformable. The observed behaviour demonstrates the capability of the composite material to absorb energy induced by cyclic loading.

It was observed that S2RM and S3RM at 0% chips content exhibit almost similar axial strains. This is because both are uniform sandy material. S4RM exhibits higher axial strain compared to uniform sand. This implies that the cyclic load yields a better densification in non-uniform material than in uniform material, which is well-known. The axial strain from sand rubber chips mixtures at 10% chips content demonstrates that S2RM generates lower strain compared to that of S3RM which is lower than that of S4RM. A small amount of rubber chips initially added to sand S2 reduces its voids ratio in contrast to sands S3 and S4. S4RM at 30% chips content exhibits smaller strains compared to that at 20%. Pure rubber chips exhibit smaller cyclic deformation compared to mixtures at

10% chips content. This indicates that increasing the rubber chips at higher contents beyond those used may increase the resistance to cyclic deformation.

It can be observed from all curves that the cyclic strains increase logarithmically with the cycles number. The respective equation (22) can be used to approximate the cyclic deformation measured in cyclic triaxial tests:

$$\varepsilon_{1,cy}[\%] = c_2 \cdot \ln(N) + c_3 \tag{22}$$

$N \geq 1$ is the number of loading cycles, a and b are the constants given in Table 10.

Table 10: Constants c_2 and c_3 for cyclic axial strain in equation (22)

χ [%]	dry S2RM		wet S2RM		loose and dry S2RM		dry S3RM		dry S4RM	
	c_2	c_3	c_2	c_3	c_2	c_3	c_2	c_3	c_2	c_3
0	0.017	0.147	0.03	0.0125	0.023	0.246	0.0384	0.244	0.011	0.187
10	0.060	0.511	0.065	0.31	0.099	0.623	0.144	0.581	0.087	0.728
20	0.100	0.583	0.136	0.51	0.288	0.94	0.175	0.698	0.181	1.092
30	0.196	0.707	0.25	1.06	0.346	0.743	0.171	0.660	0.22	1.092
100	0.155	-0.28					0.155	-0.28	0.155	-0.28

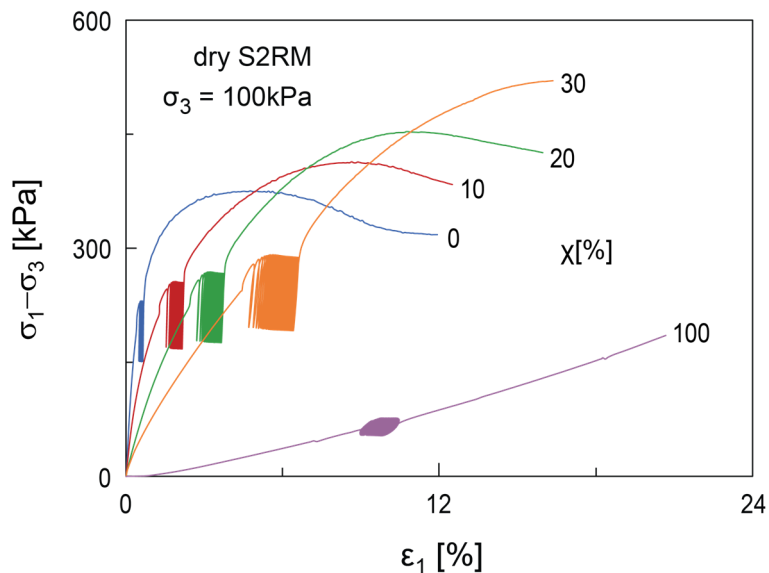


Figure 51: Stress-strain curves for pre-cyclic monotonic, cyclic and post cyclic monotonic test for dry S2RM

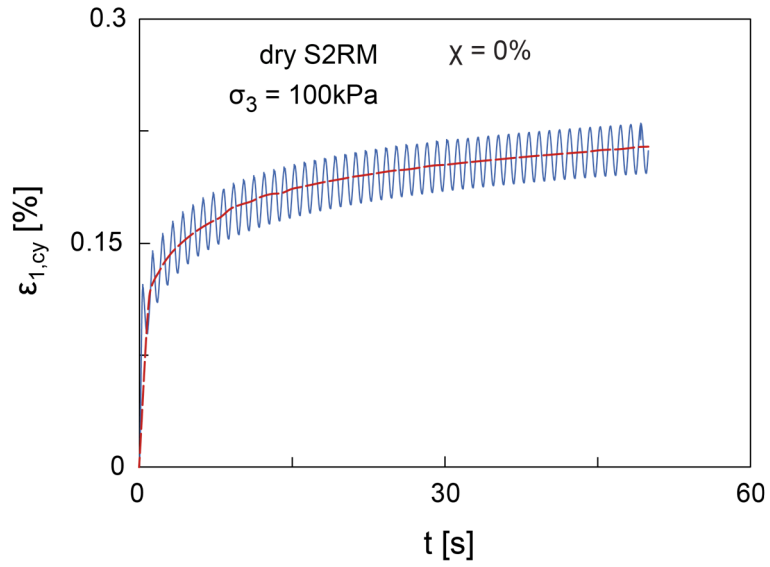
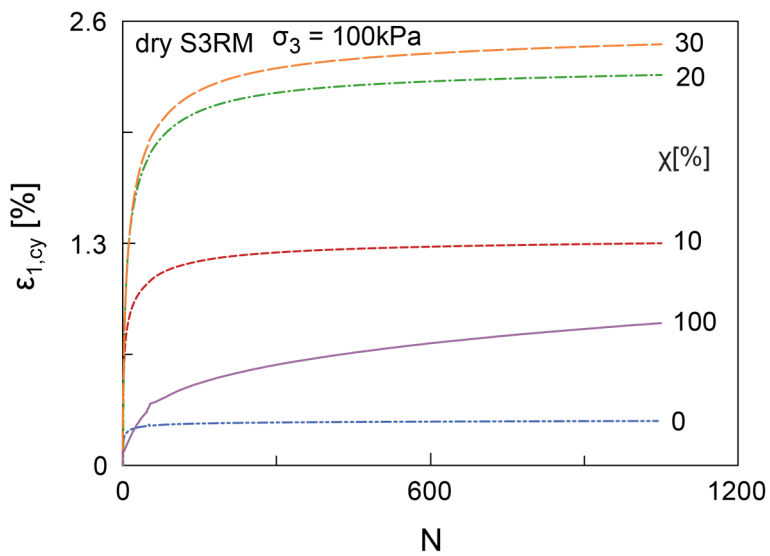
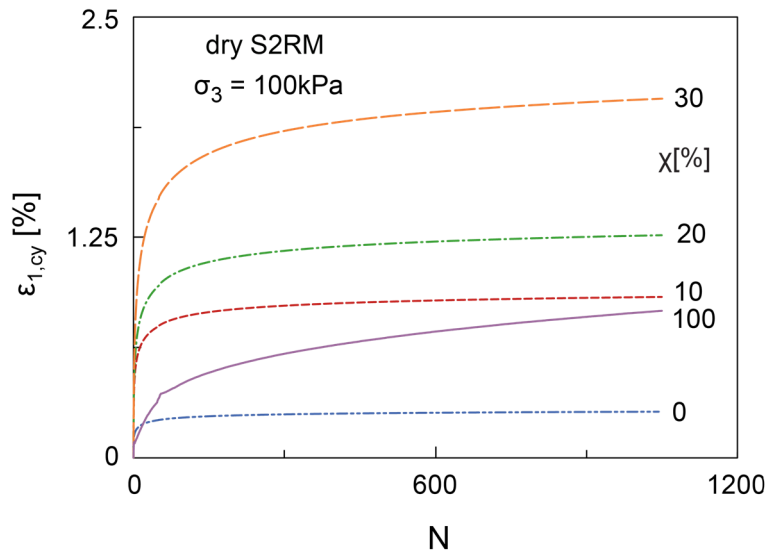


Figure 52: Evolution of cyclic strain with time over 50 cycles in dry S2RM



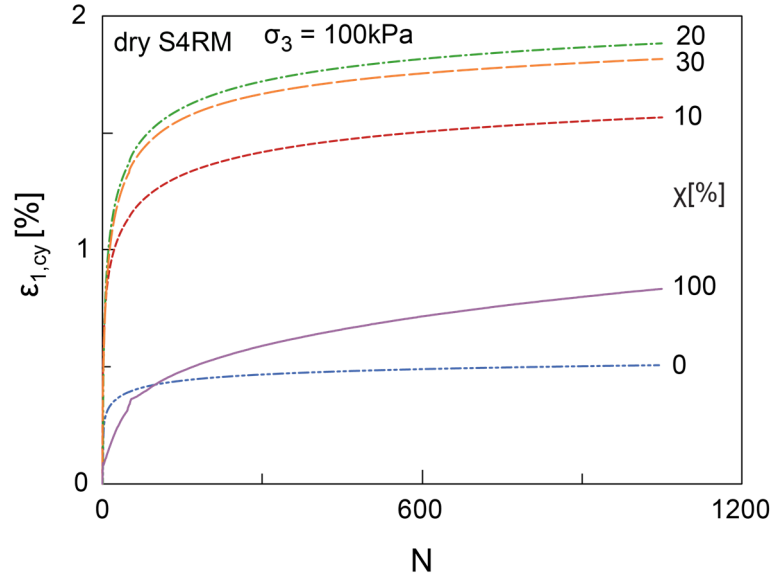


Figure 53: Average cyclic axial strains vs. number of cycles for dry S2RM, S3RM and S4RM at various chips contents

5.5.2 Young's modulus and damping ratio

Dynamic Young's modulus E_d vs. number of cycles N and damping ratio D vs. N are presented in Figure 54 for dry S2RM and in Figure 55 for dry S4RM. It can be seen in these figures that E_d increases and D decreases with the number of cycles; except for the specimens made only of rubber chips. This is due to densification of the granular material resulting in an increase in material stiffness. It can also be observed that increasing the rubber chips content in the mixtures decreases E_d and increases D . The results for wet S2RM not shown herein follow the same trend. Surprisingly, pure rubber chips specimen exhibits slightly minimum damping ratio compared to that of sands at 20% chips content but still higher than that of SRM at 0 and 10%. The cyclic tests on pure rubber chips yielded $E_d = 3.2$ MPa ($G_d = 1.21$ MPa) which is approximately 90 times lower than the corresponding value of pure sand. Stable values of E_d and D were reached after approximately 200 cycles. The same was observed for S3RM. Whenever required, one may calculate the secant shear modulus and shear strain using equations (15) and (16), respectively, assuming Poisson's ratio between 0.3 and 0.4 for dry conditions. The relationship given in equation (23) can be used to approximate the mixture stiffness with the parameters given in Table 11.

$$E_d[\text{MPa}] = c_4 \cdot \ln(N) + c_5 \quad (23)$$

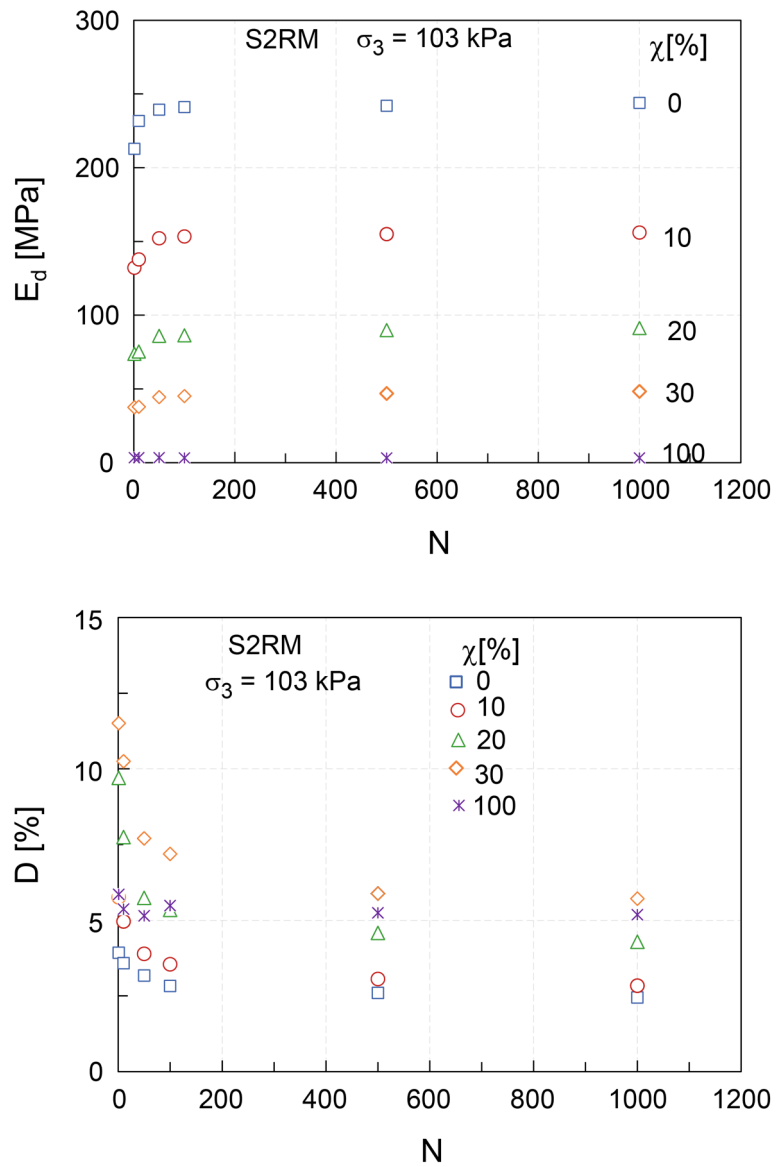


Figure 54: Cyclic Young's modulus vs. number of cycles and damping ratio vs. number of cycles for S2RM

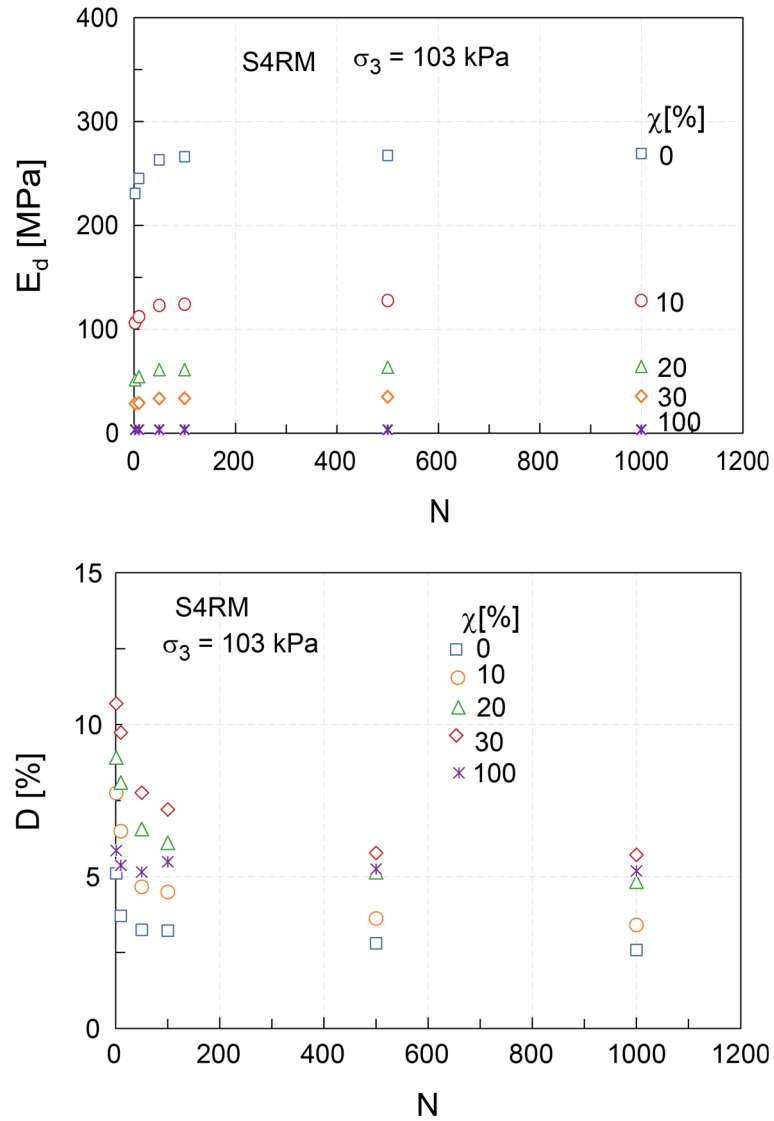


Figure 55: Cyclic Young's modulus vs. number of cycles and damping ratio vs. number of cycles for S4RM

Table 11: Parameters c_2 and c_3 for dynamic Young's modulus in equation (23)

χ [%]	dry S2RM		wet S2RM		loose and dry S2RM		dry S3RM		dry S4RM	
	c_4	c_5	c_4	c_5	c_4	c_5	c_4	c_5	c_4	c_5
0	4.28	218	2.855	231.4	3.31	150.5	3.5	231.6	6.19	231.4
10	3.77	132.7	2.86	130.8	2.94	94.8	4.06	116.2	3.68	104.8
20	2.81	72.5	2.40	64.7	2.63	49.8	2.67	45.5	2.16	50.3
30	1.71	36.4	1.56	34	1.15	24.3	0.01	26	1.27	27.1
100	-0.02	3.33	-0.02	3.33	-	-	-0.02	3.33	-0.02	3.33

5.5.3 Post cyclic shear strength

For all unsaturated specimens post cyclic, strain controlled monotonic tests were performed applying a strain rate of 0.1mm/min. The stress at failure was taken equal to the peak deviatoric stress or the maximum value at 15% axial strain whichever occurs first. Figure 56 compares the stress-strain curves for standard single stage triaxial test and the triaxial test at multi-stage, i.e. static, cyclic and post cyclic static, on a duplicate specimen for S2RM at 10% chips content. It can be seen that both tests followed nearly the same lines but with the post cyclic static curve slightly higher than that of the standard single stage triaxial test. The effect of cyclic load on post cyclic shear strength is visualized in Figure 57 for dry S2RM at various chips contents. It can be seen that cyclic loading contributes to the increased post cyclic shear strength compared to that of common single stage triaxial tests. The same behaviour, not shown herein is observed for the data from wet S2RM and dry S4RM. A marginal or no effect was observed for the S3RM.

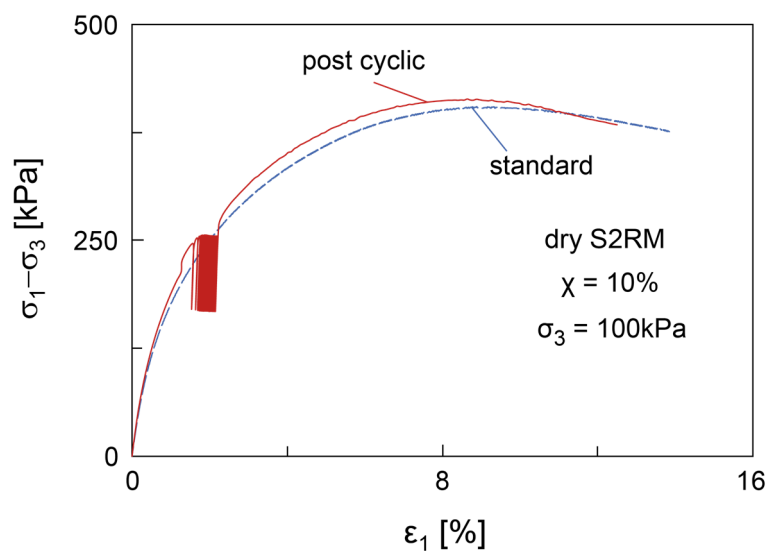


Figure 56: Comparison of stress-strain for standard and post cyclic static triaxial tests for S2RM

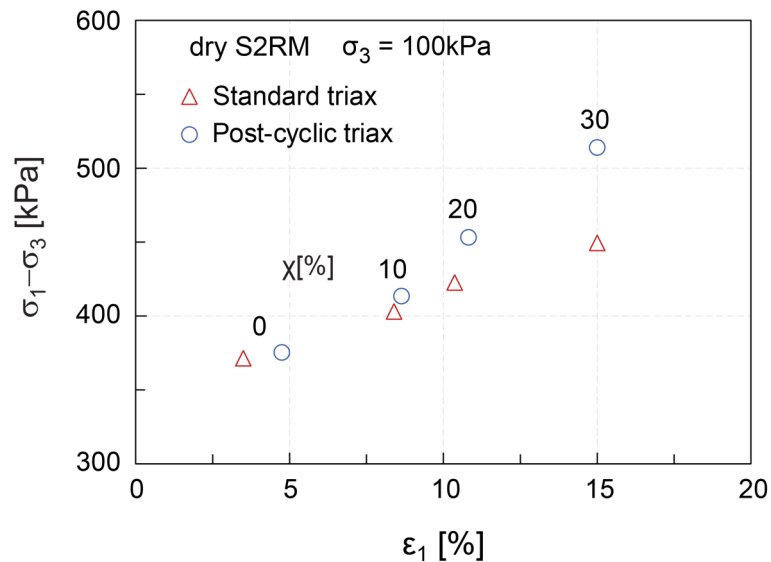


Figure 57: Maximum static shear strength from standard and post cyclic triaxial tests for dry S2RM at various chips contents.

5.6 Sample conditions before and after cyclic testing

Sand rubber chip specimens before and after undrained cyclic testing were subjected to a freezing process to allow cutting and visual observation of the mixture formation. Samples were initially frozen for 2 hours on the base pedestal of the triaxial equipment using dry ice as shown in Figure 58 prior to further freezing in the freezer for 2 days under -20°C . The frozen samples were cut longitudinally in order to identify the position and orientation of the rubber chips and the overall formation of sand rubber chips mixtures. It is clear from Figure 59 that compacting the wet mixtures does not alter the mixture formation. During sample preparation the rubber chips take various random positions and orientations. As can be seen in Figure 60 there is no evidence of rubber chips movement within the liquefied specimen.



Figure 58: Sample freezing left dry ice and right a two days frozen sample in freezer after sample preparation



Figure 59: Sand S2 at 30% chips content before test



Figure 60: Sand S2 at 30% chips content after cyclic test

5.7 Discussion

Cyclic strength was determined from a series of tests on saturated and unsaturated sand rubber chips mixtures at various rubber chips contents under different loading conditions. For saturated undrained tests, isotropically consolidated medium sand S2 specimens subjected to various cyclic stress ratio confirmed that that increasing *CSR* reduces the cyclic resistance. Obviously the increase of the relative density increases the resistance to liquefaction of sand.

For saturated sand rubber-chips mixtures, anisotropically consolidated and cyclically loaded under undrained condition, adding 10% chips increases the cyclic axial strains and decreases the resistance to liquefaction. For tests under drained conditions, adding chips up to 20% chips increases volume change and cyclic axial strain. This behaviour was observed in all sands at the selected relative densities of 30% and 50%. This can be due to the decreased density and lower ductility of the composite material. Further increase of chips increases the resistance to liquefaction, and decreases the axial strain and the volume change. Cyclic resistance for pure sand S2 at $I_D = 0.5$ is higher than that of sand with at 30% rubber chips. Pure sand S3 at I_D of 0.3 and 0.5 as well as sand S3 at 30% chips content did not liquefy. This implies that the inclusion of chips contents beyond those used in this study may yield a higher resistance to liquefaction and decrease in cyclic deformation.

For saturated specimens, anisotropically consolidated and cyclically loaded under drained conditions, cyclic loading initiated excess pore water pressure that

yielded liquefaction in some of the specimens. This may be caused by the high amplitude and the relatively high loading frequency (1 Hz) applied. It can also be due to the reduced rigidity and low ductility of the material, particularly for sand rubber mixtures. For the specimens that did not liquefy, the excess pore water pressure initiated at the beginning of cycling dissipated after some number of cycles.

The increase of the resistance to liquefaction, decrease of axial and volumetric strains for the mixtures at higher rubber chips content is associated with the increased ductility in the composite material. This in turn also prevents liquefaction flow failure. The increase of the resistance to liquefaction may also be attributed to the rigidity of rubber chips which is lower than that of sand. The dynamic Young's modulus and damping ratio from the cyclic triaxial tests under saturated condition reveal that increasing the rubber chips decreases the modulus and increases damping. For higher chips contents the results show the stabilization of shear modulus value after a large number of cycles.

For unsaturated material, increasing the number of loading cycles increases the cyclic deformation, increases the dynamic Young's modulus and decreases the damping ratio. This may be attributed to the material densification during cyclic loading. Adding 10% rubber content decreases the material density, decreases the ductility thus resulting in increased cyclic deformation. A progressive increase of rubber chips content yields a continuous decrease of density and rigidity and compressibility resulting in an increase of the deformation.

It was observed that the material stiffness decreases and damping ratio increases for any inclusion of rubber chips in sand. It is known that soil material derives its damping from the friction between particles. Including rubber chips in sand increases the capability of the composite material to dissipate energy through the rubber particle deformation. The material densification induces the higher post cyclic shear strength compared to standard triaxial tests.

Rubber chips contents used were limited to 30% by dry mass. Higher values were not considered as they yield too high compressibility that restricts the application in practice. However, the findings from cyclic triaxial tests suggest that the chips contents beyond those used may increase the cyclic strength, and this would require a pre-load prior to construction activities. The findings from this study

suggest that rubber chips in sand may turn the mixture to excellent performance as foundation seismic isolation measure.

6 Resonant column tests

6.1 Equipment and calibration

6.1.1 Equipment

The dynamic response of the wet sand rubber chips mixtures was measured using a Stokoe-type resonant column device shown in Figure 61. This equipment was supplied by GDS. It comprises a drive system capable to excite a cylindrical sample in torsion or flexure. The drive system contains a drive plate that bears four magnets at its ends, see Figure 61. During torsional tests, four pairs of coils are coupled in series and apply a net torsion torque on the specimen. The excitation is induced by accelerometer connected to the top of the drive plate. Peak strain in torsion or flexure can be measured by a proximeter sensor and the axial deformation by a linear vertical displacement transducer (LVDT) mounted on the resonant column top plate. Each coil is associated with a sensor responsible for transmitting the sample response to the resonant column (RC) control box.

Specimen can be prepared on top of the solid base pedestal and the cell pressure is applied to the specimen through pressurizing fluid in a triaxial chamber by a 2 MPa pneumatic cell pressure controller. If saturated samples are considered, the saturation can be accomplished using both the 2 MPa pneumatic cell pressure and appropriate back pressure/volume controllers of 2 MPa. The back pressure and volume change can be measured by a built in sensor while pore pressure by an external pore pressure transducer connected to the base pedestal. The system has a high-speed 16-bit data acquisition system with control card and interface panel. This is directly connected to the computer through a USB from which a commercial software responsible for test control is running the system.

6.1.2 Device calibration

The fixed-free configuration is used. It corresponds to a cylindrical solid specimen of polar mass moment of inertia I , fixed at the base and excited by a torsional moment at the head induced by the accelerated weight of a drive system with polar mass moment of inertia I_0 , as can be seen in Figure 62. The latter includes the inertia of drive plate and the top cap connecting the drive head with

the soil specimen. If an additional plate (porous stone, perforated steel plate) is placed between the soil specimen and the top cap, its inertia is added to I_0 .

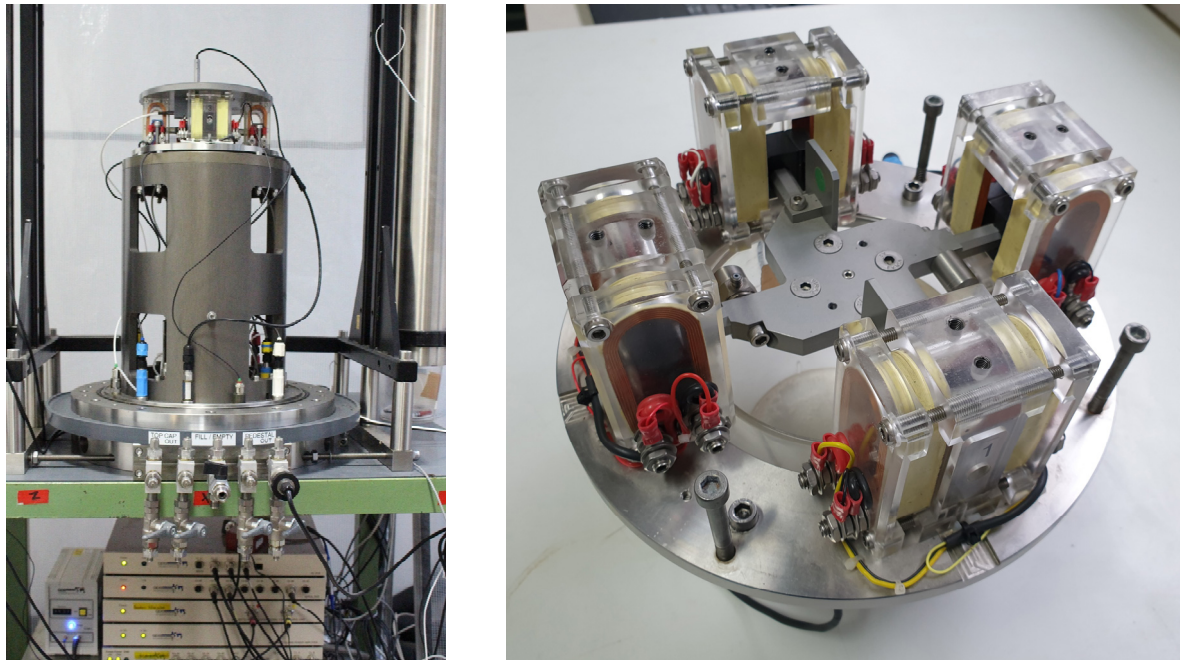


Figure 61: Fixed-free Stokoe-type resonant column apparatus (left) and the drive system (right)

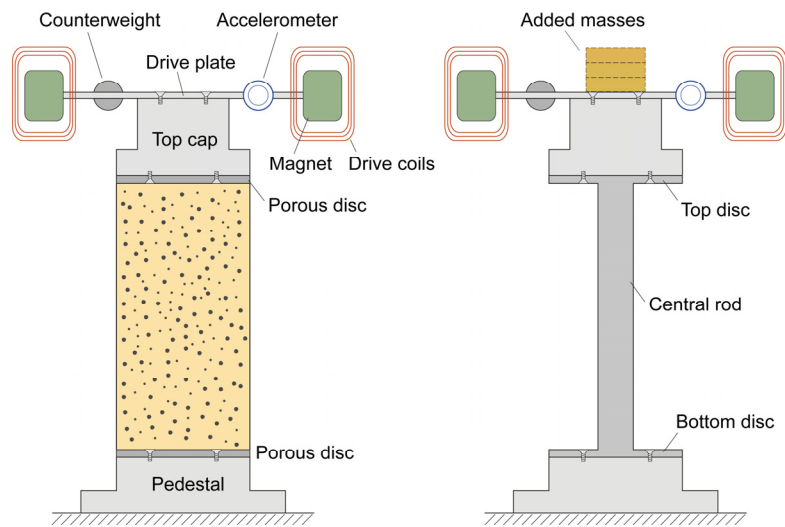


Figure 62: Section view of the resonant column device in the test (left) and during calibration (right), Vrettos & Banzibaganye (2022)

For linear elastic material behavior and purely torsional shear wave propagation (one dimensional) in the cylindrical specimen of diameter d and length l , the

equation relating the natural undamped circular frequency of the system ω_n to the shear wave velocity V_S in the specimen is given by (Richart et al., 1970):

$$\beta \cdot \tan \beta = \frac{I}{I_0} \quad (24)$$

where

$$\beta = \frac{\omega_n \cdot l}{V_S} \quad (25)$$

V_S may be written in terms of the shear modulus G and the mass density ρ

$$V_S = \sqrt{\frac{G}{\rho}} \quad (26)$$

In the test, the damped resonant frequency ω_r is measured rather than ω_n . For small values of damping ratio D (e.g. $D < 0.1$) we have $\omega_r \approx \omega_n$. β in equation (24) may be easily determined using the Excel Solver. A very good approximation may be derived that allows a fast, explicit calculation of the solution. Details are given in Vrettos & Banzibaganye (2022). While I for the cylindrical specimen is given in terms of its mass m and diameter d ($I = m \cdot d^2/8$), the determination of I_0 can only be performed experimentally by an appropriate calibration procedure due to the complex layout of the device (cross-arms, magnets, accelerometer, counterweight). The standard technique comprises a set of aluminum specimens with central rod and a disc at each of its two ends, see Figure 63. Aluminum exhibits very small damping thus justifying the assumption of linear elasticity. The calibration procedure is straightforward: The aluminum specimen is connected to the top cap of the drive head using screws. Masses (usually three) with known polar mass moment of inertia $\Delta I_{m,i}$ are sequentially added to the drive head, and the resonant frequency $\omega_{r,i}$ is measured. The top disc of the calibration specimen with polar mass moment of inertia I_1 is counted as an added mass too. For each distinct stage, the total moment of inertia can be given by the following:

$$I_{m,i} + I_1 = \frac{k}{\omega_{r,i}^2} - I_0 - \frac{I}{2.9} \quad , i = 1, 2, 3 \quad (27)$$

where $I_{m,i}$ is the total added mass inertia at stage i , I is the inertia of the central rod and k the torsional stiffness of the central rod. The contribution of I is

neglected in routine testing, thus assuming a SDOF system, since usually $I \ll I_0$ holds. The term I is however kept in the derivation.

By curve fitting the data set $(I_{m,i}; 1/\omega_{r,i}^2)$ using linear regression one determines pairs $(I_0; k)$ for each calibration specimen. The coefficient of determination is close to 1. I_0 is determined in this way for various calibration specimens of different central rod diameter, and a single average value is derived for subsequent use in soil specimen testing.

In a similar manner, one may determine I_0 from the frequencies measured at two configurations with different added masses of polar mass moment of inertia $I_{m,i} < I_{m,j}$ (Tatsuoka & Silver, 1980)

$$I_0 = \frac{I_{m,j} - I_{m,i} \cdot (\omega_{r,i} / \omega_{r,j})^2}{(\omega_{r,i} / \omega_{r,j})^2 - 1} - I_1 - \frac{I}{2.9}, \quad i < j \quad (28)$$

This approach yields for every calibration specimen different values for I_0 with non-negligible scatter and an averaging procedure is necessary to derive a single value.

Experimental evidence reveals that the variation of I_0 with frequency (different calibration specimens) is significant. Hence, when testing a wide range of soils, a function $I_0 = I_0(\omega_r)$ must be derived from the discrete set of values obtained for calibration bars of different central rod thickness, either by piecewise linear interpolation or by a global curve fitting equation (Clayton et al., 2009).

Calibration using common aluminium bars

The calibration procedure using the added masses is applied. The performance of the device was investigated for different specimen diameters but only the results for the 100 mm diameter specimen are presented herein. Several calibration bars were employed so as to cover the expected frequency range in the subsequent testing for pure soils and their mixture with tyre rubber chips, see Figure 63. The geometry of the calibration bars is defined in terms of the diameter of the top and bottom disc d_1 (equal to the nominal specimen diameter in soil testing) and the central rod diameter d . The bars used for $d_1 = 100$ mm had $d = 10, 12.5, 15, 17.5, 20, 22.5, 25$ and 30 mm. The standard test method based on sweeping the frequency around resonance was applied. Damping was

determined by the free-vibration decay method. For complete operational details it is referred to the handbook provided by the manufacturer (GDS Instruments, 2015).



Figure 63: Various aluminium calibration bars used for the calibration

Three weights of known mass moment of inertia were successively added to the drive head. Applying equation (27) with the assumption that $I \ll I_0$ holds for all calibration bars yields for each bar the inertia of the drive head I_0 . The curves $I_{m,i}$ vs. $1/\omega_{r,i}^2$ are customarily plotted in a single graph for all calibration bars, as done herein in Figure 64, and fall on almost straight lines with a coefficient of determination close to 1.

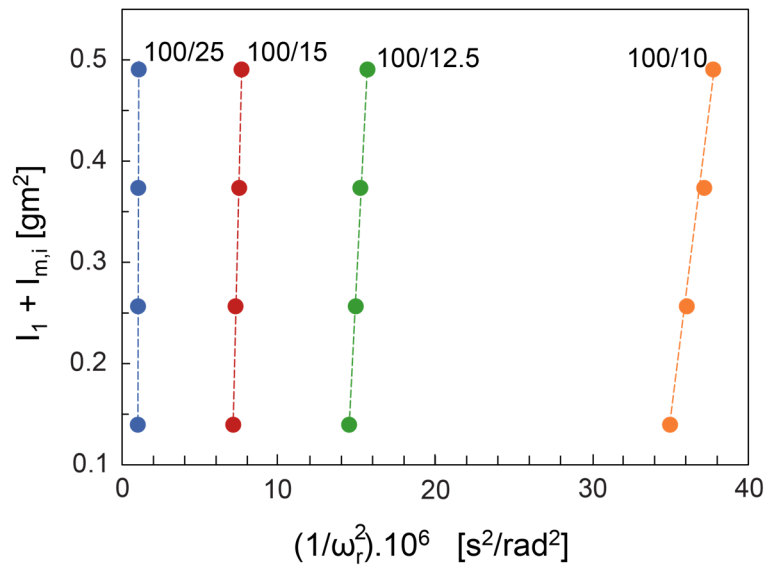


Figure 64: Results of the calibration using added masses for 100 mm bars. Curve labels indicate d_1/d in mm and the dashed lines are for the regression based on equation (27).

At the end of the calibration, the values of I_0 for the drive plate as function of frequency for 100 mm diameter specimens for all calibration bars starting from the thinnest were deduced. These are shown in Figure 65. A linear interpolation of I_0 between distinct values is applied during the data reduction in the soil tests.

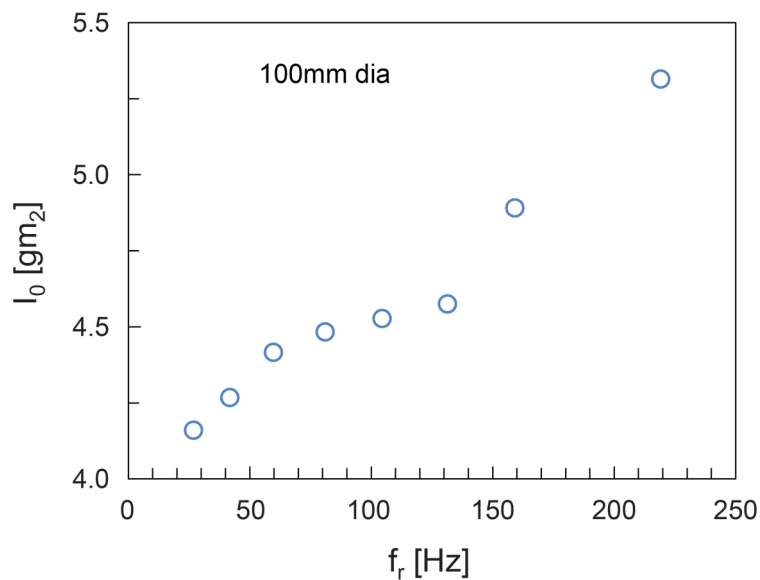


Figure 65: Drive head inertia vs. resonant frequency as determined by the calibration approach using added masses for the 100 mm specimen size.

6.2 Sample preparation and testing method

Specimens of 100 mm diameter and 200 mm in height were prepared following the standard procedure described in ASTM D 4015 - 15e1 (2015) that requires the specimen diameter to be at least six times the largest particle size. The preparation technique is described by Banzbaganye et al. (2019). Material tested comprises a) pure sands S2, S3 and S4, b) mixtures of these sands with rubber chips at 10, 20 and 30% content. Wet tamping was applied to prevent segregation of particles. The total target mass of the sample was divided into five equal portions, each transferred in a sample preparation mould and compacted to achieve a thickness of 40 mm totalling 200 mm. A small vacuum of approximately 10 kPa was applied to ensure the stability of the specimen during the removal of the mould as well as the connection to the drive plate. Figure 66 shows the test specimen at 10% rubber chips content.

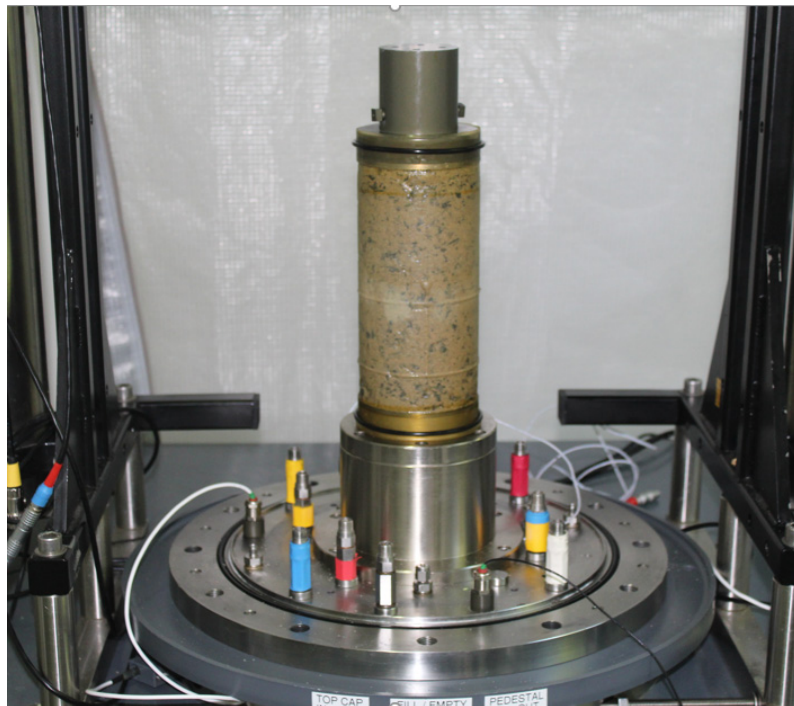


Figure 66: Test specimen before starting the resonant column testing

Some of the specimens containing higher concentration of rubber chips under this vacuum experienced a higher axial compression which required an adjustment of the level of the coils. In general, sand S3 at 30% chips content was soft and the tests were stopped at intermediate strain amplitudes. The tests on sand S3 at 20% and 30% under confining stress of 300 kPa yielded contact between the magnets and the bottom part of the coils and were cancelled. The

target relative density in all tests was $I_D = 0.5$. The test data are summarized in Table 12 where ρ_d is the dry density of the composite material and χ the percentage of rubber chips.

Table 12: Sample properties and test conditions for resonant column tests

<i>Soil</i>	χ [%]	ρ_d [g/cm ³]	I_D [-]	Soil type	σ_3 [kPa]	G_{\max} [MPa]	D_{\min} [%]
S2	0	1.484	0.5	S2	50	63.2	0.37
					100	82.1	0.36
					200	117.8	0.29
					300	140.3	0.23
					400	160.9	0.35
	10	1.393	0.5	S2	50	38.2	0.76
					100	51.4	0.7
					200	70.1	0.63
					300	85.2	0.69
	20	1.287	0.5	S2	50	19.4	1.08
					100	27.7	1.1
					200	39.5	0.96
					300	48	0.98
	30	1.171	0.5	S2	50	10.2	1.88
					100	15	1.82
					200	22.3	1.8
300					28.3	1.8	
S3	0	1.558	0.5	S3	50	80.3	0.4
					100	111.7	0.4
					200	153.4	0.4
					300	183.8	0.37
					400	213.6	0.38
	10	1.365	0.5	S3	50	28.7	0.87
					100	40.3	0.83
					200	58	0.79
					300	69.2	0.68
	20	1.228	0.5	S3	50	14	1.6
					100	19	1.51
					200	29.3	1.4

	30	1.095	0.5	S3	50	5.3	2.39
					100	8.3	2.35
					200	14.7	2.18
S4	0	1.615	0.5	S4	50	72.2	0.38
					100	97.7	0.38
					200	138.6	0.43
					300	170	0.39
					400	189	0.38
	10	1.436	0.5	S4	50	33.7	0.86
					100	44.2	0.79
					200	64.6	0.71
					300	77.8	0.66
	20	1.307	0.5	S4	50	15.1	1.08
					100	22.5	1.01
					200	33.5	0.96
					300	41.4	0.98
	30	1.189	0.5	S4	50	9	1.56
					100	13	1.52
					200	20.6	1.35
300					25.7	1.28	

Each solid specimen was consolidated to the specified cell pressure as given in Table 12. Tests were performed according to the specifications in ASTM D 4015-15e1 (2015). A harmonic torsional excitation was applied to the solid cylindrical specimen through the electromagnetic drive system. By monitoring the amplitude of the applied voltage and frequency, the maximum peak strain with the associated resonant frequency of the specimen are obtained.

A series of multi-stage tests were first performed and were followed by distinct single stage tests. In the multi-stage tests, the low amplitude tests (soil remains within the elastic limit) were conducted by stepwise increasing the effective confining stress in 50 kPa intervals up to 400 kPa. At each confining stress level (stage) the shear modulus is monitored at several strains within the elastic response range. Loading was stopped as soon as the modulus decayed approximately by 3%. The subsequent unloading (reduction of amplitude) to small strains with measurement of shear modulus provided a control that no degradation occurred. Cell pressure was then increased to the next higher level

and the test was repeated. For sand-rubber chips mixtures stages started from 50 kPa and went up to 300 kPa. In every testing stage the specimen was allowed to consolidate for a period of approx. 40 minutes to reach an equilibrium. For high-amplitude testing a fresh sample was tested at each distinct confining stress level. In intermediate strain testing a series of loading-unloading-reloading was performed in order to measure modulus degradation. The first unloading was performed at the beginning of the curve decay and then at $G/G_{\max} = 0.97, 0.9, 0.85$ and 0.80 .

6.3 Calculation for shear strain

As soon as the strain level exceeds an elastic threshold value, non-linear effects become evident by a reduction of the shear modulus and an increase of the damping ratio. The definition of the representative shear strain in the specimen requires some assumptions, since the induced strain field in the solid cylindrical specimen is inhomogeneous: it varies in the axial (x) and the radial (r) direction. The general case for the fixed-free configuration is considered, as reflected by equation (24). At the natural circular frequency ω_n , the distribution of the shear strain amplitude is expressed in terms of the twist angle θ :

$$\gamma(x,r) = r \frac{\partial \theta}{\partial x} = \frac{r \cdot \theta_l}{l} \cdot \frac{\beta}{\sin \beta} \cdot \cos\left(\frac{\beta \cdot x}{l}\right) \quad (29)$$

where $\theta_l = \theta(x=l)$ is the twist angle at the top of the specimen and β is defined by equation (25), see Vrettos & Banzibaganye (2022). If the inertia ratio I_0/I is sufficiently high, β is small and the terms containing β cancel which implies that the twist angle $\theta(x)$ varies linearly along the specimen axis, from zero at the base to a maximum θ_l at the head. The twist angle θ_l is determined in the test from the output of the accelerometer that is mounted on the drive head by taking into account the offset from the rotation axis and the corresponding conversion factors for the device (Drnevich et al., 1978).

Several rules have been suggested to calculate the equivalent homogeneous shear strain γ_{eq} of the specimen by defining an appropriate equivalent radius that is conveniently specified as fraction of the specimen radius r_0 :

$$\gamma_{eq} = \alpha \cdot r_0 \cdot \theta_l / l \quad (30)$$

The factor α commonly applied to the data reduction of the Stokoe-type apparatus (Isenhower et al., 1987) is based on the suggestion by Chen & Stokoe (1979) to set $\alpha = 0.82$ for shear strain amplitudes below 0.001 % and $\alpha = 0.79$ at 0.1%. These values were derived by a priori assuming suitable nonlinear stress-strain relationships for a variety of soils. Based on these findings, an average $\alpha = 0.8$ is recommended for routine testing by the ASTM D4015. This recommendation was applied in all tests.

6.4 Results for sands

6.4.1 Small strains response

Resonant tests were performed on the three sands S2, S3 and S4 specimens at various confining stress in the range of 50 to 400kPa. As mentioned above the values of I_0 were taken dependent on frequency according to Figure 65. At the low shear strain limit in the tests, the resonant frequency is determined from the readings at three slightly different input voltages to prove that no material degradation or slippage occurred. Table 12 summarizes the recorded values of G_{\max} and D_{\min} . Figure 67 plots G_{\max} vs. σ_0 for all sands as obtained from the multistage tests with stepwise increasing confining stress level. The well-known dependence of shear modulus on effective confining stress is confirmed in all test series. For the comparison with published experimental data on sand, the criteria for the selection are the median grain size d_{50} , the uniformity coefficient C_u , and the relative density in the tests as expressed by the void ratio e . The comprehensive databank by Wichtmann & Triantafyllidis (2009) encompasses a large variety of silica sands with some of them fitting into the grain size distributions investigated herein: sand S2 is similar to sand L3 ($d_{50} = 0.35$, $C_u = 1.5$), sand S3 close to sand L4 ($d_{50} = 0.6$, $C_u = 1.5$), and sand S4 similar to sand L11 ($d_{50} = 0.6$, $C_u = 2.5$). The data in that study are derived from the tests on a free-free type of resonant column device with specimen size 100 mm in diameter and 200 mm in height. In that study, numerical values for each particular sand are given by means of the general equation:

$$G_{\max} = A \cdot F(e) \cdot (\sigma'_0 / p_a)^n \cdot p_a \quad (31)$$

where $F(e) = (a-e)^2/(a+e)$, σ'_0 is the effective confining stress (cell pressure), p_a is the atmospheric pressure (100 kPa), and the constants A , a and n were

determined via curve fitting to the experimental data. For the three sands, the corresponding values A , a , n are as follows: L3: 1620, 1.77, 0.42; L4: 2023, 1.67, 0.41; L11: 2240, 1.47, 0.48, Wichtmann & Triantafyllidis (2009). The respective curves are included in Figure 67. The agreement with our results is very good for all three sands, at all confining stresses. The same holds for other specimen sizes. For details see Vrettos & Banzibaganye (2022).

The damping ratio at small strains has also been assessed. Equipment damping is a well-known source of potential error. The generation of a counter electromotive force in the magnets during the free vibration decay after the power is shut off at resonance is prevented by the software utilized for control and data acquisition of the device (GDSLAB). The apparatus damping is negligible as also confirmed in the very recent study by Facciorusso & Madiari (2020) on a similar Stokoe-type RC apparatus. In the soil tests the small strain damping ratio D_{\min} was less than 0.4 % with a slight tendency to decrease at higher confining stresses.

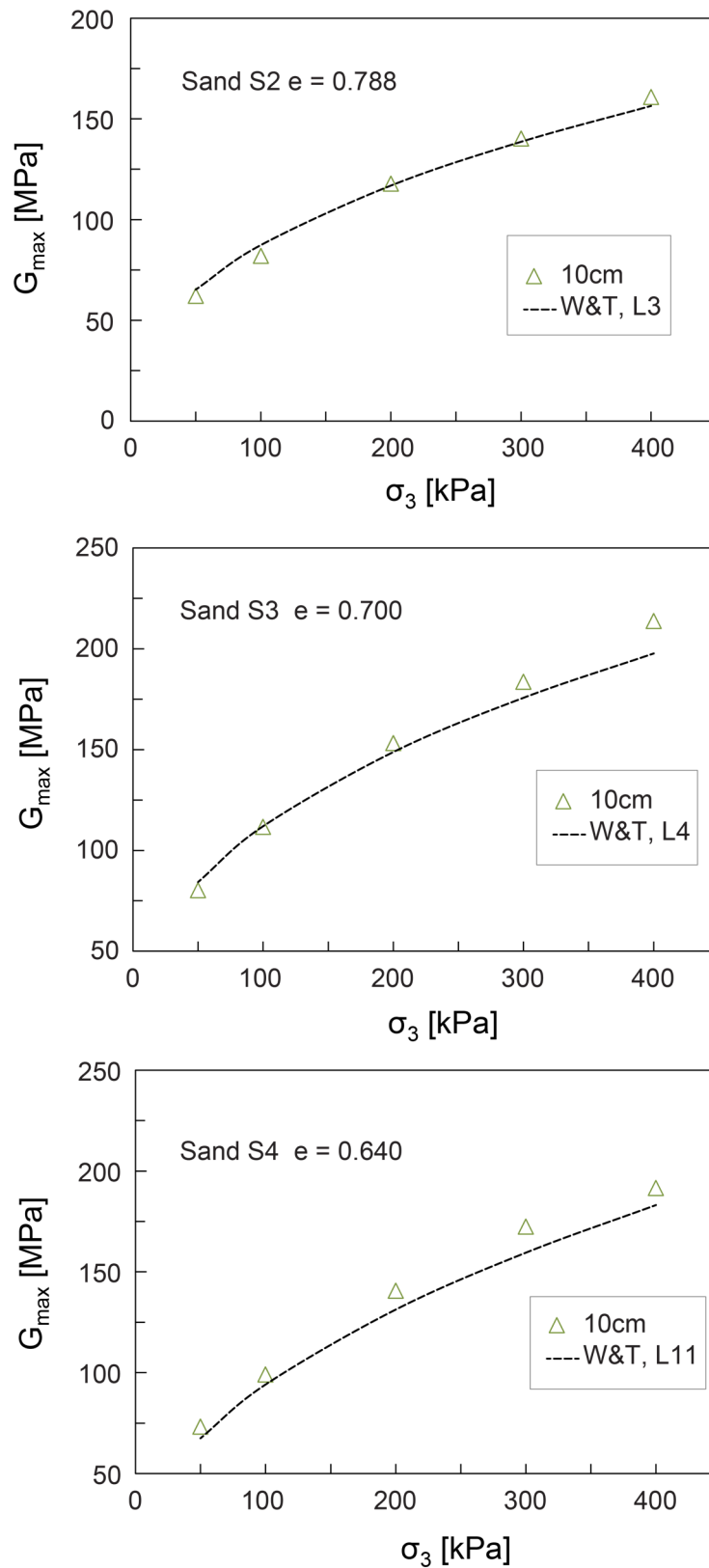
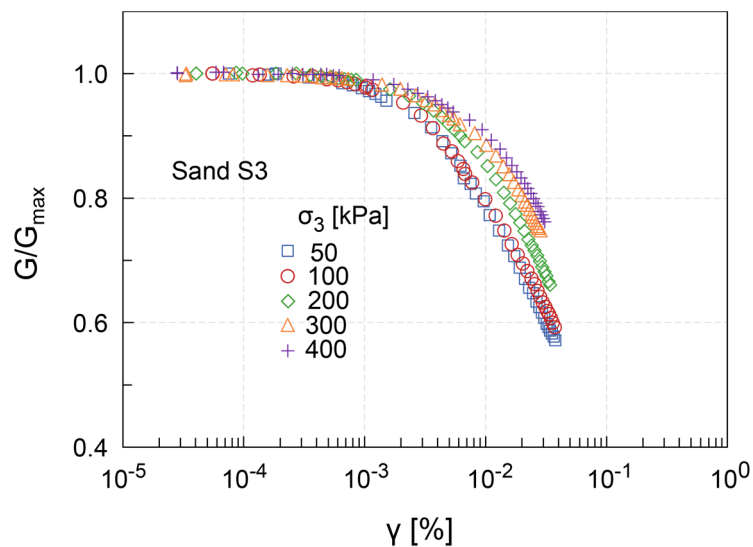
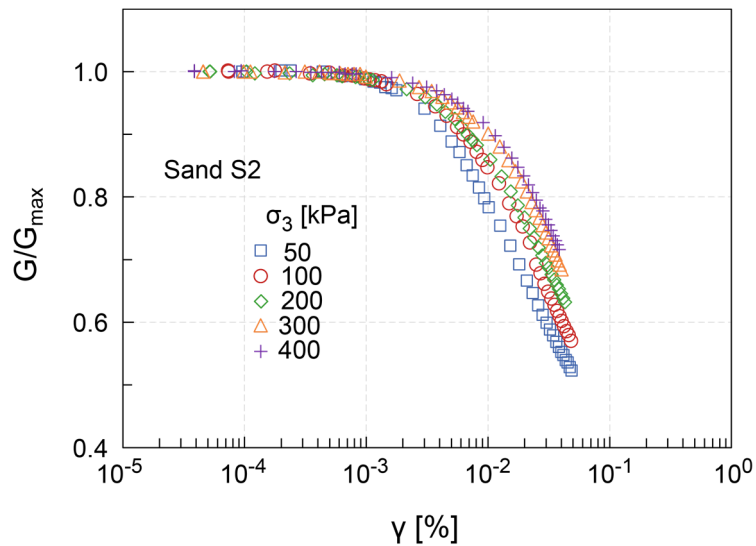


Figure 67: Maximum shear modulus vs. confining stress for the three sands. The dashed lines (W&T) are the data by Wichtmann & Triantafyllidis (2009)

6.4.2 Intermediate strains response

Figure 68 and Figure 69 present the shear modulus reduction and damping increase with shear strain amplitude for sands S2, S3 and S4. The curves were obtained at different confining stresses in a single stage testing. The results confirm the well-known trends that the shear modulus reduction becomes stronger as the confining stress decreases whereas the damping increases, see Figure 69. The influence of confining stress on the shear modulus reduction and damping ratio curves is further described in the next sections. It can be deduced from the results that the degradation of shear modulus is stronger as the sand becomes more non-uniform, increasing $C_u = 1.5, 1.7$ and 2.7 for S3 to S2 and S4 respectively, see Figure 70. This is in accordance with the findings reported in the comprehensive study by wichtmann & Triantafyllidis (2013) thus providing additional validation of the calibration and the testing procedure.



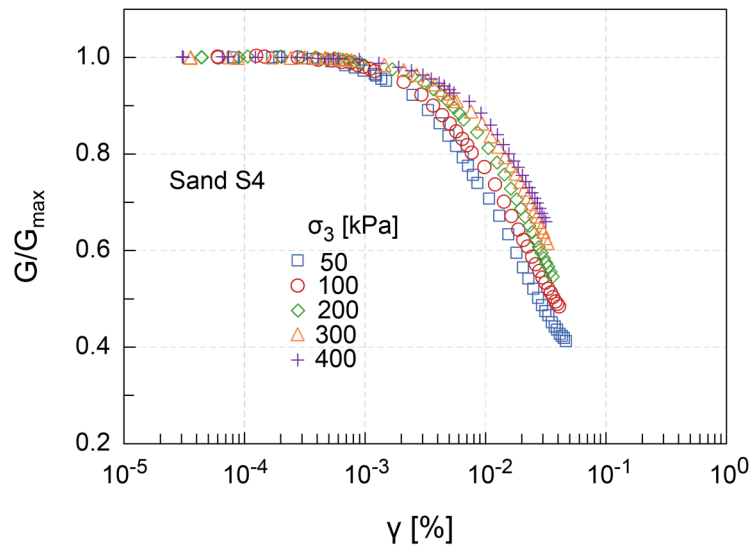
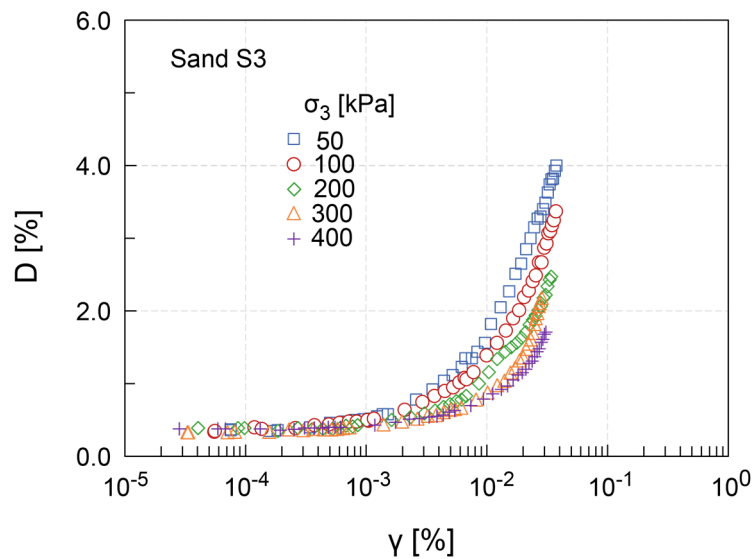
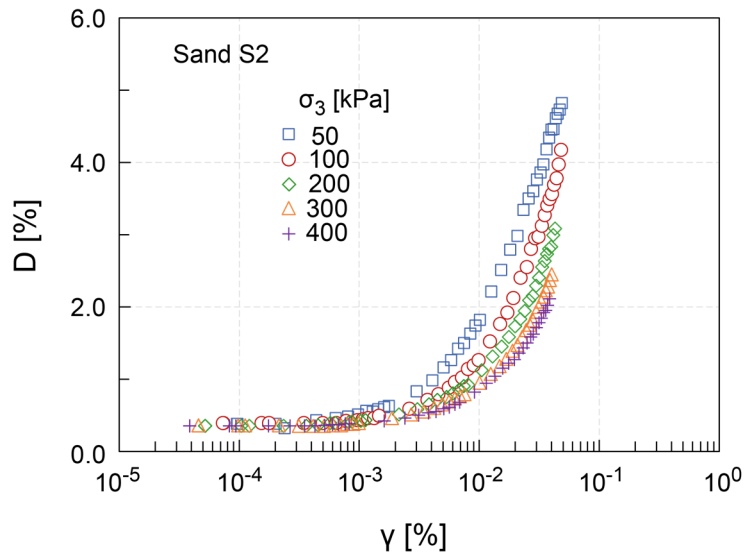


Figure 68: Shear modulus reduction G/G_{\max} vs. shear strain amplitude at different confining stresses for sands S2, S3 and S4.



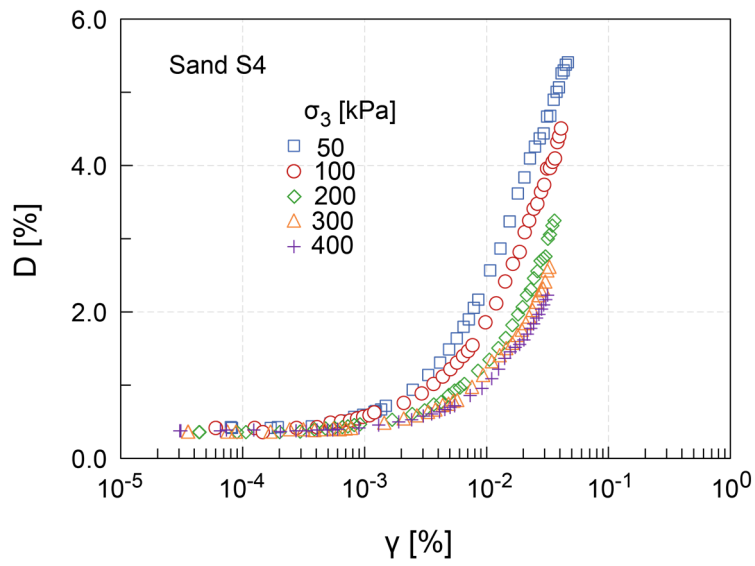
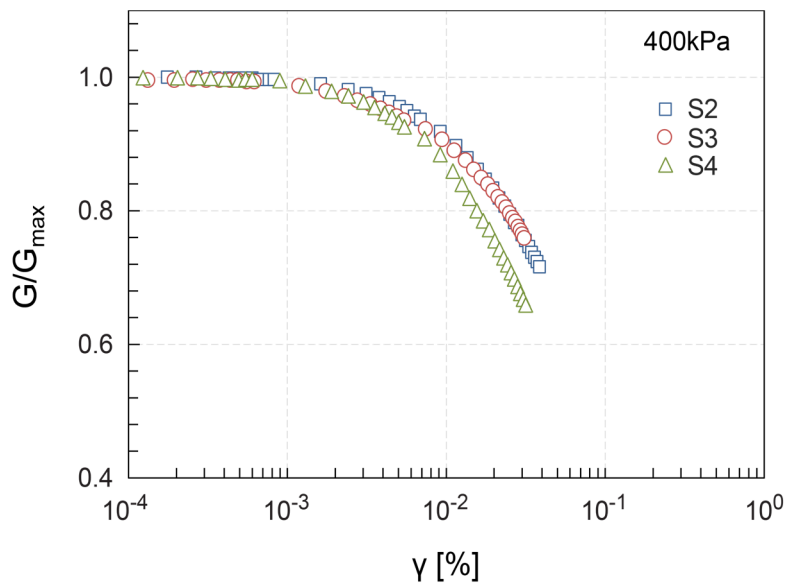


Figure 69: Damping ratio D vs. shear strain amplitude at different confining stresses for sands S2, S3 and S4



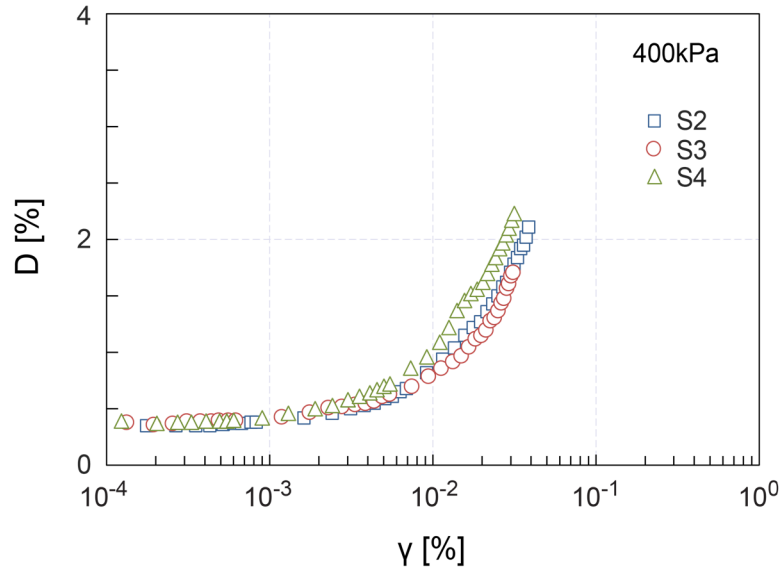


Figure 70: Shear modulus reduction G/G_{\max} and damping ratio vs. shear strain amplitude at confining stress of 400 kPa for sands S2, S3 and S4

6.5 Results for sand rubber mixtures

6.5.1 Small strains response

Values for the small strains shear modulus G_{\max} for sands S2, S3 and S4 mixed with rubber chips at different contents are given in Table 12. The respective shear strain amplitudes were in the order of 10^{-4} % for both the sands and their mixtures. As shown in Figure 71, G_{\max} increases with increasing confining stress and decreases with increasing rubber chips content. For pure rubber chips a shear modulus of around 1.2 MPa was obtained from cyclic triaxial tests (see section 5.5.2 in the present thesis) and similar values are reported in the literature by Anastasidis et al. (2009). The slower decrease of G_{\max} with strain compared to pure sand is attributed to the decreased density, increased elasticity and compressibility in the mixtures.

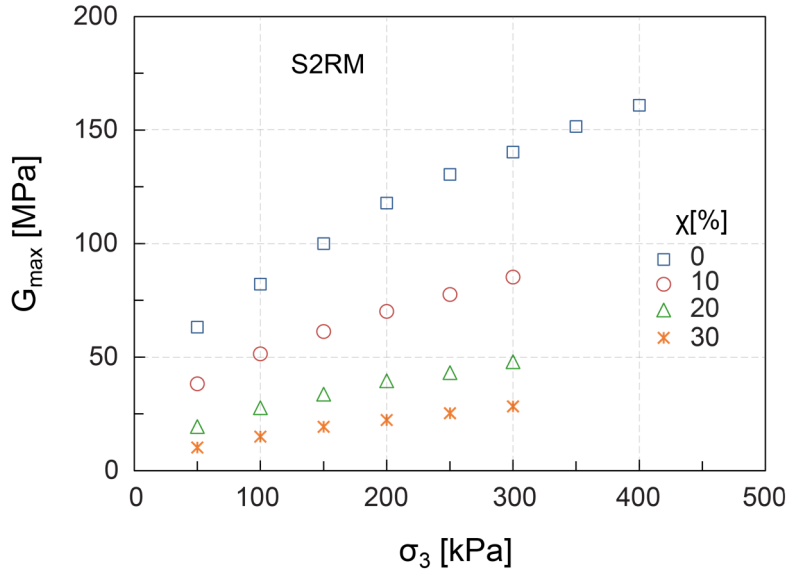


Figure 71: G_{\max} vs. confining stress for S2RM at different rubber contents; $I_D = 0.5$

It can be observed in Figure 72 that, as expected, pure sand with larger particles exhibit higher G_{\max} value compared to sand with smaller ones. Pure sand S3 with $d_{50} = 0.77$, tested at 100 kPa exhibits $G_{\max} = 111.7$ MPa, while sand S2 with $d_{50} = 0.32$ yielded with $G_{\max} = 82.1$ MPa, and sand S4 with $d_{50} = 0.5$ gives $G_{\max} = 97.7$ MPa. The addition of rubber material, for example 10%, yields a stronger degradation of shear modulus in sands with larger grain sizes. G_{\max} for these mixtures at a confining stress of 100 kPa is 40.3 MPa for S3RM, 51.4 MPa for S2RM and 44.2 MPa for S4RM. The reduction is approximately 64% for S3RM, 37% for S2RM and 54.7% for S4RM. The same is observed for rubber contents of 20 and 30% and at other confining stresses. These results suggest a better interaction of rubber chips and sand particles with smaller grain size. The increase of sand grain size results in a weaker interaction with rubber chips. It can be suggested that the response of the mixture at lower rubber contents is controlled by sand-to-sand contacts while at higher rubber contents the rubber-to-rubber contact strongly affects the overall behavior of the mixture.

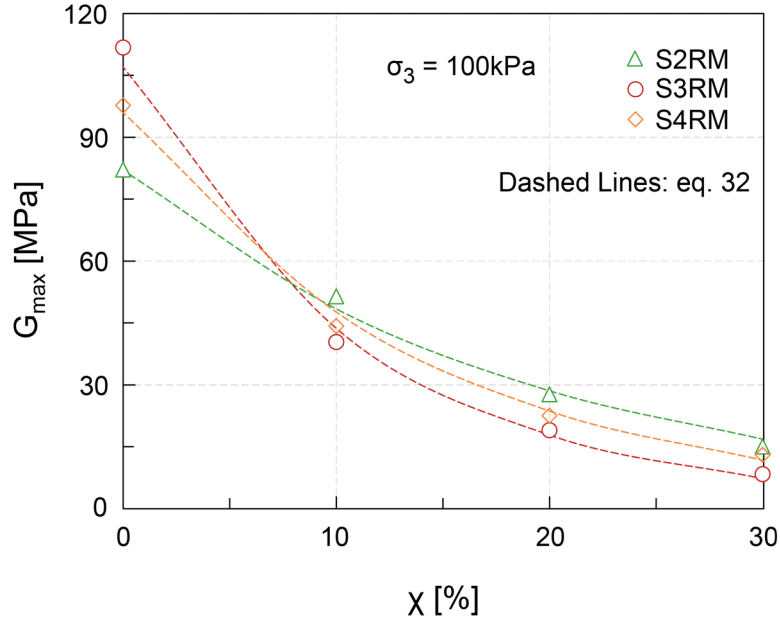


Figure 72: Maximum shear modulus vs. rubber chips content for different types of mixtures at 100kPa

From the experimental data a design equation for the stress-dependence G_{\max} is derived. A simple power law can be used with a fixed exponent equal to 0.5 which is widely accepted in soil dynamics (Handin, 1978). Curve-fitting yields equation (32) with the parameters summarized in Table 13 for different types of sand rubber mixture.

$$G_{\max} = A_G \cdot \exp(-d_G \cdot \chi) \left(\frac{\sigma_3}{p_a} \right)^{0.5} p_a \quad (32)$$

for $0 \leq \chi \leq 30\%$; $50 \leq \sigma_3 \leq 400$ kPa with χ in percentage.

Table 13: Constants for equation (32) for different types of sand rubber mixture

Material	A_G	d_G
Sand S2 & S2RM	820	0.0527
Sand S3 & S3RM	1070	0.0895
Sand S4 & S4RM	960	0.0700

This equation may be used to approximately predict the response at higher rubber contents that could not be measured due to the high compressibility of the mixture. For $\chi = 0.5$, the predicted G_{\max} for S2RM at 100kPa is 5.88 MPa instead of 82 MPa for pure sand. For S4RM G_{\max} at 100kPa reduces to 2.05 MPa instead of 96 MPa for pure sand. For S3RM at 100 kPa the predicted $G_{\max} = 1.21$ MPa

instead of 107 MPa for pure sand. These data show that already at this rubber content the material behaves almost similar to pure rubber chips. It can be seen from Table 13 that A and d increase with increasing median grain size of the sand.

The data for the minimum damping ratio D_{\min} show in Figure 73, as expected, a weak dependence on confining stress but a significant increase with the rubber chips content. For pure rubber chips, a D_{\min} value of around 6% was obtained from cyclic triaxial tests and similar values are reported in the literature (Anastasiadis et al., 2009). From the data sets $D_{\min}; \sigma_3$ a relationship is derived. Curve-fitting yields equation (33) with constants given in Table 14.

$$D_{\min}[\%] = A_D \cdot \exp(d_D \cdot \chi^{0.68}) \quad (33)$$

where χ is given in percentage, $0 \leq \chi \leq 30\%$; $50 \leq \sigma_3 \leq 400$ kPa

Table 14: Constants for equation (33) for different types of sand rubber mixture

Material	A_D	d_D
Sand S2 & S2RM	0.30	0.174
Sand S3 & S3RM	0.36	0.182
Sand S4 & S4RM	0.37	0.135

The G_{\max} and D_{\min} data with the predictions plotted in Figure 73 and Figure 74 for 100 kPa show an accuracy of the proposed design equations. The same trend was obtained for other confining stresses covered in this study.

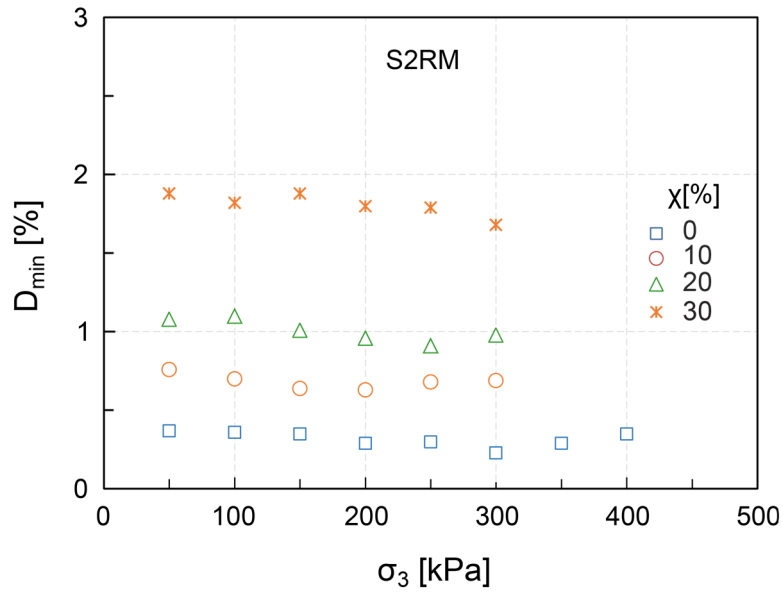


Figure 73: Minimum damping ratio vs. confining stress for S2RM at different rubber contents

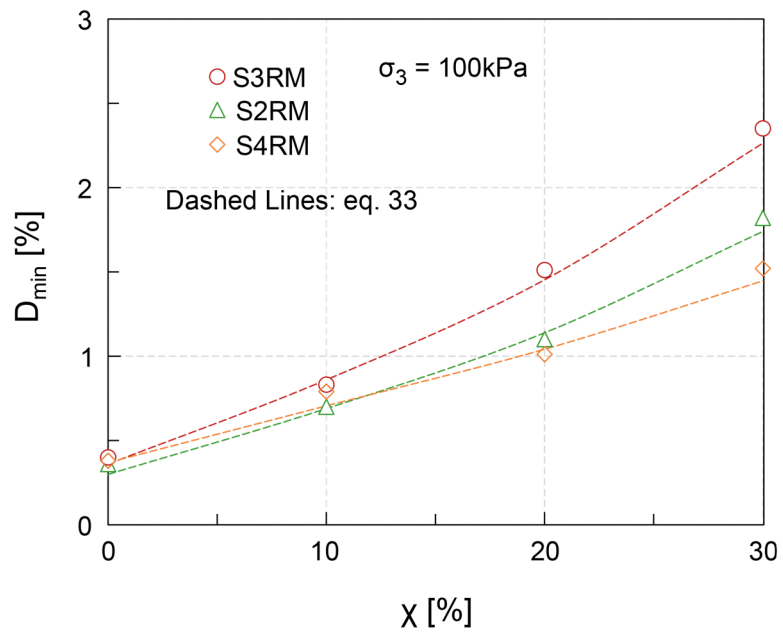


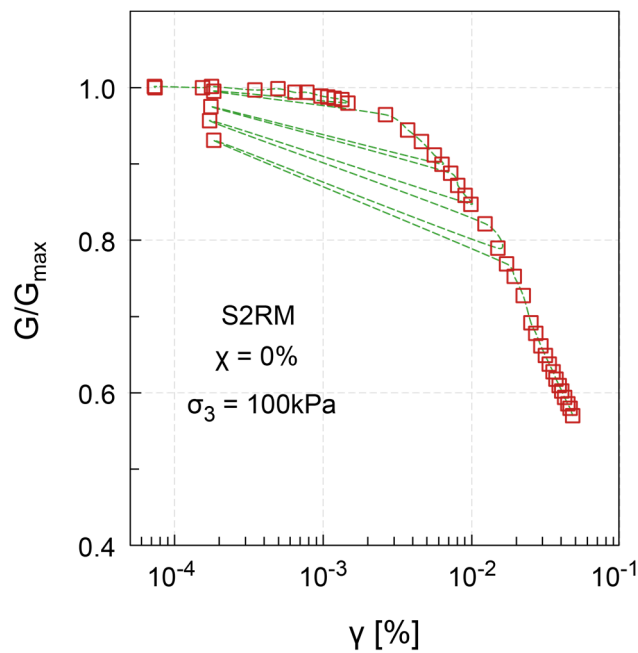
Figure 74: Minimum damping ratio vs. rubber chips content for different types of mixtures at 100kPa

6.5.2 Intermediate strain response

To evaluate the shear modulus and damping ratio of sand rubber mixtures at intermediate strain levels, higher amplitude torsional resonant column tests were performed at various mean confining stresses. Due to the large specimen size and inertia, the maximum attainable strain level in the specimen is limited. As

expected, the experimental results show a reduction of shear modulus and an increase of damping ratio after an elastic threshold shear strain is exceeded. It has been observed that increasing the confining stress increases the shear modulus (G) or shear modulus reduction (G/G_{\max}) and decreases the damping ratio (D). Increasing the rubber chips contents decreases G , increases G/G_{\max} and D .

During these tests, a sequence of loading-unloading-reloading were performed. Figure 75 displays typical results for S2RM at 0 and 10% chips contents at 100kPa. The results show that loading upto $G/G_{\max} = 0.97$ yields a small strain value of $G/G_{\max} \approx 1$ in unloading. Further loading reduced the small strain G/G_{\max} value. This is an indication of the elastic threshold shear strain amplitude that corresponds to the loading $G/G_{\max} \approx 0.97$. For S2RM at 0/10/20/30 % chips content this strain value is around $1.47 \times 10^{-3}/1.92 \times 10^{-3}/2.54 \times 10^{-3}/4.53 \times 10^{-3}$ %. These data show that increasing rubber chips content increases the elastic threshold shear strain. The increase is also noticed in other confining stresses. The same trend was obtained for S3RM and S4RM at different confining stresses. More results for the tests at 100 kPa can be seen in the appendix. These observations elucidate the role of rubber chips in the absorption of vibration energy.



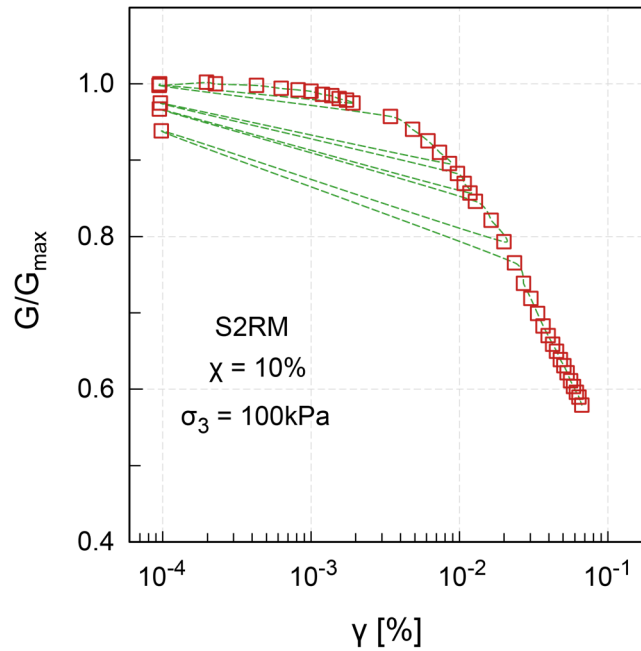


Figure 75: G/G_{\max} vs. shear strain amplitude for S2RM at $\chi = 0/10\%$, $\sigma_3 = 100\text{kPa}$

G/G_{\max} vs. $\log \gamma$ and D vs. $\log \gamma$ curves are plotted from Figure 76 to Figure 84. These curves were obtained from high amplitude tests at confining stresses from 50 up to 300 kPa for sand rubber mixtures specimens. The rubber chips contents used are 0/10/20/30% by dry mass, as before in the cyclic tests. The influence of confining stress on the behaviour of the mixture is presented in Figure 76 & Figure 77 for S2RM, Figure 78 & Figure 79 for S3RM and Figure 80 & Figure 81 for S4RM. It is inferred from these figures that, as expected, increasing the confining stress increases G/G_{\max} and decreases D for all specimens leading to a more-linear shape of $G/G_{\max} - \log \gamma - D$ curves. The extended range of linear behaviour refers to the increased shear strain amplitude before the G/G_{\max} value drops and at the same time the movement of the non-linear curve to the top right.

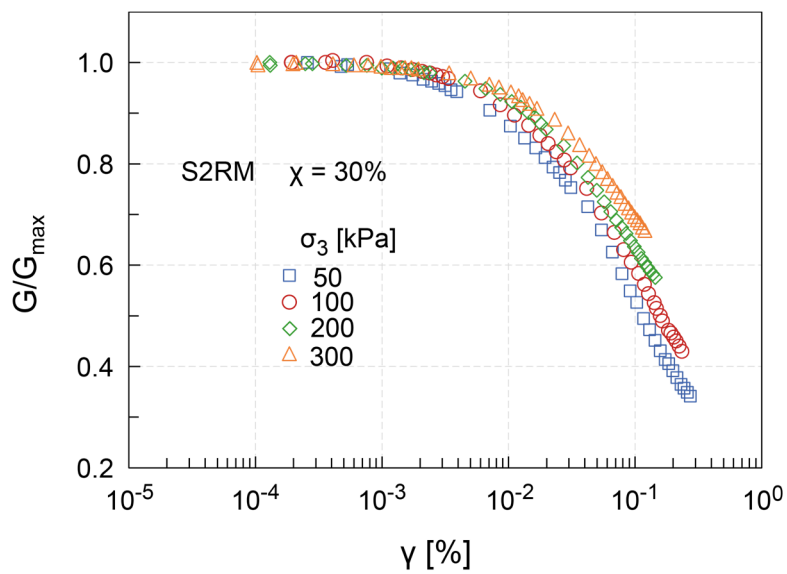
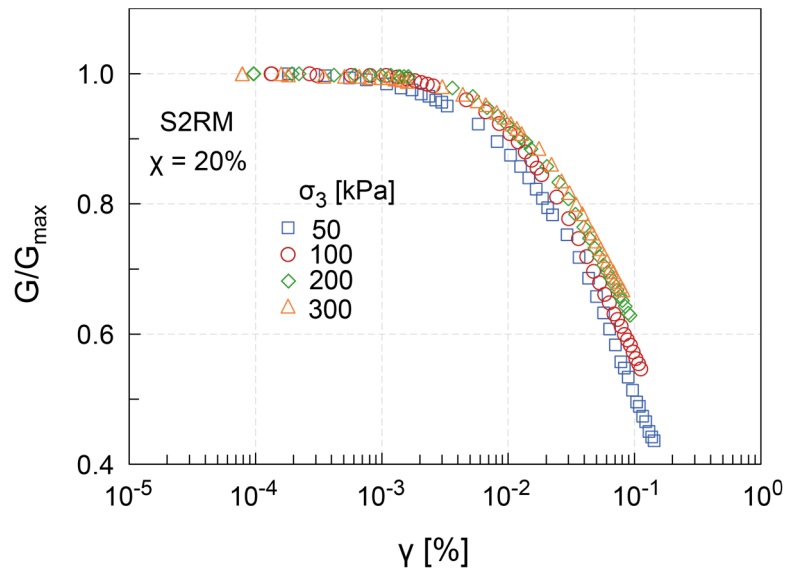
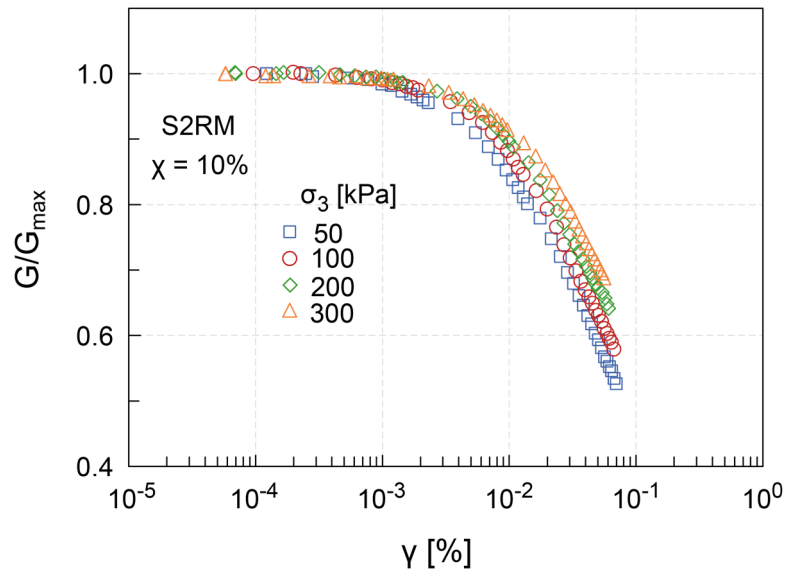


Figure 76: G/G_{\max} vs. $\log \gamma$ for S2RM at different confining stresses and at various rubber contents

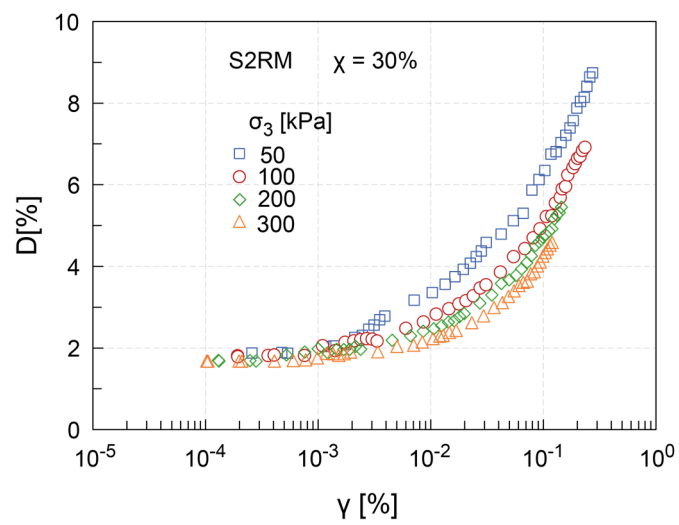
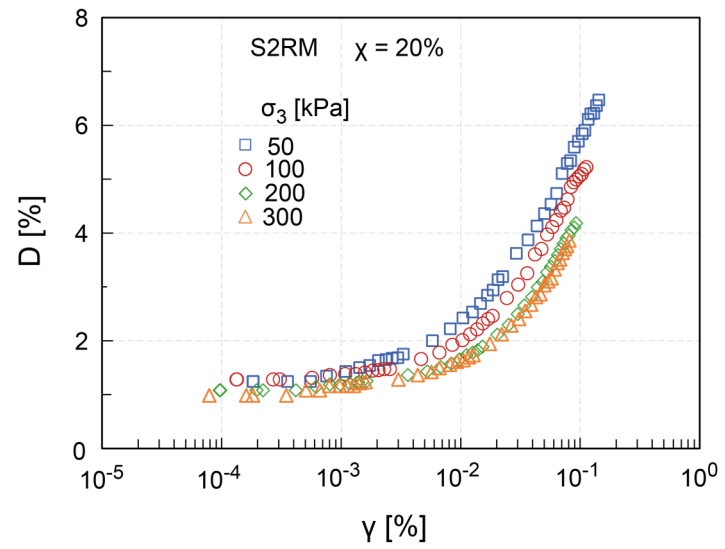
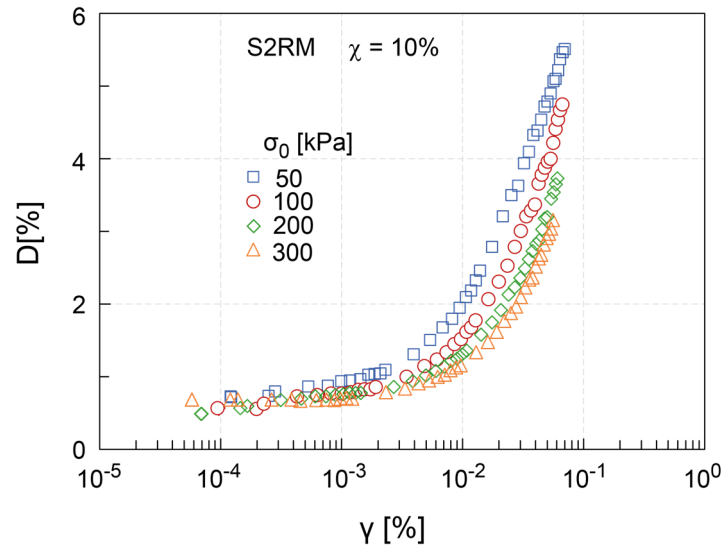


Figure 77: G/G_{\max} vs. $\log \gamma$ for S2RM at different confining stresses and at various rubber contents

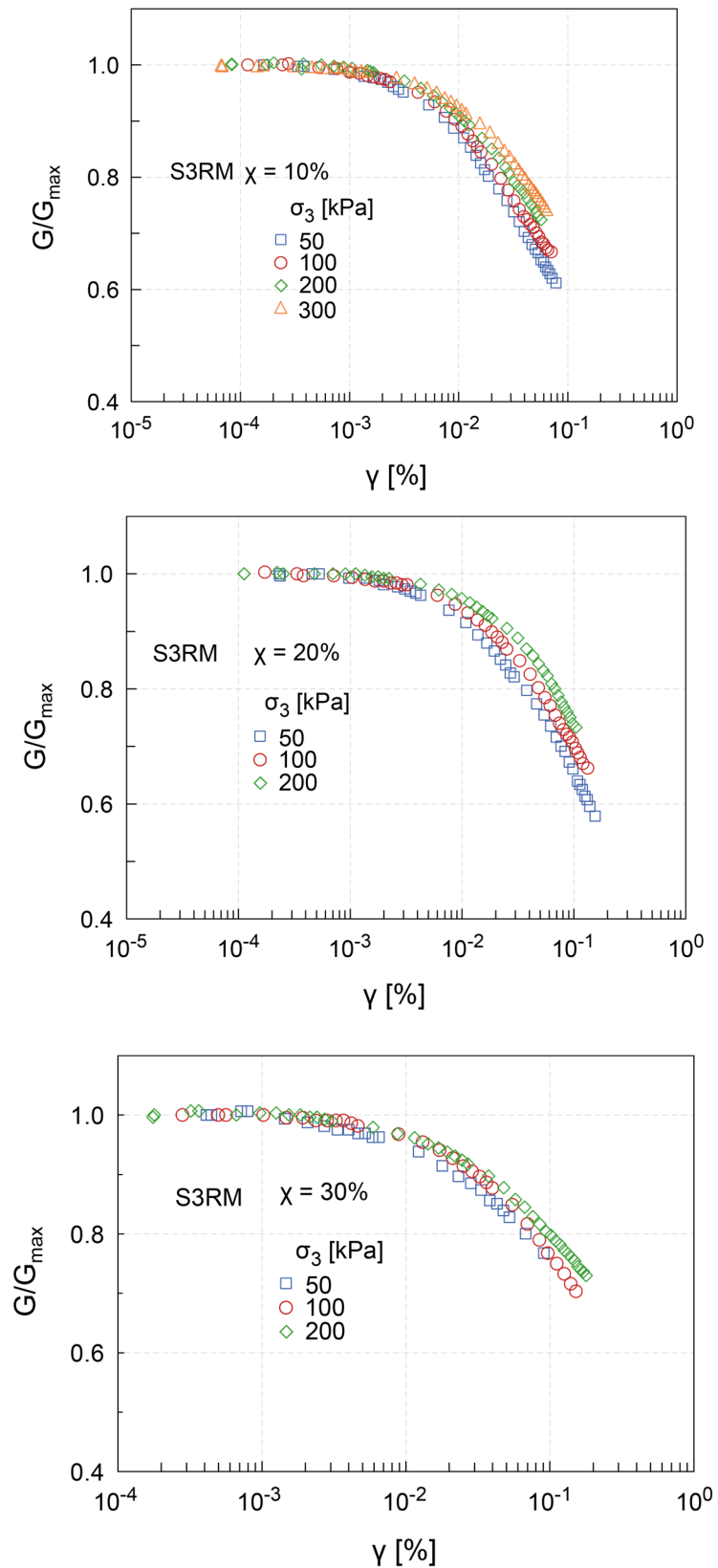


Figure 78: G/G_{\max} vs. $\log \gamma$ for S3RM at different confining stresses and at various rubber contents

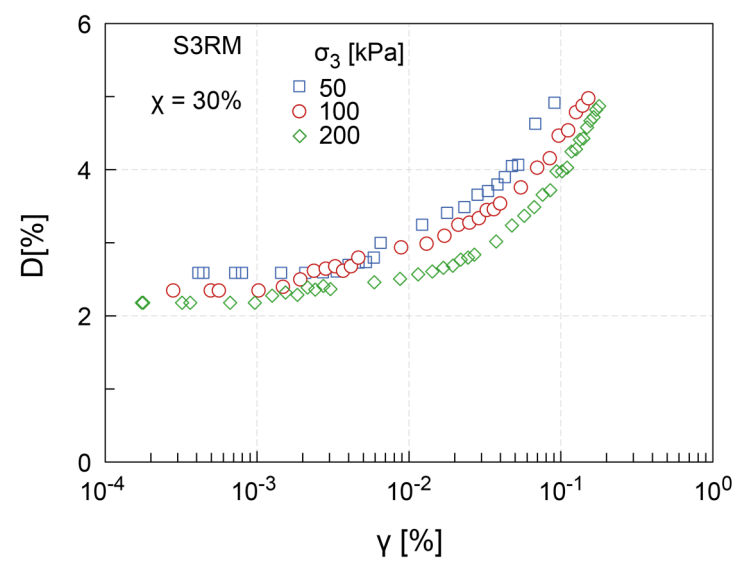
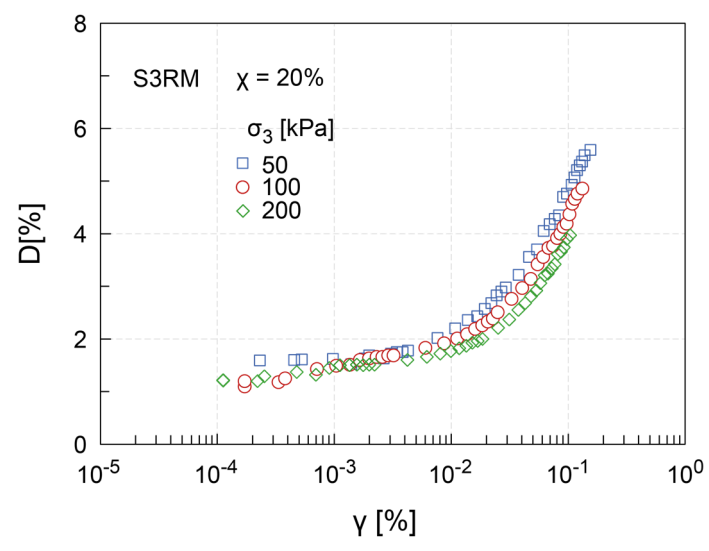
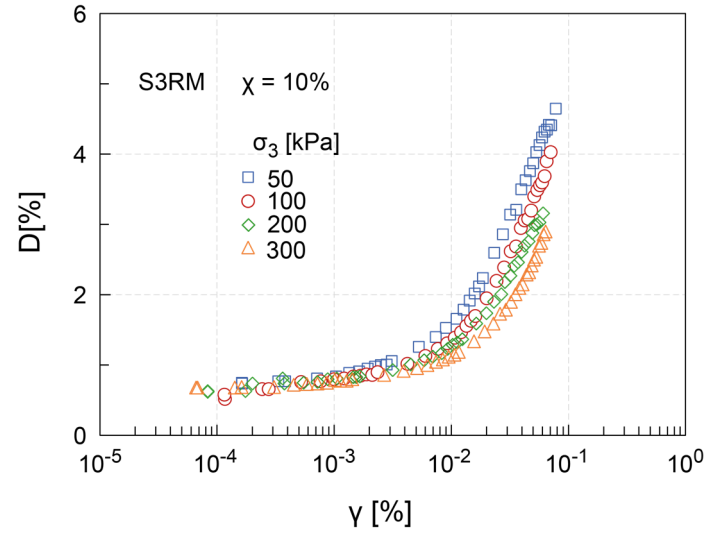


Figure 79: D vs. $\log \gamma$ for S3RM at different confining stresses and at various rubber contents

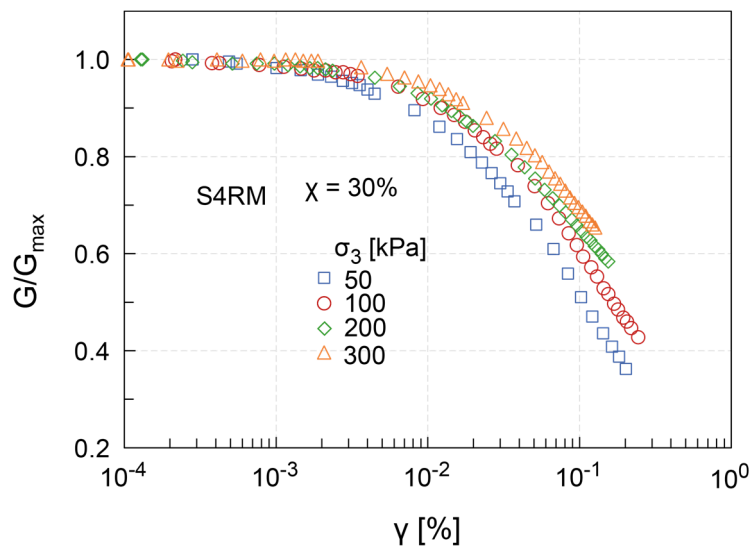
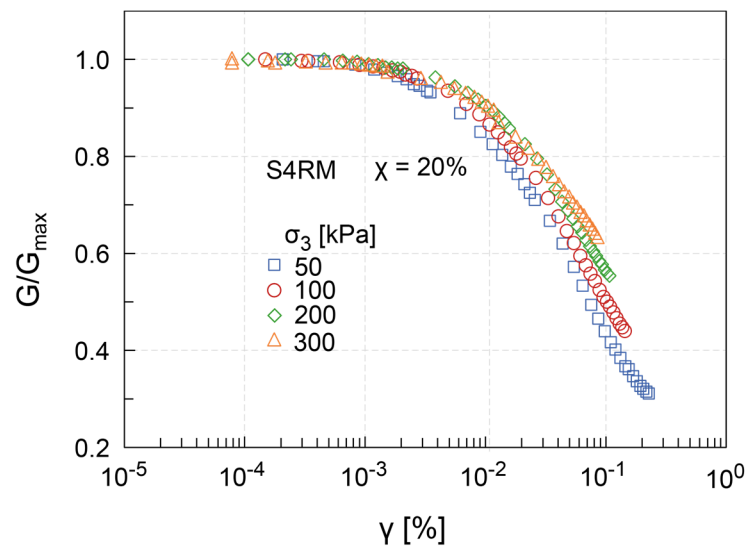
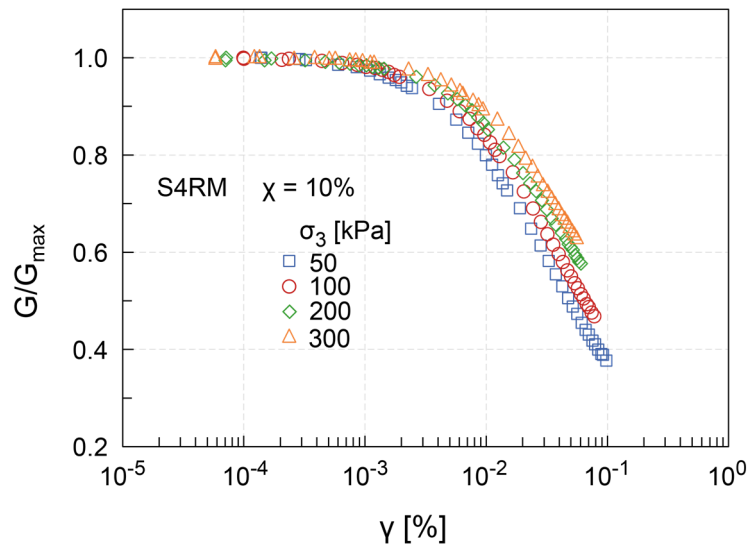


Figure 80: G/G_{\max} vs. $\log \gamma$ for S4RM at different confining stresses and at various rubber contents

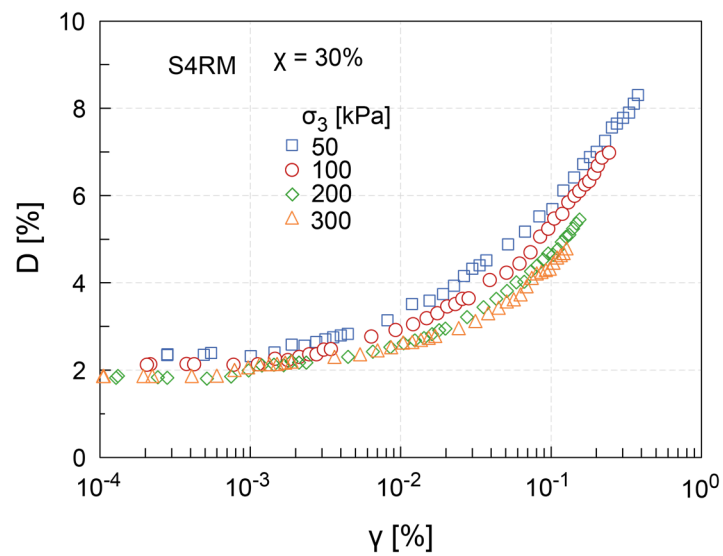
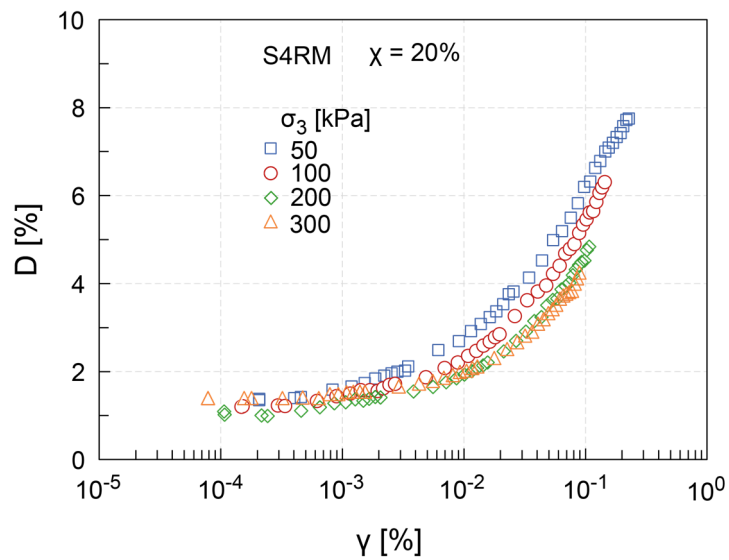
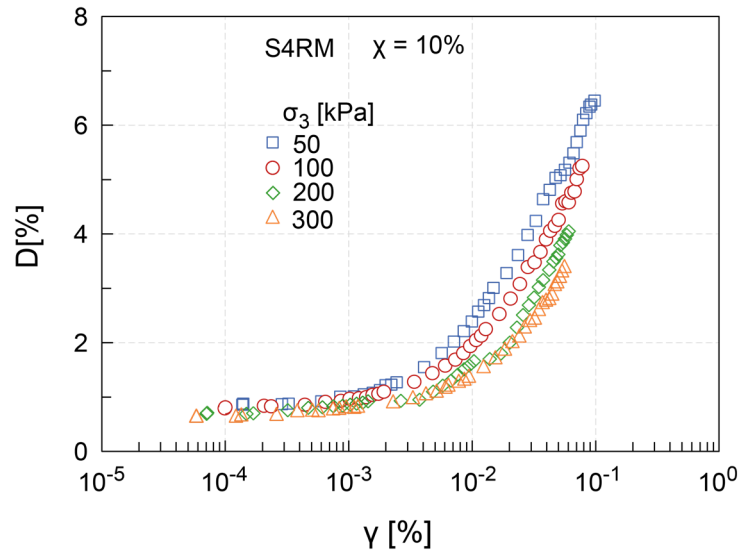


Figure 81: D vs. $\log \gamma$ for S4RM at different confining stresses and at various rubber contents

Figure 82 to Figure 84 display the effect of rubber chips content on the mixture's dynamic behaviour. The results are for the tests at 100 kPa. It is inferred from these figures that increasing the rubber chips content increases the shear strain amplitude. At any particular shear strain, increasing the rubber chips content increases both G/G_{\max} and D . Increasing the rubber content leads to the extended range of linear behaviour of the G/G_{\max} - and - D - $\log \gamma$ curves. This behaviour was also observed for the specimens at other confining stresses, i.e. 50, 200 and 300 kPa.

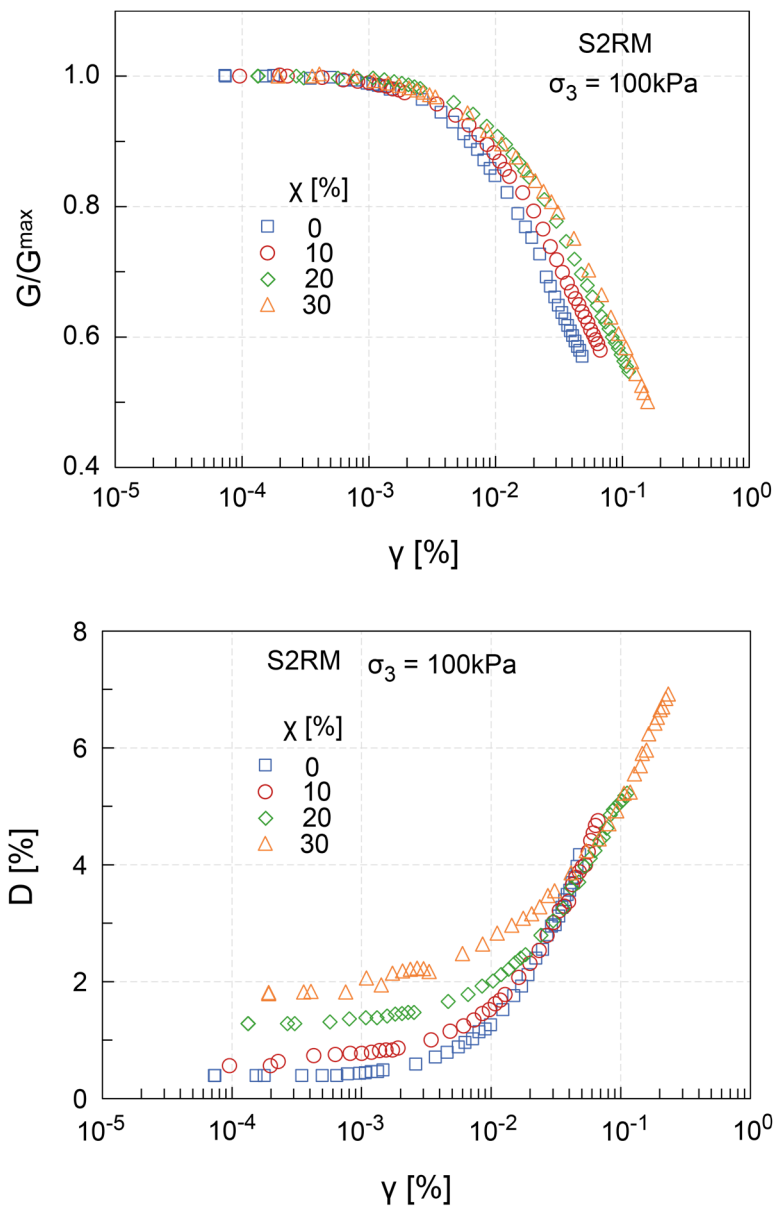


Figure 82: G/G_{\max} vs. $\log \gamma$ and D vs. $\log \gamma$ for S2RM at different rubber chips contents, $\sigma_3 = 100\text{kPa}$

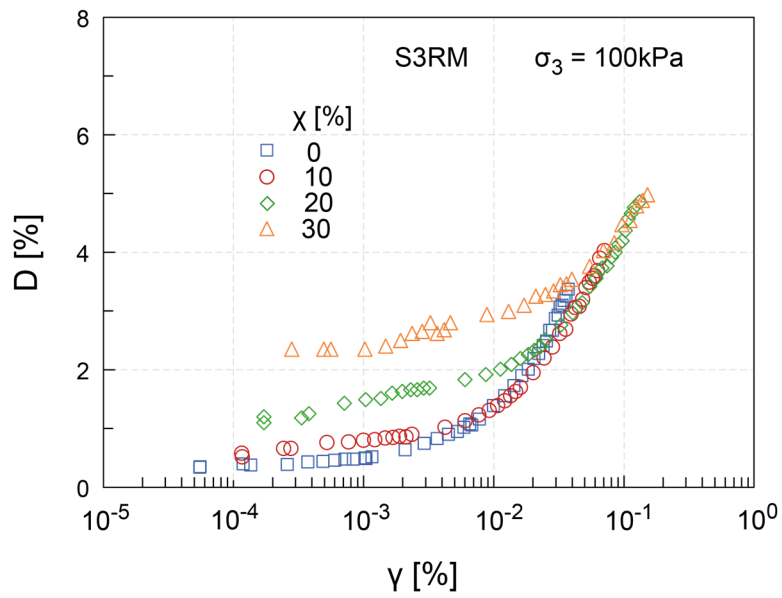
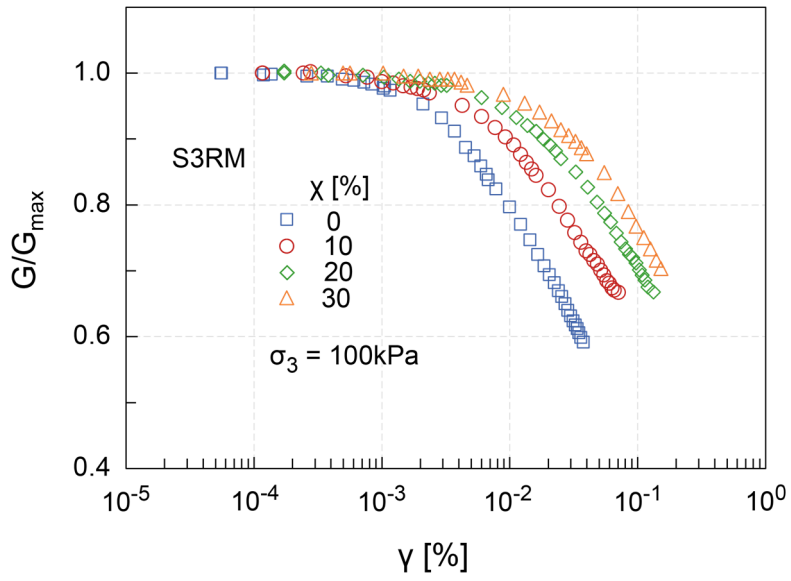


Figure 83: G/G_{\max} vs. $\log \gamma$ and D vs. $\log \gamma$ for S3RM at different rubber chips contents, $\sigma_3 = 100\text{kPa}$

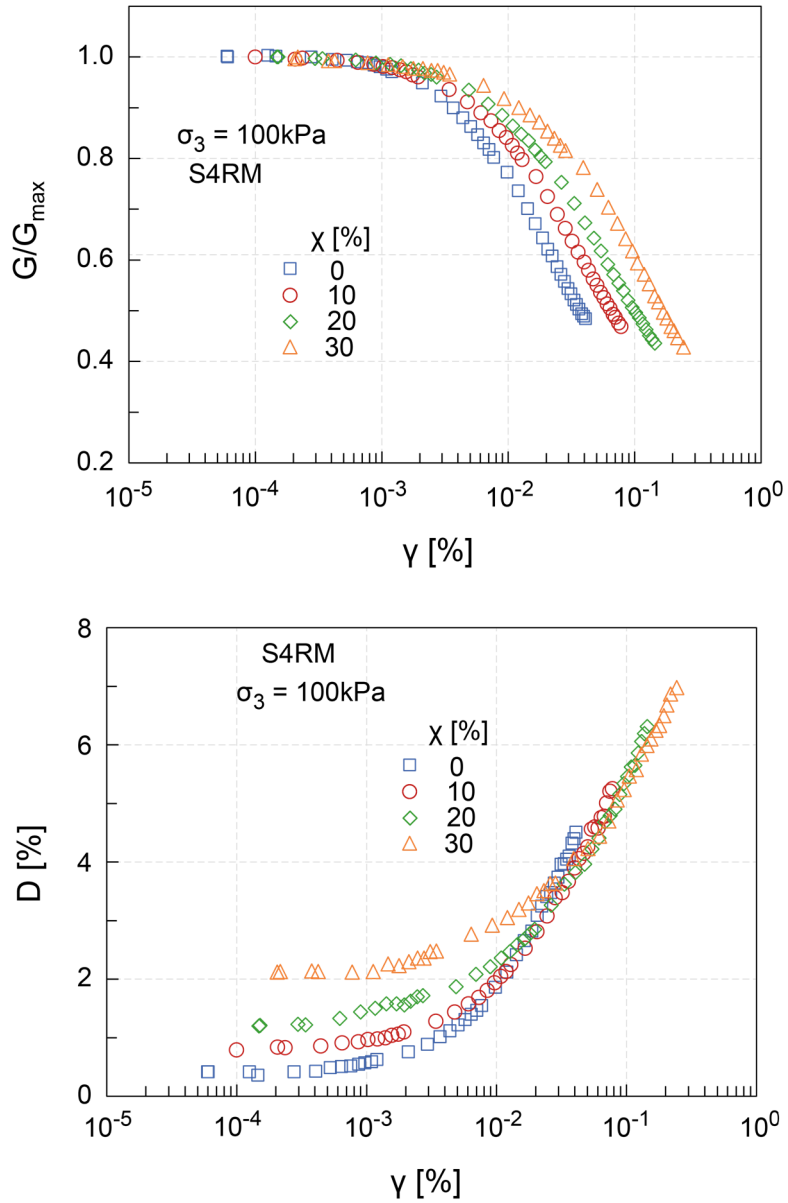


Figure 84: G/G_{\max} vs. $\log \gamma$ and D vs. $\log \gamma$ for S4RM at different rubber chips contents, $\sigma_3 = 100\text{kPa}$

The shear modulus reduction curves obtained from various sand rubber mixtures can be approximated by means of a non-linear hyperbolic law suggested among others by Vrettos & Savidis (1999) taking into account the rubber chips content and the confining stress.

$$\frac{G}{G_{\max}} = \frac{1}{1 + g_1 \cdot \gamma^{\alpha_1}} \quad (34)$$

The parameter g is obtained by fitting equation (34) in the experimental data for S2RM, S3RM, and S4RM and fixing the parameter $\alpha_1 = 0.9$. An example is

shown in Figure 85 for S2RM at 100 kPa. It can be deduced that by considering a mixture formed by one type of sand at a single confining stress, increasing the rubber content decreases the values of g_1 . Alternatively, by keeping the percentage of rubber chips constant and increasing the confining stress yield a decreasing trend of g_1 values. This implies that for the decreased g_1 values the G/G_{\max} curve becomes more linear. The parameter g_1 can be estimated by equation (35) with constants given in Table 15.

$$g_1 = A_q \cdot \exp(d_q \cdot \chi) \left(\frac{\sigma_3}{p_a} \right)^{-0.3} \quad (35)$$

where χ is in percentage, $0 \leq \chi \leq 30\%$; $50 \leq \sigma_3 \leq 400$ kPa

Table 15: Constants for equation (35)

Material	A_q	d_q
Sand S2 & S2RM	11.53	-0.026
Sand S3 & S3RM	12.29	-0.058
Sand S4 & S4RM	18.82	-0.042

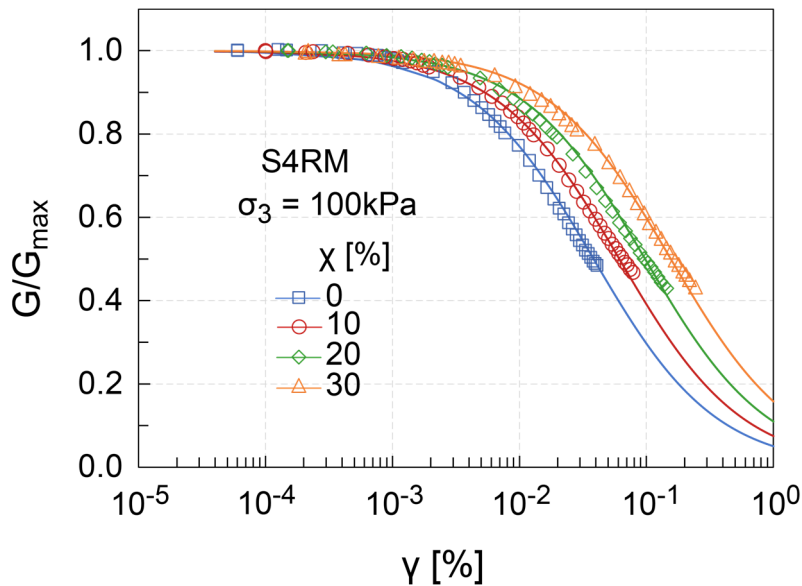


Figure 85: G/G_{\max} vs. $\log \gamma$ and D vs. $\log \gamma$ for S4RM at different rubber chips contents; $\sigma_3 = 100$ kPa; the solid lines are from equation (34)

6.6 Discussion

In this Chapter the resonant column test was applied as a suitable laboratory technique to evaluate the dynamic behaviour of sands and sand rubber mixtures at small to intermediate strain levels. The mixtures were prepared at different rubber contents and tested under various confining stresses.

With regard to the small strain response, increasing the confining stress increases G_{\max} and marginally decreases D_{\min} . For the modulus, this is due to the increased net effective stress at the particle contact resulting in stronger soil structure. As rubber content in the mixture increases, G_{\max} decreases and D_{\min} increases. This is attributed to the decreased density, increased elasticity and compressibility of rubber in the mixtures.

For intermediate strain response, the reduction of shear modulus and the increase of damping ratio are noticed as soon as a threshold shear strain is exceeded. Increasing the confining stress increases G/G_{\max} , while D decreases. It is also noticed that at the same confining stress increasing the rubber content enhances rubber-to-rubber contact and renders the specimen more flexible leading to a higher shear strain amplitude. At constant shear strain amplitude increasing rubber content increases G/G_{\max} and D values. For the mixtures at chips content less than 20% the overall response is controlled by the soil portion of the mixture while for 20% and 30% content the dynamic response is controlled both by soil particles and rubber particles.

For the three sands used, the shear modulus degradation is stronger as sand becomes more non-uniform but with no appreciable influence of d_{50} . Mixing soils of larger particles with rubber chips many result in a higher void compared to soils with smaller particles for the same relative density I_D . This contributes to the drastic reduced density and accordingly the strong degradation of the shear modulus of the mixture. The increase of void may be due to the fact that the coarser soil particles hardly penetrate into voids between rubber material while this is easier for the smaller particles.

During vibration, pure sand particles may derive their damping through friction between them with a very little or no energy dissipation through particle deformation. However, damping for sand rubber mixtures may result from both

the friction between particles and the deformation of the rubber particles. As a result, increasing rubber content in the mixtures increases the damping ratio.

7. Summary and outlook

This thesis evaluates the static and dynamic behaviour of sand rubber mixtures through various laboratory investigations. The classification tests were first performed on the parent material prior to forming the sand rubber chips mixtures S2RM, S3RM and S4RM. The proportions of rubber chips used were 0/10/20/30/100% by dry mass. Density tests (Proctor density, minimum and maximum densities) were performed on the mixtures to determine the expected range of data applicable in field applications. Permeability tests were performed to evaluate the mixture drainage. The obtained data confirmed that the mixtures are light weight with improved drainage characteristic.

Next, the static behaviour in terms of compressibility and shear resistance of the composite material S2RM, S3RM, and S4RM was investigated by utilizing oedometer, direct shear test in large shear box as well as triaxial tests. The mixtures were tested in dry condition. To include the effect of water content on the mixture behaviour wet S2RM was prepared at 5% water content. For oedometer tests, mixtures were subjected to a series of vertical stresses loadings varying from 50 to 300kPa and the resulting stress strain data were evaluated. In the direct shear tests mixtures were subjected to shearing under normal stresses in the range of 50 to 200kPa. In these tests both shear force and horizontal deformation were measured. Triaxial compression tests were performed using an available dynamic triaxial testing system with the application of deviatoric force up to specimen failure. Confining stresses varied from 50 to 200 kPa. Axial deformation and volume change were measured. Saturated undrained and drained tests were also performed on pure sand S2 specimens. A B-value above 0.95 was achieved as an indication of attained high degree of saturation. In these tests excess pore water pressure and volume change were additionally measured. It was noticed that the small amount of water added does not alter the mixture behaviour. The benefit is that it prevents particle segregation. Increased rubber content increased the compressibility and shear resistance of the mixtures. A rubber chips content in the range of 20 to 30% by dry mass can be used to reinforce sand soils.

Further dynamic cyclic triaxial tests were performed to evaluate the cyclic behaviour of saturated, dry and wet mixtures. All specimens were first isotropically consolidated at 100 kPa. For saturated material a static deviatoric stress of 45 kPa was imposed prior to cyclic stage to simulate field anisotropic

consolidation condition. Some saturated specimens formed by pure sand S2 were also tested under isotropic consolidation condition for comparison. Cycling was applied stress-controlled with amplitude equal to ± 50 kPa. Both undrained and drained tests were performed on S2RM, S3RM and S4RM. Tests in dry or wet conditions were also performed. The applied pre-cyclic static deviatoric stress and the amplitude varied. They were determined from the peak deviatoric stress obtained from standard triaxial tests. For all tests the loading frequency was 1 Hz. Tests under dry or wet conditions are important particularly with regard to the occurrence of earthquake loading in the desert regions.

For saturated undrained tests, applied pre-cyclic static deviatoric stress increased the cyclic resistance. A small amount of rubber chips added to sand increased the liquefaction but also the cyclic axial strain. Further addition increased the ductility that contributed to the increased liquefaction resistance and decreased cyclic strain. In drained saturated tests volume change and axial strain increased for rubber contents up to 20% and then decreased. For dry and wet conditions, increased number of cycle induced densification and increased the material stiffness and decreased the damping ratio associated with the increased settlement particularly for loose and medium-dense specimens. Increased rubber content decreased the dynamic Young's modulus and increased the damping ratio

Resonant column tests were conducted to evaluate dynamic behaviour of various sand rubber mixtures. The device was first calibrated in order to increase the accuracy and reliability of recorded data. Aluminium calibration bars of different sizes were used and the added mass approach was applied. The Resonant tests were performed on wet S2RM, S3RM and S4RM specimens of 100 mm diameter prepared at $I_D = 0.5$ under confining stress varying from 50 to 400 kPa. The highest stress level was 400 kPa for pure sand specimens. Both small and intermediate strain responses were measured. These tests are typical to assess soil behaviour during earthquake loading. Increased confining stress increased G/G_{\max} and decreased D while changing the mixture from non-linear to linear behaviour. Further, increasing the rubber content increases elasticity and ductility in the mixtures, increases the values of G/G_{\max} and D and increased the linearity of the $G/G_{\max} - \log \gamma - D$ curves.

In summary, rubber chips in the range of 4 to 14 mm mixed with sands were found to increase the shear resistance of the mixtures. They yield to an increase

of the cyclic resistance under saturated condition, to a decrease of stiffness and to an increase of damping ratio. Increased confining stress increased G/G_{\max} and decreased damping ratio of the mixtures. Increased rubber content increased both G/G_{\max} and D . Several new design equations were proposed. Mixture compression strain ε_c [%] as function of σ_v and χ ; $\bar{\varepsilon}_u$ as function of N/N_f ; $\bar{\varepsilon}_u$ as function of $\varepsilon_{v,cy}$; G_{\max} or D_{\min} as function of σ_3 and χ ; G/G_{\max} as function of γ , σ_3 and χ . Concluding, a chips content around 30% by dry mass can be used to reinforce sands in an effective manner.

Further research should focus on large scale field trials that utilize larger rubber chips for example up to 50 mm mixed with sand to investigate their cyclic and dynamic behaviour in both wet and saturated condition. The laboratory testing of such material is restricted to the available equipment. It can be expected that the larger rubber will increase the cyclic resistance while cutting off the emitted seismic waves. From this trial, environmental effect of placing rubber chips above or below ground water table can be determined.

Literature

Ahmed, I. (1993): Laboratory Study on Properties of Rubber-Soils. Publication FHWA/IN/JHRP-93/04. Joint Highway Research Project, Indiana Department of Transportation and Purdue University, West Lafayette, Indiana.

Amuthan, M.S., Boominathan, A., Banerjee, S. (2020): Undrained cyclic responses of granulated rubber-sand mixtures, *Soils and Foundations* 60(4), 871-885. doi:10.1016/j.sandf.2020.06.007.

Anastasiadis, A., Pitilakis, K., Senetakis, K. (2009): Dynamic shear modulus and damping ratio curves of sand/rubber mixtures. *Earthquake Geotechnical Engineering Satellite Conference, XVIIth International Conference on Soil Mechanics & Geotechnical Engineering*, Alexandria, Egypt.

Anastasiadis, A., Senetakis, K., Pitilakis, K., Gargala, C., Karakasi, I. (2011): Dynamic behavior of sand/rubber mixtures. Part I: Effect of rubber content and duration of confinement on small-strain shear modulus and damping ratio, *Journal of ASTM International* 9(2), 1-19. doi: 10.1520/JAI103680.

Anastasiadis, A., Senetakis, K., Pitilakis, K. (2012): Small-strain shear modulus and damping ratio of sand-rubber and gravel-rubber mixtures, *Geotechnical and Geological Engineering* 30, 363-382. doi:10.1007/s10706-011-9473-2.

Anvari, S.M., Shooshpasha, I., Kutanaei, S.S. (2017): Effect of granulated rubber on shear strength of fine-grained sand, *Journal of Rock Mechanics and Geotechnical Engineering*, 9, 936-944.

ASTM D3999-2003: Standard test methods for the determination of the modulus and damping properties of soils using the cyclic triaxial apparatus.

ASTM D4015-15e1: Standard Test Methods for Modulus and Damping of Soils by Fixed-Base Resonant Column Devices, ASTM International, West Conshohocken, PA.

ASTM D5311/D5311M-13 Standard Test Method for Load Controlled Cyclic Triaxial Strength of Soils. ASTM International, West Conshohocken, PA, 2015.

ASTM D6270-20, Standard Practice for Use of Scrap Tires in Civil Engineering Applications, ASTM International, West Conshohocken, PA

ASTM D7181-20: Method for Consolidated Drained Triaxial Compression Test for Soils, ASTM International, West Conshohocken, PA

Bahadori, H., Manafi, S. (2015): Effect of tyre chips on dynamic properties of saturated sands, *Journal of Physical Modelling in Geotechnics* 15(3), 116-128. doi: 10.1680/jphmg.13.00014.

Bahadori, H., Farzalizadeh, R. (2018): Dynamic properties of saturated sand mixed with tyre powders and tyre shreds, *International Journal of Civil Engineering* 16(4), 395-408. <https://doi.org/10.1007/s40999-016-0136-9>.

Bałachowski, L., Gotteland, P. (2007): Characteristics of tyre chips-sand mixtures from triaxial tests, *Archives of Hydro-Engineering and Environmental Mechanics* 54(1), 3–14.

Balunaini, U., Mohan, V.K.D., Prezzi, M., Salgado, R. (2014): Shear strength of tyre chip–sand and tyre shred–sand mixtures, *Geotechnical Engineering* 167(6): 585–595.

Banzibaganye, G., Becker, A., Vrettos, C. (2019): Static and cyclic triaxial tests on medium sand and tire chips mixtures, *Proceedings of 17th African Regional Conference on Soil Mechanics and Geotechnical Engineering*, Cape Town, South Africa, 163-168.

Banzibaganye, G., Vrettos, C. (2022): Sand-tyre chips mixtures in undrained and drained cyclic triaxial tests, *Proceedings of the Institution of Civil Engineers - Ground Improvement*. 175(1): 23–33 doi:10.1680/jgrim.20.00046.

Becker, A., Vrettos, C. (2011): Bodenmechanische Untersuchungen an Mischungen von rolligen und bindigen Böden mit Gummi aus Recyclingprozessen, *Bauingenieur* 87, 548-556.

Bernal-Sanchez, J., McDougall, J., Barreto, D., Marinelli, A., Dimitriadi V., Anbazhagan, P., Miranda, M. (2019): Experimental assessment of stiffness and damping in rubber-sand mixtures at various strain levels. *Earthquake Geotechnical Engineering for Protection and Development of Environment and Constructions – Silvestri & Moraci* (Eds), ISBN 978-0-367-14328-2.

Bosscher, P.J., Edil, T.B., Eldin, N.N. (1993): Construction and performance of a shredded waste tire test embankment, *Transportation Research Record* 1345, Transportation Research Board, Washington, D.C., 44-52.

Brophy, M., Graney, J. (2004): Groundwater effects from highway tire shred use, *Environmental Forensics* 5(2), 79-84.

Cabalar, A.F. (2011): Direct shear tests on waste tires-sand mixtures, *Geotechnical and Geological Engineering* 29, 411-418.

Chen, A.T.F., Stokoe, K.H. (1979): *Interpretation of strain-dependent modulus and damping from torsion soil tests*. Rep. No. USGS-GD-79-002, NTIS No. PB298749, U.S. Geological Survey, Menlo Park, CA.

Chen, G., Zhao, D., Chen, W., Juang, C.H. (2019): Excess pore water pressure generation in cyclic undrained testing, *Journal of Geotechnical and Geoenvironmental Engineering*, 04019022. doi:10.1061/(ASCE)GT.1943-5606.0002057.

Chenari, J.R., Alaie, R., Fatahi, B. (2019): Constrained compression models for tire-derived aggregate-sand mixtures using enhanced large scale oedometer testing apparatus, *Geotechnical and Geological Engineering* 37, 2591–2610. doi:10.1007/s10706-018-00780-2.

Becker, A. (2017): Untersuchungen zu neuartigen und gängigen Methoden der Baugrundertüchtigung, Veröffentl. des Fachgebietes Bodenmechanik und Grundbau der TU Kaiserslautern, Heft 17.

Clayton, C.R.I., Priest, J.A., Bui, M.T., Zervos A, Kim S.G. (2009): The Stokoe resonant column apparatus: Effects of stiffness, mass and specimen fixity, *Géotechnique*, 59(5), 429-437. doi:10.1680/geot.2007.00096.

Daniell, J.E., Khazai, B., Wenzel, F.V.A. (2012): The worldwide economic impact of earthquakes, Paper No. 2038. *Proceedings of the 15th World Conference of Earthquake Engineering*, Lisbon, Portugal.

Das, S., Bhowmik, B. (2020): Dynamic behaviour of sand-crumbed rubber mixture at low strain level. *Geotechnical and Geological Engineering* 38, 6611-6622. doi:10.1007/s10706-020-01458-4.

DIN 18127:2012-09 Soil, investigation and testing - Proctor test.

DIN 18127-100X Soil, investigation and testing - Maximum and minimum density test

DIN EN ISO 17892-10: 2018 Geotechnical investigation and testing - laboratory testing of soils - Part 10: Direct shear tests.

DIN EN ISO 17892-11: 2019 Geotechnical investigation and testing - laboratory testing of soils - Part 11: Permeability tests.

DIN EN ISO 17892-5: 2017 Geotechnical investigation and testing - laboratory testing of soils - Part 5: Incremental loading oedometer tests.

DIN EN ISO 17892-9: 2018 Geotechnical investigation and testing - laboratory testing of soils - Part 9: Consolidated triaxial compression tests on water saturated soils.

Drnevich, V.P., Hardin, B.O., Shippy, D.J. (1978): Modulus and damping of soils by the resonant column test, *Dynamic Geotechnical Testing, STP 654* (Silver, M., Tiedemann, D., Eds.), ASTM International, West Conshohocken, PA, 91-125.

Edeskär, T. (2006): Use of tyre shreds in civil engineering applications - technical and environmental properties, Doctoral thesis, Lulea University of Technology.

Edil, T. B., Bosscher, P.J. (1994): Engineering properties of tire chips and soil mixtures, *Geotechnical Testing Journal* 17(4), 453-464. doi:10.1520/GTJ10306J.

Egglezos, D.N., Bouckolavas, G. D. (1998): Analytical relationships for earthquake induced pore pressure in sand, clay and silt. *11th European Conference on Earthquake Engineering* 1998 Balkema, Rotterdam.

Ehsani M., Shariatmadari, N., Mirhosseini, S. M. (2015): Shear modulus and damping ratio of sand-granulated rubber mixtures, *Journal of Central South University* 22, 3159-3167.

Eldin, N.N., Senouci, A.B. (1992): Use of scrap tires in road construction. *Journal of Construction Engineering and Management* 118(3), 561-576.

Esmaili, M., Mosayebi, S.A., Nakhaee, N. (2013): Performance of shred tire mixed with railway subgrade in reduction of train induced vibrations, *International Journal of Advances in Railway Engineering* 1(1), 37-49.

Facciorusso, J., Madiari, C. (2020): On cohesive soil damping estimation by free vibration method in resonant column test. *Geotechnical Testing Journal*, 43(6), 1499-1518. doi:10.1520/GTJ20180241.

- Feng, Z.-Y., Sutter, K.G. (2000): Dynamic properties of granulated rubber-sand mixtures, *Geotechnical Testing Journal* 23(3), 338-344.
- Foose, B.G.J., Benson, C.H., Bosscher, P.J. (1996): Sand reinforced with shredded waste tyres, *Journal of Geotechnical Engineering*, 122(9), 760-767.
- Ghazavi, M. (2004): Shear strength characteristics of sand-mixed with granular rubber, *Geotechnical and Geological Engineering* 22, 401–416.
- GDS Instruments (2015): GDS resonant column: The GDS resonant column system handbook. Hook, U.K; 2015.
- GDSLAB Resonant Column V2.4.8 [Computer software], Hook, U.K., GDS Instruments
- Geosyntec Consultants Inc. (2008): *Guidance Manual for Engineering Uses of Scrap Tires*, Report to Maryland Department of the Environment.
- Gray, D.H., Ohashi, H. (1983): Mechanics of fiber reinforcement in sand, *Journal of Geotechnical Engineering* 109(3), 335-353.
- Hall, T. J. (1991): Reuse of shredded tire material for leachate collection systems, *Proceedings of 14th Annual Madison Waste Conference*, University of Wisconsin-Madison.
- Hardin, B.O. (1978): The Nature of stress-strain behavior of soils, *Earthquake Engineering and Soil Dynamics*, Proceedings of the ASCE Geotechnical Engineering Division Specialty Conference, Pasadena, 1978, Vol. 1, 3-90.
- Hazarika, H., Pasha, S.M.K., Ishibashi, I., Yoshimoto, N., Kinoshita, T., Endo, S., Karmokar, AK., Hitosugi, T. (2020): Tire-chip reinforced foundation as liquefaction countermeasure for residential buildings, *Soils and Foundations* 60(2), 315-326. doi:10.1016/j.sandf.2019.12.013.
- Hazarika H, Kohama E, Sugano T (2008) Underwater shake table tests on waterfront structures protected with tire chips cushion, *Journal of Geotechnical and Geoenvironmental Engineering* 134(12), 1706–1719.
- Hong, Y., Yang, Z., Orense, R.P., Lu, Y. (2015): Investigation of sand-tire mixtures as liquefaction remedial measure, *Proceedings of the Tenth Pacific Conference on Earthquake Engineering Building an Earthquake-Resilient Pacific*, Sydney, Australia.

- Hoppe, E.J. (1998): Field study of shredded-tire embankment, *Transportation Research Record No. 1619*, Transportation Research Board, Washington, D.C., 47-54.
- Hoppe, M., Oman, M. (2013): Use of Tire Derived Products (TDP) in Roadway Construction, Report by Braun Intertec Corporation to Minnesota Department of Transportation, Rep. No. MN/RC 2013-20
- Humphery, D.N., Sandford, T.C. (1993): Tyre shreds as lightweight subgrade fill and retaining wall backfill, Proceedings of the Symposium on Recovery and Effective Reuse of Discarded Materials and By-products for Construction of Highway Facilities, Federal Highway Administration, Washington, D.C.
- Humphrey, D.N., Katz, L.E. (2000): Five-year field study of the effect of tyre shreds placed above the water table on groundwater quality, *Transportation Research Record No. 1714*, Transportation Research Board, Washington, D.C., 18-24.
- Humphrey, D.N., Katz, L.E. (2001): Field study of the water quality effects of tyre shreds placed below the water table, *Proceedings of the International Conference on Beneficial Use of Recycled Materials in Transportation Applications*, Arlington, VA, 699-708.
- Hyodo, M., Hyde, A.F.L., Aramaki, N., Nakata, N. (2002): Undrained monotonic and cyclic shear behaviour of sand under low and high confining stresses, *Soils and Foundations* 42(3), 63-76.
- Indraratna, B., Qi, Y., Heitor, A. (2018): Evaluating the properties of mixtures of steel furnace slag, coal wash, and rubber crumbs used as subballast. *Journal of Materials in Civil Engineering* 30 (1), 04017251.
- Isenhower, W.M., Stokoe, K.H., Allen, J.C. (1987): Instrumentation for torsional shear/resonant column measurements under anisotropic stresses, *Geotechnical testing Journals* 10(4),183-191.
- Kaneko, T., Orense, R.P.M., Hyodo, M., Yoshimoto, N. (2013): Seismic response characteristics of saturated sand deposits mixed with tire chips, *Journal of Geotechnical and Geoenvironmental Engineering* 139 (4), 633-643.
- Kowalska, M., Chmielewski, M. (2017): Mechanical parameters of rubber-sand mixtures for numerical analysis of a road embankment, *IOP Conference Series: Materials Science and Engineering* 245: 052003.

Li, B., Huang, M., Zeng, X. (2016): Dynamic behavior and liquefaction analysis of recycled-rubber sand mixtures, *Journal of Materials in Civil Engineering* 28(11),1-14. doi:10.1061/(ASCE)MT.1943-5533.0001629.

Madhusudhan, B.R., Boominathan, A., Banerjee, S. (2017): Static and large-strain dynamic properties of sand–rubber tire shred mixtures, *Journal of Materials in Civil Engineering* 29(10), 04017165. doi:10.1061/(ASCE)MT.1943-5533.0002016

Madhusudhan, B.R., Boominathan, A. Banerjee, S. (2019): Factors affecting strength and stiffness of dry sand-rubber tire shred mixtures, *Geotechnical and Geological Engineering* 37(4), 2763-2780.

Madhusudhan, B.R., Boominathan, A., Banerjee, S. (2020): Cyclic simple shear response of sand- rubber tyre chip mixtures, *International Journal of Geomechanics* 20(9):04020136. doi:10.1061/(ASCE)GM.1943-5622.0001761

Masad, E., Taha, R., Ho, C., Papagiannakis, T. (1996): Engineering properties of tyre soil mixtures as lightweight fill material, *Geotechnical Testing Journal* 19(3), 297-304.

Mashiri, M.S. (2014): *Monotonic and cyclic behaviour of sand tyre chips (STCh) mixtures*, Dissertation, University of Wollongong.

Mashiri, M.S., Vinod, J.S., Sheikh, M.N., Tsang, H.-H. (2015): Shear strength and dilatancy behavior of sand-tyre chip mixtures, *Soils and Foundations* 55(3), 517-528.

McCartney, J.S., Ghaaowd, I., Fox, P.J., Sanders, M.J., Thielmann, S.S., Sander, A.C. (2017): Shearing behavior of tire-derived aggregate with large particle size. II: cyclic simple shear, *Journal of Geotechnical and Geoenvironmental Engineering* 143(10), 04017079.

Nakhaei, A., Marandi, S, Sani Kermani, S., Bagheripour, M. (2012): Dynamic properties of granular soils mixed with granulated rubber, *Soil Dynamics and Earthquake Engineering* 43, 124-132. doi:10.1016/j.soildyn.2012.07.026.

Pistolas, G.A., Anastasiadis, A., Pitilakis, K. (2018): Dynamic behaviour of granular soil materials mixed with granulated rubber: effect of rubber content and granularity on the small-strain shear modulus and damping ratio, *Geotechnical and Geological Engineering* 36, 1267–1281. doi:10.1007/s10706-017-0391-9.

- Pitilakis, D., Anastasiadis, A., Vratsikidis, A., Kapouniaris, A., Massimino, M. R., Abate, G., Corsico, S. (2021): Large scale field testing of geotechnical seismic isolation of structures using gravel-rubber mixtures, *Earthquake Engineering and Structural Dynamics* 50, 2712-2731. doi: 10.1002/eqe.3468
- Rao, G.V., Dutta, R.K. (2006): Compressibility and strength behaviour of sand-tyre chip mixtures, *Geotechnical and Geological Engineering* 24, 711–724.
- Reddy, S. B., Krishna, A. M. (2015): Recycled tire chips mixed with sand as lightweight backfill material in retaining wall applications: An experimental investigation, *International Journal of Geosynthetics and Ground Engineering*, 1, 31. doi:10.1007/s40891-015-0036-0.
- Richart, F.E., Hall, J.R., Woods, R.D. (1970): *Vibrations of Soils and Foundations*, Prentice Hall, Englewood Cliffs, NJ, USA.
- Rios, S., Kowalska, M., Viana da Fonseca, A. (2021): Cyclic and dynamic behavior of sand–rubber and clay-rubber mixtures, *Geotechnical and Geological Engineering*, 39, 3449–34671. doi: 10.1007/s10706-021-01704-3.
- Rowhani, A., Zainey, T.J. (2016): Scrap tyre management pathways and their use as fuel - A review, *Energies* 9, 888. doi:10.3390/en9110888.
- Salgado, R., Yoon, S., Siddiki, N. Z. (2003): *Construction of tyre shreds test embankment*. Technical Report FHWA/IN/JTRP - 2002/35.
- Senetakis, K., Anastasiadis, A., Pitilakis, K. (2012): Dynamic properties of dry sand/rubber (SRM) and gravel/rubber (GRM) mixtures in a wide range of shearing strain amplitudes, *Soil Dynamics and Earthquake Engineering* 33 38–53. doi:10.1016/j.soildyn.2011.10.003.
- Senetakis, K., Anastasiadis, A., Pitilakis, K., Souli, A. (2012): Dynamic behavior of sand/rubber mixtures, Part II: Effect of rubber content on G/Go- γ -DT curves and volumetric threshold strain. *Journal of ASTM International* 9(2). doi: 10.1520/JAI103711.
- Shariatmadari, N., Karimpour-Fard, M., Shargh, A. (2018): Undrained monotonic and cyclic behavior of sand-ground rubber mixtures. *Earthquake Engineering and Engineering Vibration* 17(3), 541-553.

- Tasalloti, A., Gabriele Chiaro, G., Murali, A., Banasiak, L. (2021): Physical and mechanical properties of granulated rubber mixed with granular soils – A literature review, *Sustainability* 13, 4309. doi:10.3390/su13084309.
- Tatsuoka, F., Silver, M. (1980): New method for the calibration of the inertia of resonant column devices. *Geotechnical Testing Journal* 3(1), 30-34. <https://doi.org/10.1520/GTJ10471J>.
- Thomas, B.S., Gupta, R.C., Panicker, V.J. (2016): Recycling of waste tyre rubber as aggregate in concrete: Durability-related performance. *Journal of Cleaner Production* 112(1), 504-513. doi:10.1016/j.jclepro.2015.08.046.
- Towhata, I. (2008): *Geotechnical Earthquake Engineering*, Springer Series in Geotechnics and Geoengineering.
- Tsang, H.-H., Lo, S.H., Xu, X., Sheikh, M.N. (2012): Seismic isolation for low-to-medium-rise buildings using granulated rubber–soil mixtures: numerical study, *Earthquake Engineering and Structural Dynamics* 41, 2009–2024.
- Twin City Testing Corporation (1990): *Waste Tires in Sub-grade Road Beds*, Report on the Environmental Study of the Use of Shredded Waste Tires for Roadway Sub-grade Support, Minnesota Pollution Control Agency.
- Vinot, V., Baleshwar, S. (2013): Shredded tire-sand as fill material for embankment applications, *Journal of Environmental Research and Development* 7(4A), 1622–1627.
- Vrettos, C., Banzibaganye, G. (2022): Effect of specimen size and inertia on resonant column tests applied to sand, *Soil Dynamics and Earthquake Engineering* (in print).
- Vrettos, C., Savidis, S. (1999): Shear modulus and damping for Mediterranean clays of medium plasticity. In: Seco e Pinto P (ed) *Earthquake Geotechnical engineering: Proceedings of the Second International Conference on Earthquake Geotechnical Engineering*. A.A. Balkema, Rotterdam, vol 1, pp 71–76.
- Warith, M.A., Rao, S.M. (2006): Predicting the compressibility behaviour of tire shred samples for landfill applications, *Waste Management* 26(3), 268-276. doi: 10.1016/j.wasman.2005.04.011.

- Wichtmann, T., Triantafyllidis, T. (2009): Influence of the grain-size distribution curve of quartz sand on the small strain shear modulus G_{\max} . *Journal of Geotechnical and Geoenvironmental Engineering* 135(10), 1404-1418. [https://doi.org/10.1061/\(ASCE\)GT.1943-5606.0000096](https://doi.org/10.1061/(ASCE)GT.1943-5606.0000096).
- Wichtmann, T., Triantafyllidis, T. (2013): Effect of uniformity coefficient on G/G_{\max} and damping ratio of uniform to well-graded quartz sands, *Journal of Geotechnical and Geoenvironmental Engineering* 139(1): 59–72. doi:10.1061/(ASCE)GT.1943-5606.0000735.
- Wu, W.Y., Benda, C.C., Cauley, R.F. (1997): Triaxial determination of shear strength of tire chips, *Journal of Geotechnical and Geoenvironmental Engineering* 123(5), 479–482.
- Youwai, S., Bergado, D.T. (2003): Strength and deformation characteristics of shredded rubber tyre sand mixtures. *Canadian Geotechnical Journal* 40, 256-264.
- Yoon, S., Prezzi, M., Siddiki, N.Z., Kim, B. (2005): Construction of test embankment using sand-tire shred mixture as fill material, *Waste Management* 26, 1033-1044.
- Zhou, E., Wang, Q. (2019): Experimental investigation on shear strength and liquefaction potential of rubber-sand mixtures, *Advances in Civil Engineering*, Article ID 5934961.
- Zornberg, J.G., Cabral, A.R., Viratjandr, V. (2004): Behaviour of tyre shred sand mixtures, *Canadian Geotechnical Journal* 41, 227-241.

Appendices

A Proctor tests

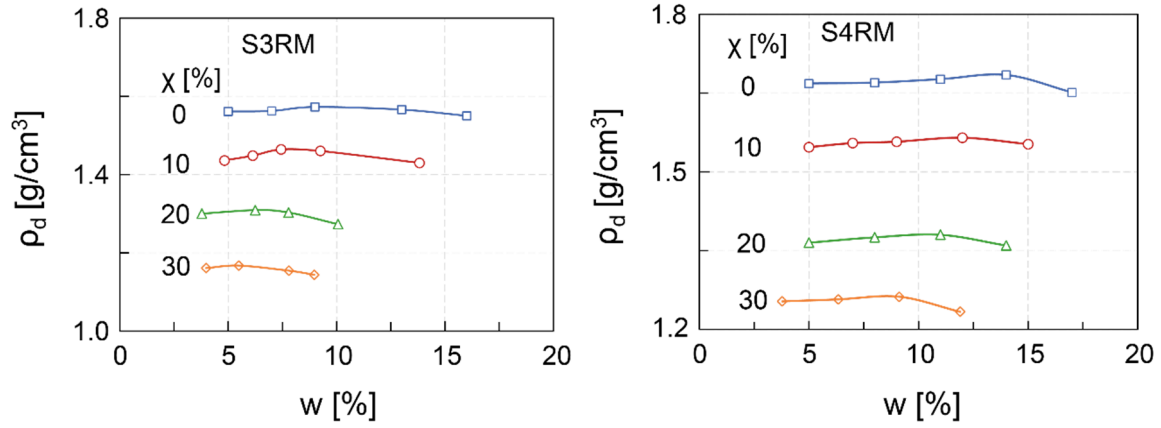


Figure A-1: Dry density vs. moisture content for S3RM and S4RM

B Static tests

- Oedometer tests

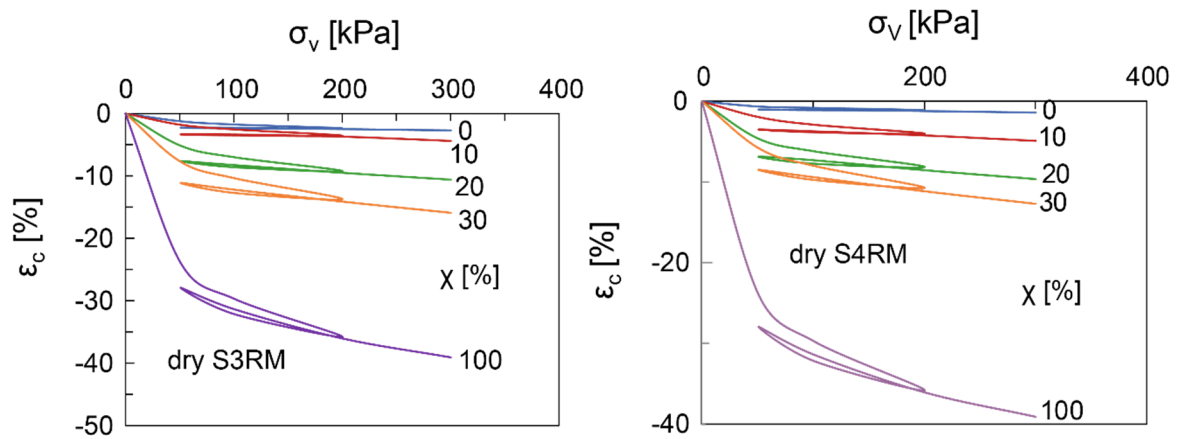


Figure B-1: Stress vs. strain for S3RM and S4RM

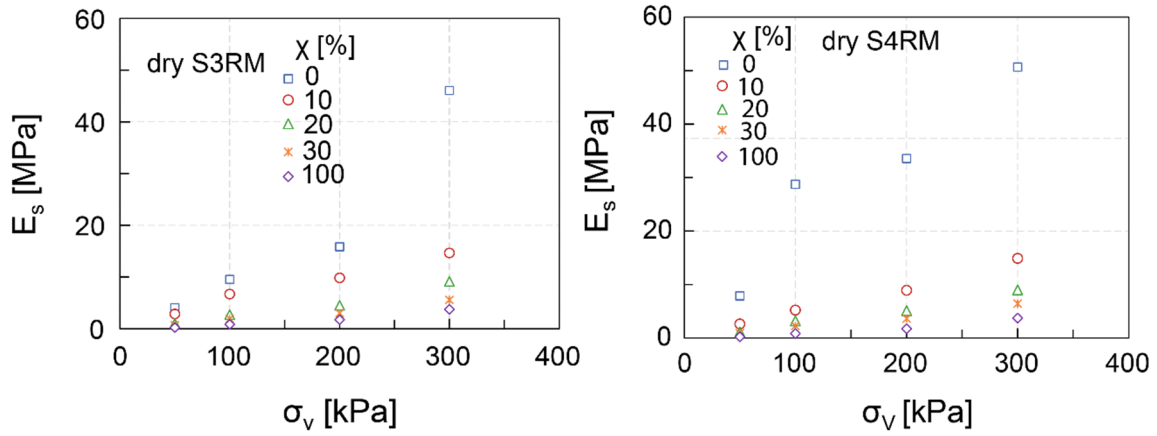
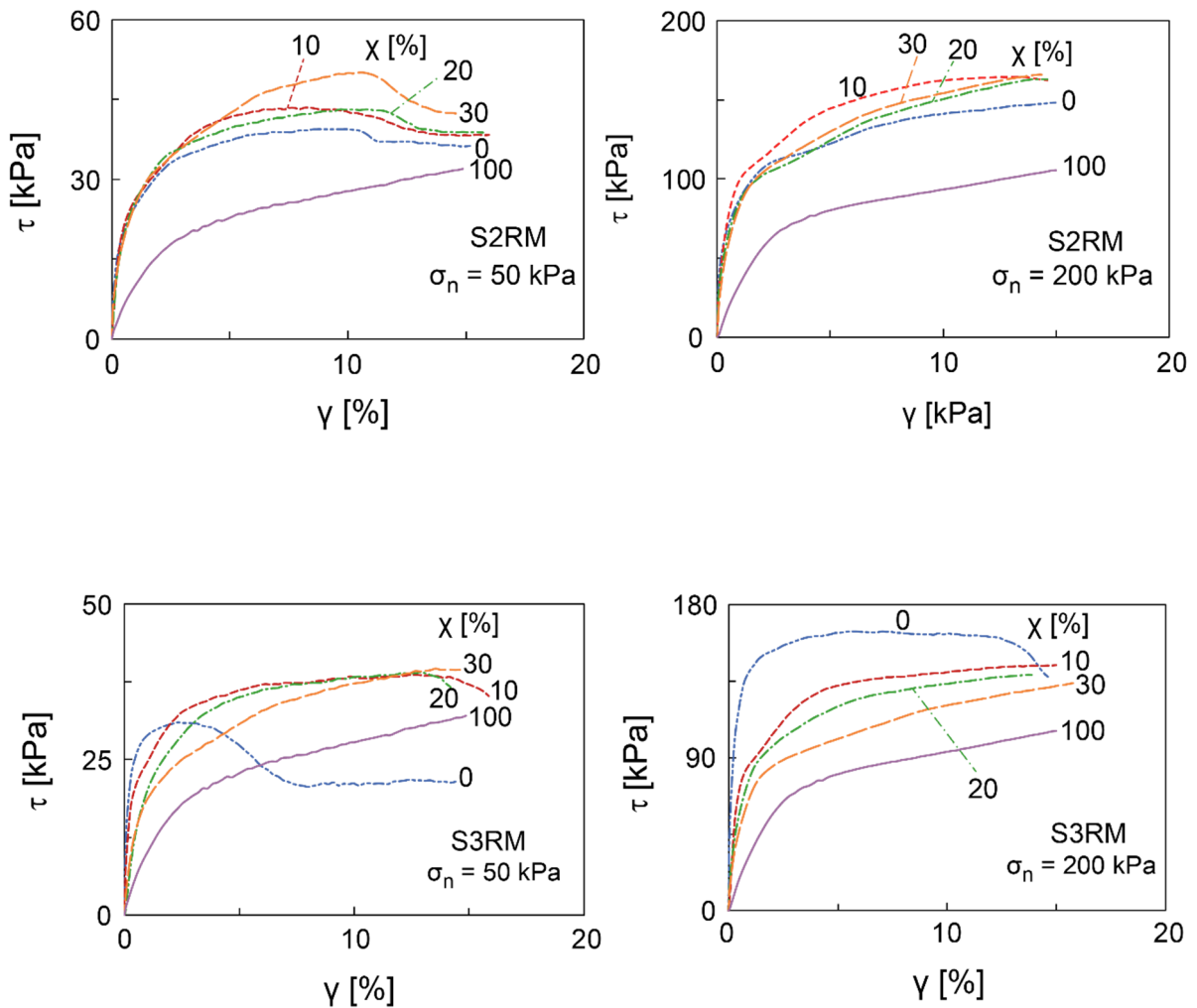


Figure B-2: Constrained modulus vs. vertical strain for dry S3RM and S4RM

• **Direct shear tests**



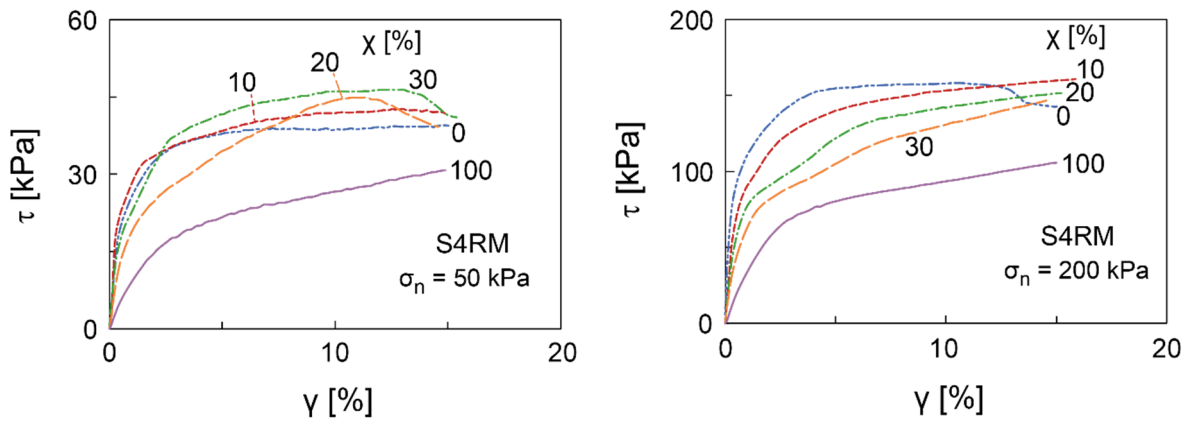
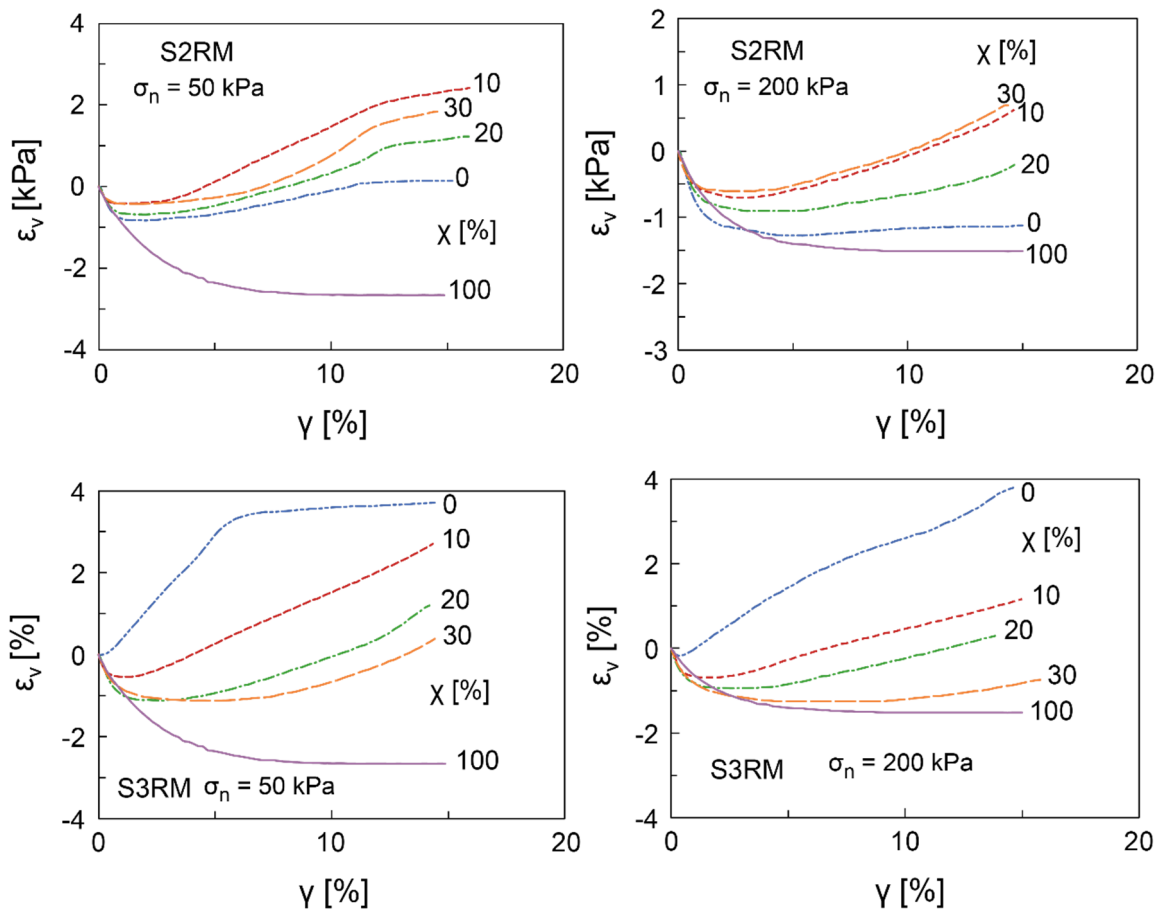


Figure B-3: Shear stress vs. shear strain for various dry sand rubber chips mixtures



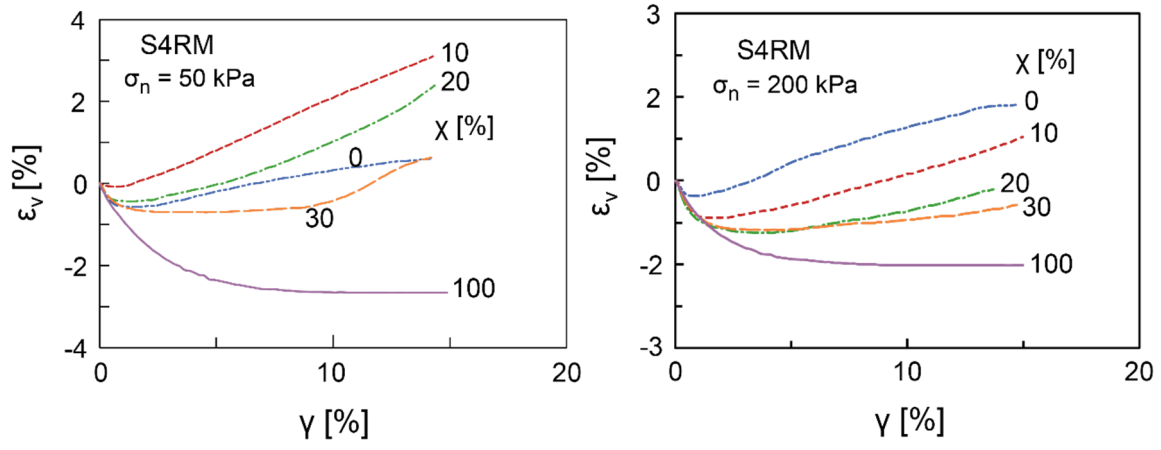
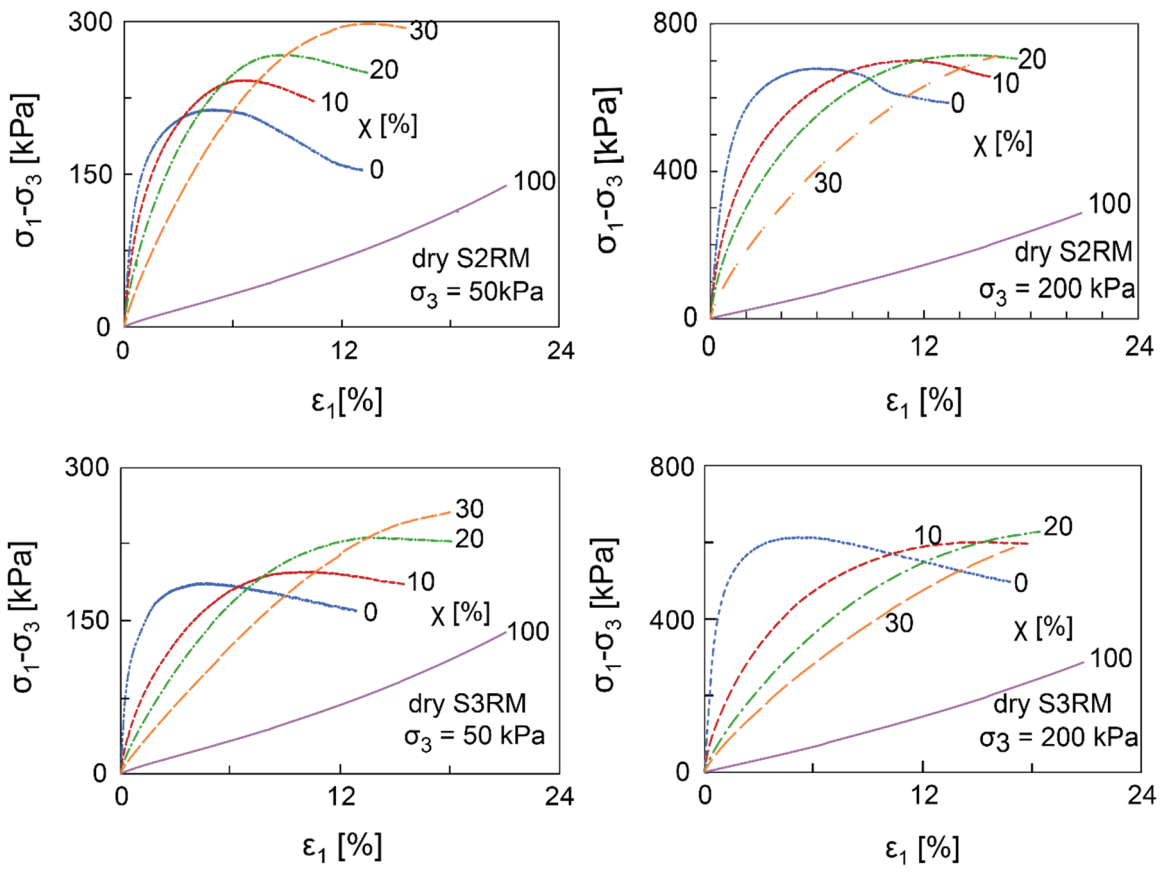


Figure B-4: Volumetric strain vs. shear strain for various dry sand rubber chips mixtures

• **Triaxial compression tests**



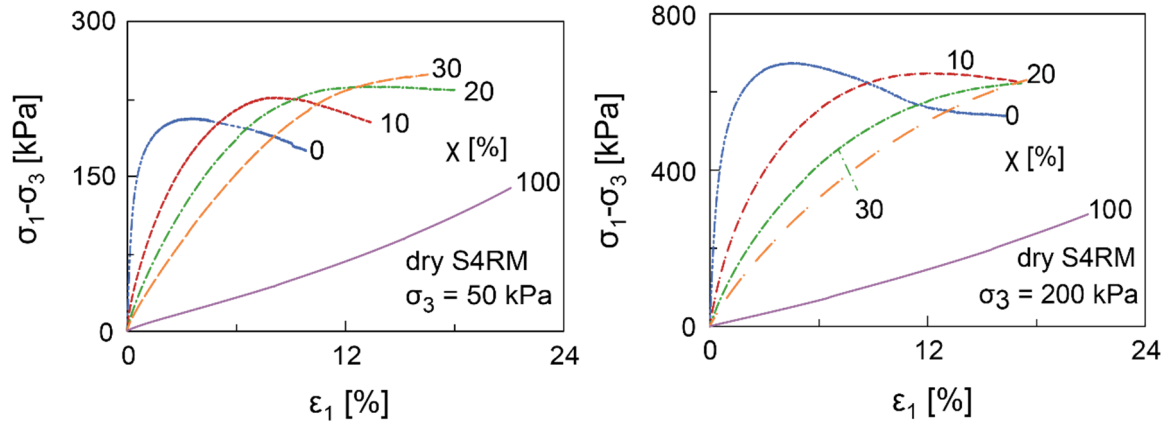
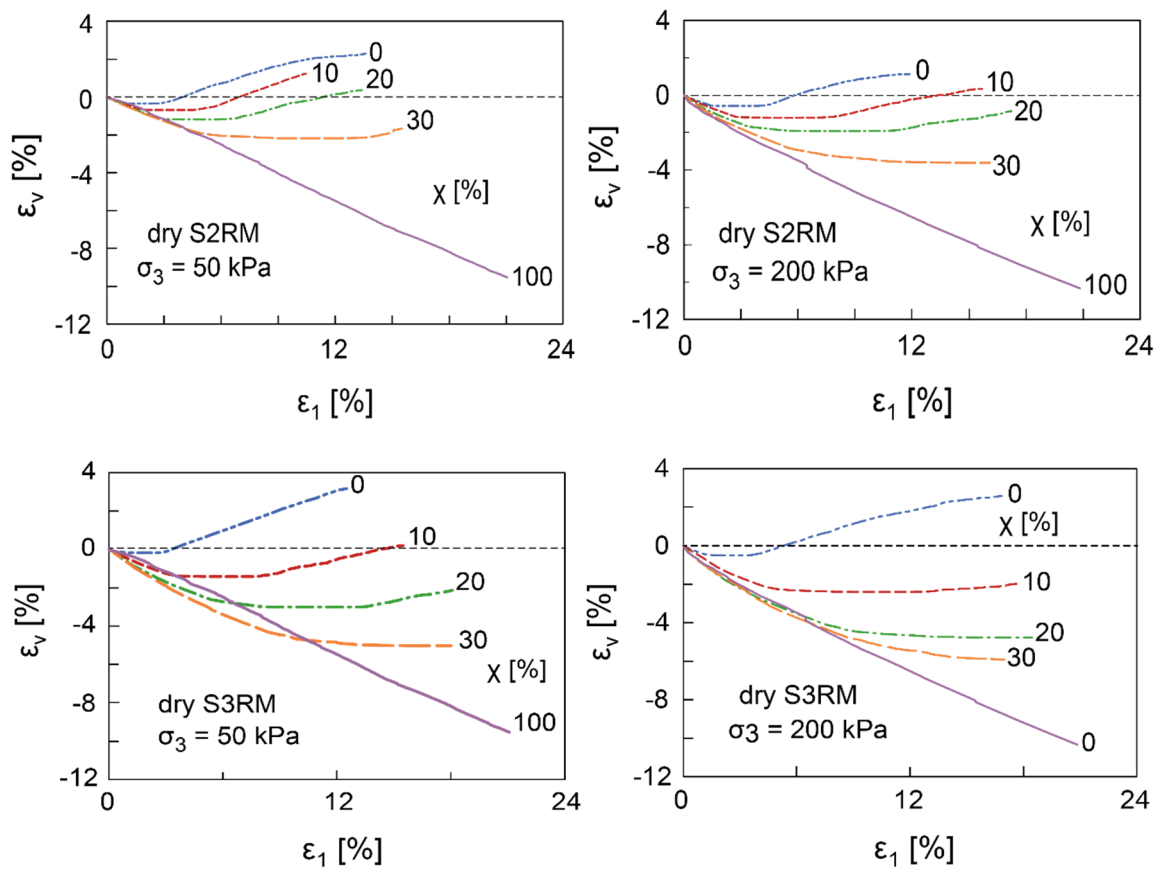


Figure B-5: Deviatoric stress vs. axial strain for different sand rubber mixtures



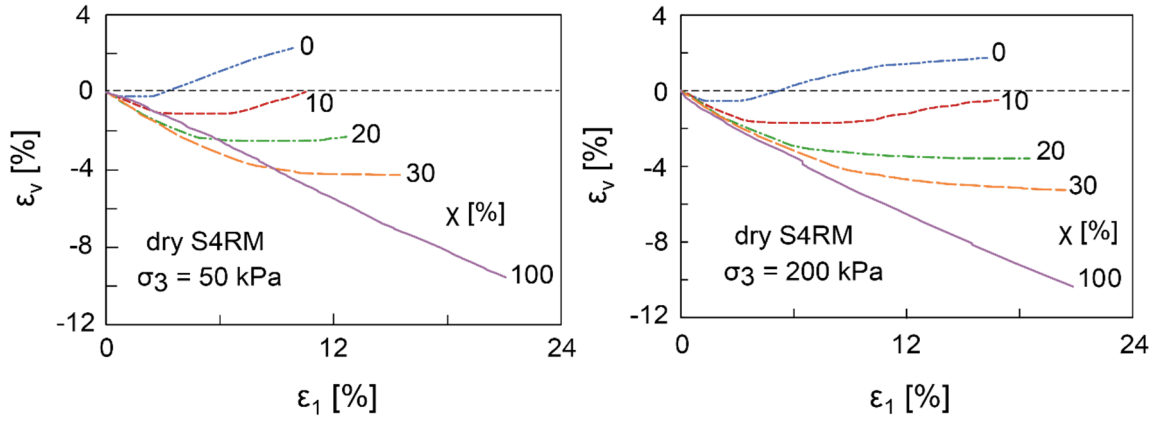


Figure B-6: Volumetric strain vs. axial strain for different sand rubber mixtures

C Cyclic triaxial tests

- Saturated undrained tests

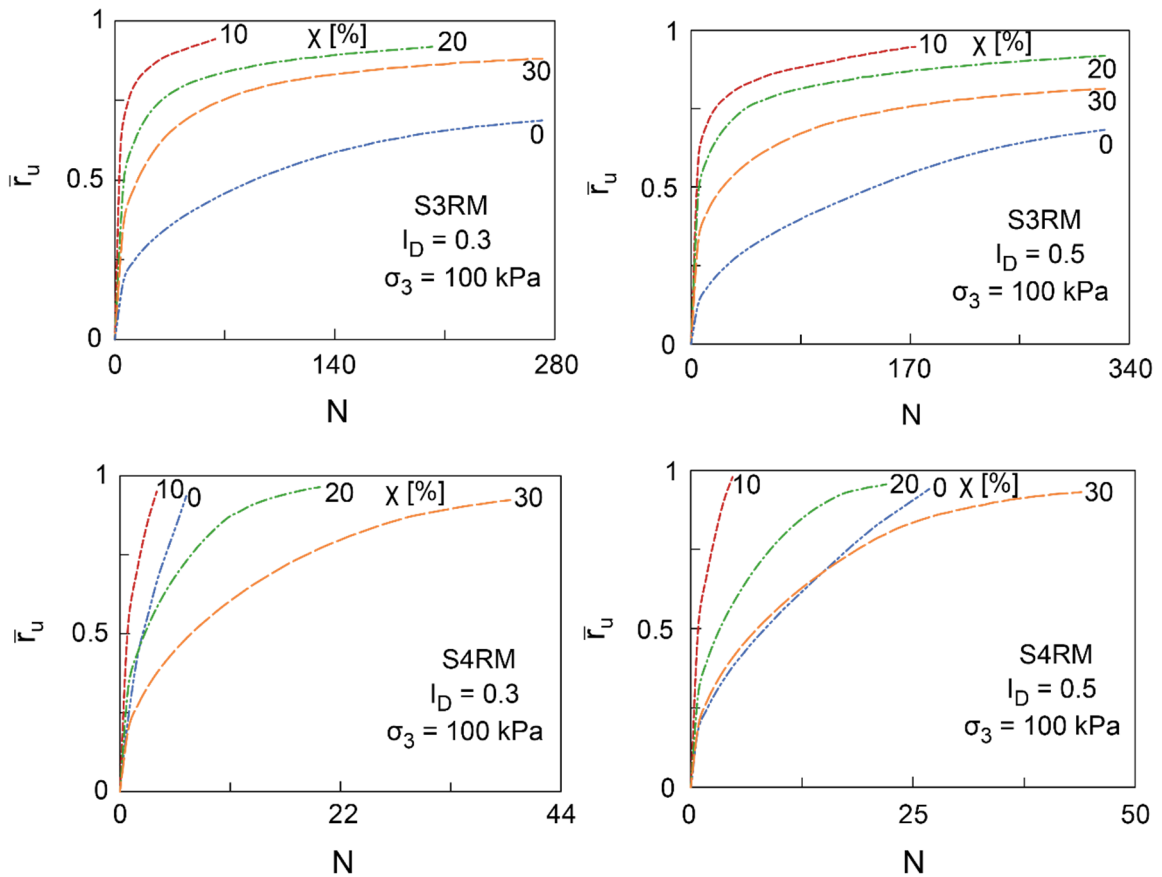


Figure C-1: Average pore pressure ratio vs. number of cycles for S3RM and S4RM, CAU tests

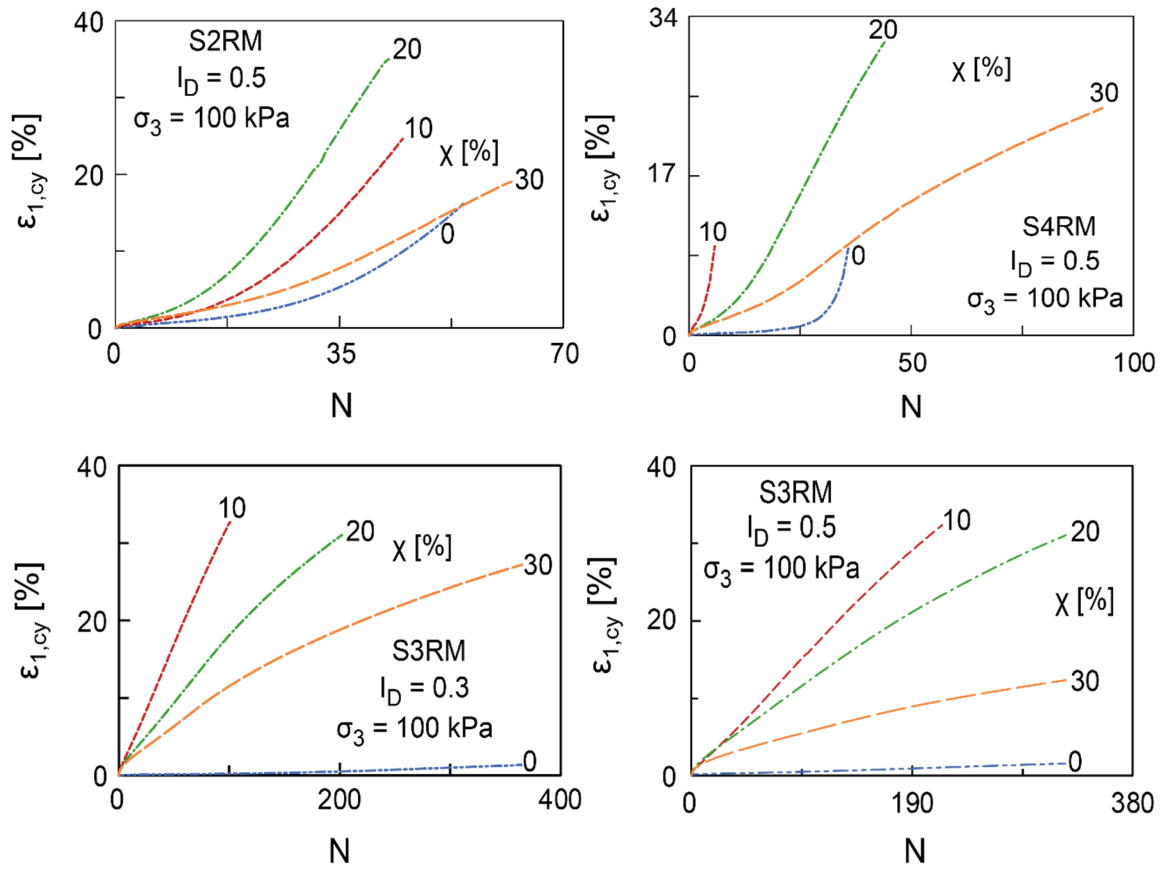
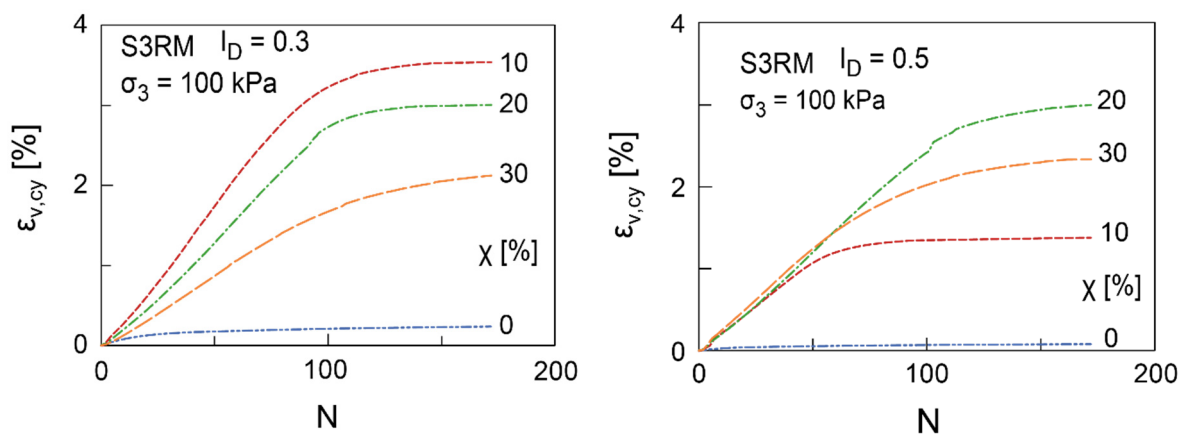


Figure C-2: Average cyclic axial strain vs. number of cycles for S2RM, S3RM and S4RM, CAU tests

• **Saturated drained tests**



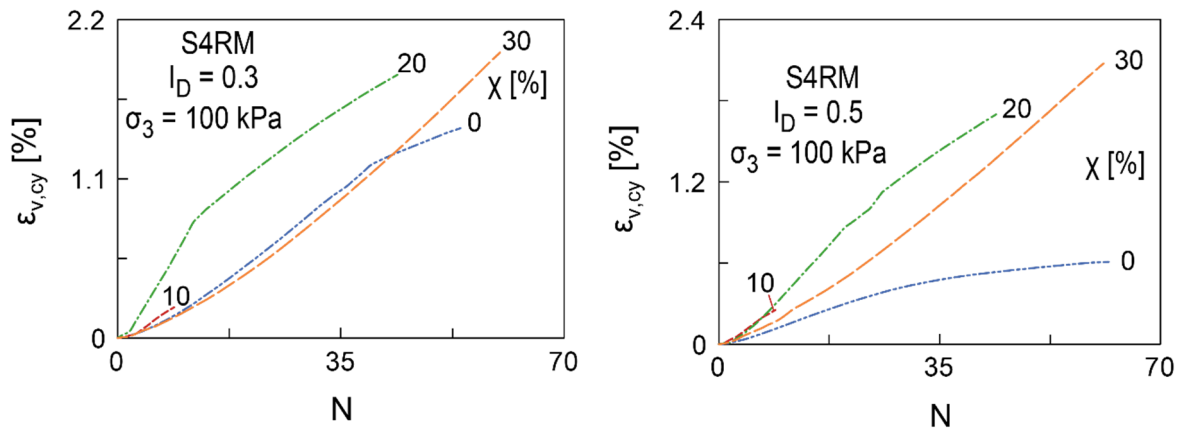


Figure C-3: Average volumetric strain vs. number of cycles for S3RM and S4RM, CAD tests

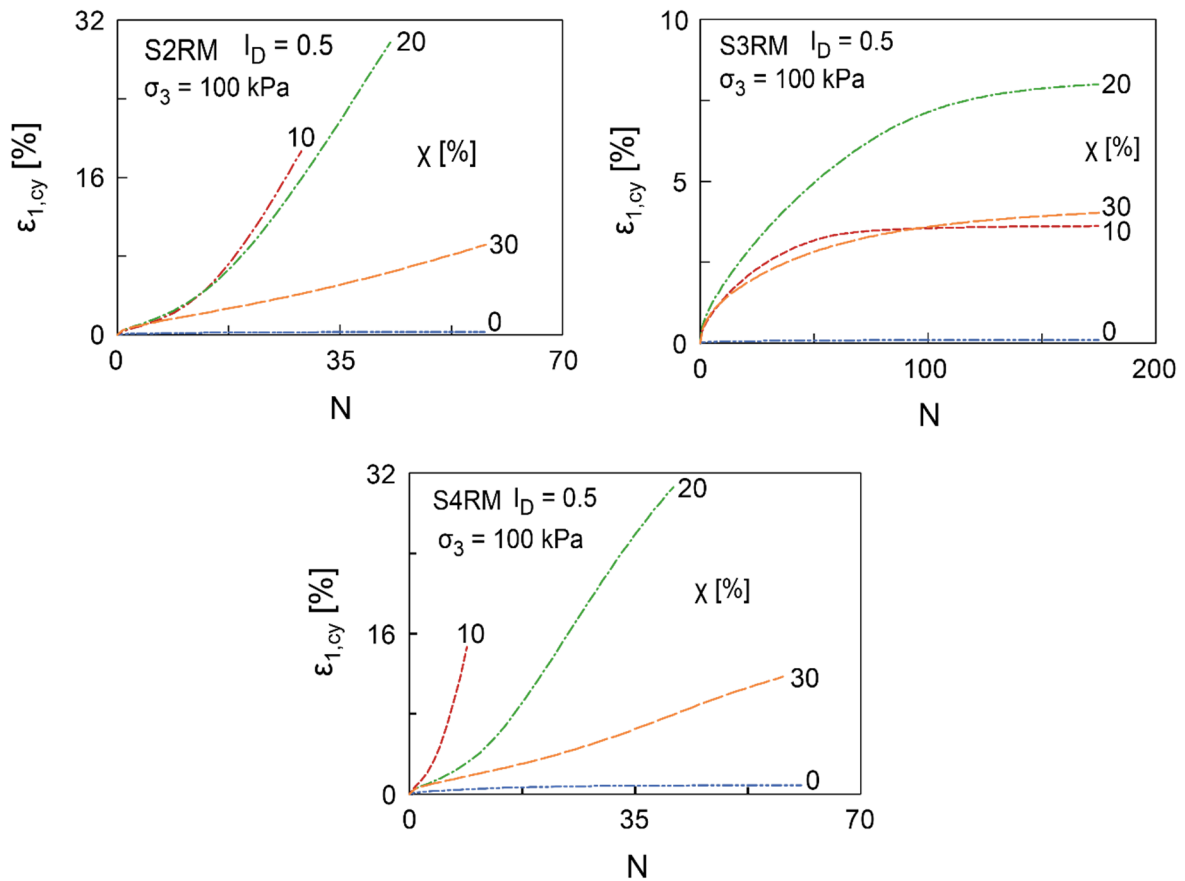


Figure C-4: Average cyclic axial strain vs. number of cycles for S2RM, S3RM and S4RM, CAD tests

• **Dry drained tests**

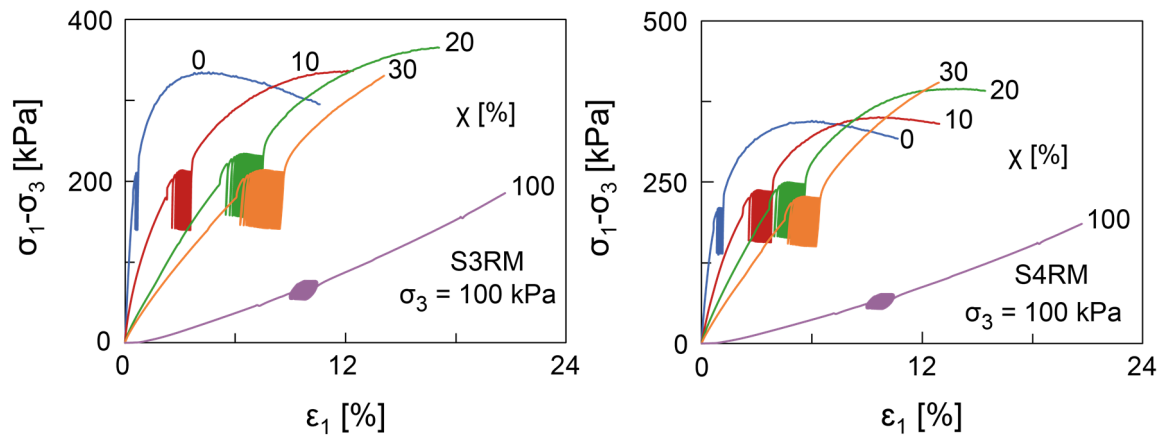


Figure C-5: Stress vs strain curves for S3RM and S4RM

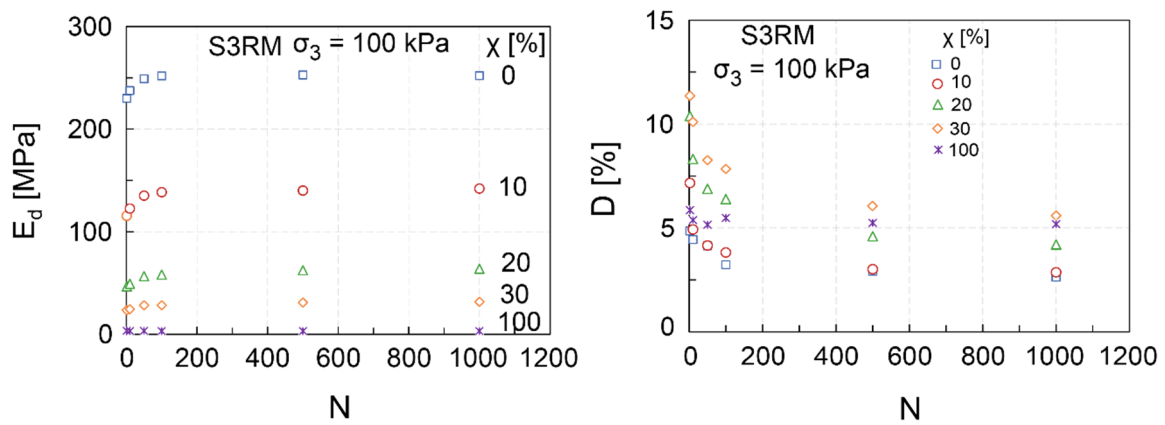


Figure C-6: Dynamic young modulus and damping ration Vs. number of cycles for S3RM

D Resonant column tests

- Loading-unloading-reloading

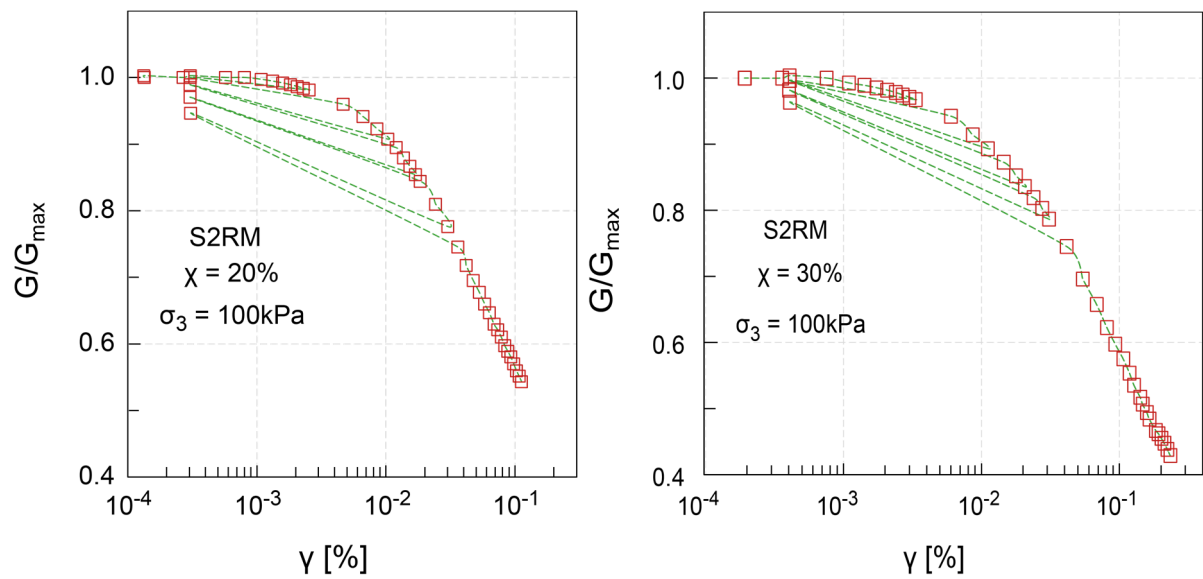


Figure D-1: G/G_{\max} vs $\log \gamma$ for S2RM

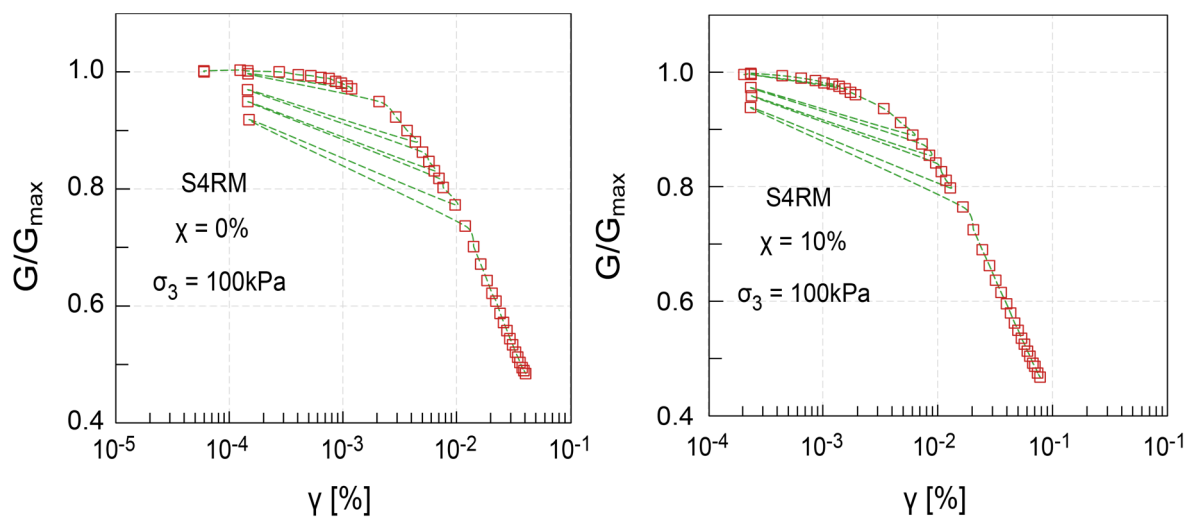


Figure D-2: G/G_{\max} vs $\log \gamma$ for S4RM

Lebenslauf

Beruflicher Werdegang

- 03/2018 - 03/2022 Wissenschaftlicher Mitarbeiter, Fachgebiet Bodenmechanik und Grundbau der TU Kaiserslautern
- 07/2014 - 06/2017 Assistant Lecturer and Head of Soil Mechanics Laboratory, School of Engineering, Department of Civil, Environmental and Geomatics Engineering, University of Rwanda (beurlaubt von 07/2017 bis 03/2022)
- 07/2014 - 06/2017 Bauingenieur bei Associated Technologies Ltd, Kist Consulting Company, Ltd sowie Conset Ltd in Kigali, Rwanda; Durchführung von geotechnischen Untersuchungen

Studium

- 10/2017 - 03/2022 Doktorand am Fachgebiet Bodenmechanik und Grundbau der TU Kaiserslautern
- 02/2012 - 06/2014 Master of Science in Bauingenieurwesen mit Vertiefung Geotechnik, University of Cape Town, South Africa
- 09/2006 - 07/2010 Bachelor of Science in Bauingenieurwesen und Umwelttechnologie, University of Rwanda (ehemals KIST), Kigali

Auszeichnungen

- 07/2021 - 03/2022 Promotionsstipendium des Fachgebiets Bodenmechanik und Grundbau der TU Kaiserslautern
- 07/2017 - 06/2021 Promotionsstipendium, Deutscher Akademischer Austauschdienst (DAAD)
- 02/2010 - 12/2013 Master Stipendium der Regierung von Rwanda
- 91/2006 - 09/2010 Bachelor Stipendium der Regierung von Rwanda

Veröffentlichungen des Fachgebietes Bodenmechanik und Grundbau der Technischen Universität Kaiserslautern

Herausgegeben von Prof. Dr.-Ing. habil. Helmut Meißner

- Nr. 1 Johannes Vogt (1992)
Tragverhalten von Schlitzwandelementen
- Nr. 2 Frank Rogmann (1992)
Untersuchungen zum Stoffverhalten von Kohle im Hinblick auf
Hohlraumstandsicherheiten
- Nr. 3 Wolfgang Weckbecker (1993)
Beitrag zur Berechnung oberflächennaher Tunnel
- Nr. 4 Egbert Adam (2001)
Untersuchungen zum temperaturabhängigen Materialverhalten kristalliner und
sedimentärer Gesteine
- Nr. 5 Andreas Becker (2002)
Stoffmodell und numerisches Modell für zyklisch beanspruchte, teilgesättigte
Sande
- Nr. 6 Katja Abel (2002)
Zugspannungen in Kunststoffdichtungsbahnen geneigter
Deponiebasisabdichtungen
- Nr. 7 Tao Li (2002)
Zweiflächen-Stoffmodell für wassergesättigte bindige Böden unter zyklischer
Beanspruchung
- Nr. 8 Solomon Taye Abebe (2002)
Foundation pits in saturated highly expansive soils
- Nr. 9 Festschrift anlässlich des 65. Geburtstages von Prof. Dr.-Ing. habil. Helmut
Meißner und dem 20-jährigen Bestehen des Fachgebietes Bodenmechanik und
Grundbau an der Technischen Universität Kaiserslautern (2003)

Herausgegeben von Prof. Dr.-Ing. habil. Christos Vrettos

Nr. 10 Sanaa Wendling (2004)

Untersuchungen zur Entstehung von Austrocknungsrisen in mineralischen Deponieabdichtungen

Nr. 11 Yi Lei Shen (2005)

Unterfangung belasteter Fundamente durch Bohrpfähle

Nr. 12 Stefan Jung (2007)

Nichtlinearer horizontaler Bettungsmodulansatz für Trägerbohlwände in mitteldicht gelagertem Sand

Nr. 13 Markus Dobrowolsky (2008)

Quellverhalten teilgesättigter bindiger Böden mit mittlerem Quellpotential

Nr. 14 Viktoria Schwarz (2011)

Mechanisches Verhalten eines teilgesättigten Tons: Experimentelle Untersuchungen, Stoffmodell und Implementierung

Nr. 15 Thomas Becker (2012)

Materialverhalten eines teilgesättigten bindigen Bodens unter zyklischer Belastung

Nr. 16 Dong Chen (2014)

Flachgründungen auf Böden mit tiefenabhängiger Steifigkeit unter vertikaler dynamischer Belastung: Ergebnisse von numerischen Berechnungen im Frequenz- und Zeitbereich

Nr. 17 Andreas Becker (2017)

Untersuchungen zu neuartigen und gängigen Methoden der Baugrundertüchtigung

Nr. 18 Salomi Papamichael (2019)

Experimental and numerical investigations on wheel-soil interactions in calibrated near-surface soil model

Nr. 19 Gerard Banzibaganye (2022)

Static and dynamic behaviour of sand-rubber chips mixtures